Observational Study of AGB Stars In the Outer Galactic Disk

Biwei JIANG

Department of Astronomical Science
The Graduate University for Advanced Studies, Japan

日本総合研究大学院大学
数物科学研究科 • 天文科学専攻

A dissertation submitted
to
the Graduate University for Advanced Studies
in Partial Fulfillment of the Requirements
for the Degree of
Doctor of Philosophy
in School of Mathematical and Physical Science

February 5, 1997

Bibliography of publications

1. • Authors: B.W.Jiang, S.Deguchi, J.Y.Hu, T.Yamashita, E.Nishihara, S. Matsumoto & Y.Nakada
   • Title: Identification of IRAS sources in the outer disk of the Galaxy
   • Publ.: The Astronomical Journal, scheduled in April 1997

2. • Authors: B.W.Jiang, S.Deguchi, I. Yamamura, Y.Nakada, S.H.Cho & T. Yamagata
   • Title: SiO maser sources in the outer disk of the Galaxy
   • Publ.: The Astrophysical Journal Supplement Series, 1996, Vol. 106, pp.463-488

3. • Authors: B.W.Jiang, S.Deguchi, & Y.Nakada
   • Title: Optical identification of IRAS sources in the outer Galaxy
   • Publ.: The Astronomical Journal, 1996, Vol. 111 No.1, pp. 231-259

4. • Authors: B.W.Jiang, S.Deguchi, H.Izumiura, Y.Nakada & I.Yamamura
   • Title: SiO maser survey of the Galactic bulge IRAS sources: IV. Observational properties of SiO masers
   • Publ.: Publ. Astron. Soc. Japan, 1995, Vol. 47 No.6, pp. 815-827

5. • Authors: WANG Junjie, JIANG Biwei & HU Jingyao
   • Title: Optical identification and observation of the unidentified IRAS LRS sources, II. Sources with silicate feature in the region: $13^h < \alpha < 24^h$, $0° < \delta < 66°$
   • Publ.: Acta Astrophysica Sinica, Vol.14, No.3, pp.239-244, Jul. 1994

6. • Authors: J.Y.Hu, S.Slijkhuis, T.de Jong & B.W.Jiang
   • Title: A systematic study of IRAS selected proto-planetary nebula candidates I.Selection of the sample and observations of the southern objects
   • Publ.: Astron. Astrophys. Suppl. Ser., 1993, Vol.100, No.2, pp.413-430

7. • Authors: JIANG Biwei & HU Jingyao
   • Title: From AGB star to Planetary Nebulae
   • Publ.: Progress in Astronomy, 1993, Vol.11, pp.123-134

8. • Authors: JIANG Biwei & HU Jingyao
   • Title: The galactic distribution of O-rich AGB stars
   • Publ.: Chin. Astron. Astrophys., 1993, Vol.17, pp.321-328

9. • Authors: JIANG Biwei & HU Jingyao
   • Title: Optical identification and observation of the unidentified IRAS LRS sources, I. Sources with silicate feature in the region: $0^h < \alpha < 12^h$, $0° < \delta < 66°$
   • Publ.: in Chin. Astron. Astrophys., Vol.16, No.4, p.416, 1992

10. • Authors: Wang Junjie, Qian Zhongyu, Hu Jingyao, JIANG Biwei & Wang Gang
    • Title: IRAS 04000+5052: a near-infrared variable associated with HII region
    • Publ.: Acta Astrophysica Sinica, 1992, Vol.12, No.4, pp.385-388

11. • Authors: Qian Zhongyu, Hu Jingyao & JIANG Biwei
    • Title: IRAS 19213+1723 : a newly found compact HII region
    • Publ.: Acta Astrophysica Sinica, 1991, Vol.11, No.1, pp.79-81

Acknowledgements

Many people and several institutions supported and helped me during my Ph.D.-hood. I would like to thank all of them and in particular those listed in following (in alphabetic order).

Deguchi, S., Prof.
Advisor, constant encouragement and advice
Hashimoto, O., Dr.
Helpful discussion
Hu, J.-Y., Prof.
Helpful suggestion and support in Beijing observation
Izumiura, H., Dr.
Helpful discussion
Japanese Government Scholarship
Financial support
Kiso Observatory
Long-time support for my observation, friendly acceptance
Nakada, Y., Prof.
Helpful discussion and friendly care
Nakano, T., Prof.
Encouraging attention
Nobeyama Radio Observatory people
Non-stop support, help and care
Nobeyama Radio Observatory, the 45m group
Important support to my SiO maser observation
Ohnaka, K., Dr.
Friendly help and discussion
Okayama Astrophysical Observatory
Support of my NIR observation
Utsumi, K., Prof.
Helpful discussion
XingLong Observatory, Beijing Observatory
Kind support of my observation
Yamamura, I., Dr.
Friendly help

Contents

List of Figures

Chapter I

Introduction

I.1. Asymptotic Giant Branch Stars

Asymptotic Giant Branch stars (AGB stars) are low-mass (0.8-2.3 $M_\odot$ on the initial main sequence) and intermediate-mass (with an upper limit of about 8-9 $M_\odot$ on the initial main sequence mass) stars that have developed an electron-degenerate C-O core after the exhaustion of central helium. The name comes from that for low-mass stars, the evolutionary track of AGB stars in the H-R diagram approaches that of the first giant branch(Renzini & Fusi 1988). Low-mass stars develop an electron-degenerate helium core immediately following the main sequence phase. After the helium flash lifts the degeneracy and burns out all the central helium, they evolve to AGB phase with a degenerate C-O core. Intermediate-mass stars ignite helium non-degenerately after leaving the main sequence phase and then directly result in a degenerate C-O core. In the AGB phase shortly living for about a few $10^4 \sim 10^5$ years(Wood 1990; Renzini & Greggio 1990) the low- and intermediate-mass stars behave qualitatively the same and ultimately evolve into planetary nebulae and/or white dwarfs through the so-called post-AGB stage(Kwok 1993).

In AGB phase, there are two important processes whose results are not only important to evolution but also observable, the third dredge-up and the mass loss. The so-called dredge-up is a process that the base of convective envelope extends inward to "dredge-up" material newly produced by nuclear reaction and thus brings about the surface abundance changes. The first dredge-up occurs in every star as it becomes a red giant following the exhaustion of central hydrogen(Becker & Iben 1979). The second dredge-up accompanies the formation of an electron-degenerate core following the exhaustion of central helium(Becker & Iben 1980). The third dredge-up happens when the thermal pulse amplitude approaches some limiting strength in AGB phase. It results in the mixing of freshly synthesized ^{12}C and neutron-rich isotopics via helium burning and neutron capture to the stellar surface and makes it possible for an AGB star to become C-rich in view of spectroscopy. Whether or not the third dredge-up occurs depends on core mass, total mass, metallicity and mixing length of convective envelope (Wood 1983). In particular, the minimum core mass for dredge-up occurrence decreases with decreasing metallicity as well as increasing total mass and increasing mixing length.

AGB stars lose mass through stellar winds. Four mechanisms have been proposed for the mass loss that are radiative driving of the dust(Tielens 1983), radial pulsation(Bowen 1988), Alfven wave driven wind(Hartmann & MacGregor 1980) and sound wave driven wind(Pijpers

& Hearn 1989). The process is not very clear but it seems more than one mechanism have to work in some combinational way. Mass loss rates range from a detectability lower limit of 10^{-8} $M_\odot$ yr^{-1} to some 10^{-5} $M_\odot$ yr^{-1} in light of the evidence of molecular line observations. The matter driven to apart from the star's photosphere forms a circumstellar envelope expanding at velocity of the order of 10 km s^{-1}. The envelope becomes thick and cold as expanding and departing away from the photosphere. Gradually the central star becomes optically invisible and the object becomes bright at infrared and even radio wavelengths due to the re-emission from the circumstellar envelope (CSE) by transferring the photosphere radiation. With the cooling of the CSE, some solid particles condense and molecules come to existence. The interaction of the AGB wind with the so-called superwind at a rate of around 10^{-4} $M_\odot$ yr^{-1} or 10^{-3} $M_\odot$ yr^{-1} at the post-AGB phase is able to produce the asymmetrical morphology of planetary nebulae(Kwok 1982).

I.2. Observations

I.2.1. In space: IRAS and ISO

IRAS (InfraRed Astronomical Satellite) launched in 1983 discovered a large number of AGB stars during its survey covering 96% sky. IRAS made photometric observations at 12, 25, 60 and 100 μm of all of them (IRAS PSC) with the sensitivity of about 1Jy(Beichmann et al. 1988). The presence of circumstellar envelope resulted from mass loss distinguished AGB stars from other normal stars without CSEs in the IRAS color-color diagram ($logF_{25}/F_{12}$ viz $logF_{60}/F_{25}$) by showing infrared excess of normal photosphere radiation. Their color temperatures range from about 800K to 200K, much lower than that of the stellar photospheres(van der Veen & Habing 1988). The IRAS colors and fluxes are also tools to estimate the mass loss rates of AGB stars(Herman et al. 1986; Jura 1987). Many AGB stars are detected variable in the IRAS mission which surveyed most of the sky more than once. In addition to photometry, IRAS also took Low Resolution Spectra (LRS) ranging from 7.7 to 22.6 μm of the 12μm-bright sources (5425 entries in Olnon & Raimond 1986) which bifurcate the CESs of AGB stars. The C-rich CSEs exhibit an emission feature of SiC at 11.3μm and the O-rich CSEs exhibit the emission or absorption feature of silicate at 9.7μm and around 18μm.

AGB stars show a disk-plus-bulge structure in the Galaxy based on the the IRAS PSC database, mostly being long period variables in the bulge according to the multi-times photometric results of IRAS(Harmon & Gilmore 1988). In the disk, AGB stars tend to clump in the spiral arms(Jiang & Hu 1993).

The circumstellar physics of AGB stars has been one of the major subjects of ISO (Infrared Space Observatory) launched in 1995 and performing nominally in operation(Kessler 1996). With four main instruments ISOCAM, ISOPHOT, ISOSWS and ISOLWS, ISO will achieve higher sensitivity in photometry and higher resolution in spectroscopy covering wider wavelength range of 2.5 $\sim$ 240 μm than IRAS, make innovative imaging observations in the pointing mode other than the survey mode. ISO will shed light on many aspects of study of AGB stars, in particular the chemical environment and structure of circumstellar envelopes.

I.2.2. On ground

In addition to the direct results from the IRAS observation, IRAS database have been the starting points of almost all the later ground-based observations of AGB stars.

Near-infrared photometry and spectroscopy

Epchtein et al. (1987) observed 630 infrared stars at JHKL bands in near-infrared and suggested the possible discrimination of C-rich and O-rich AGB stars based on the colour indices such as $K - L$ and [12μm] - [25μm]. Follow-up observations of 516 AGB candidates at JHKLM bands by Fouqué et al. (1992) attested this result. Another large-scale and independent near-infrared photometric observations by Noguchi et al. (1991) further confirmed the difference between C-rich and O-rich AGB stars in the near-mid-infrared color-color diagram. The observational results at JHKLM bands of about 1332 candidate AGB stars are compiled by Gugliemo et al. (1993). In the diagram of $K - L$ and [12μm] - [25μm], C-rich stars aggregate in the region relatively bluer in [12μm] - [25μm] and redder in $K - L$ than the O-rich stars.

Whitelock et al.(1991, 1994) monitored the light-variation of 141 AGB stars in the Galactic bulge and 61 AGB stars in the South Galactic Pole at JHKL bands. They found that the periods of bulge Miras mainly lie in the range of 360-560 days with maximum and minimum values of 722 and 172 days. The calculated luminosities from their periods and period-luminosity relation then vary from about 6800 $L_\odot$ to 11000 $L_\odot$. The K-band amplitude ranges from 0.4mag up to 2mag. They did not find any obvious difference in the period distribution or light-curve amplitudes between the bulge and south pole AGB stars. The Galactic Miras and the Magellanic Clouds (MCs) Miras (Feast et al. 1989) conform very similar period-luminosity relations. The difference found between the Galactic and LMC AGB stars is that the near-infrared M-type Miras in the LMC have much "bluer" colors than that in the Galaxy with similar periods and pulsation properties, suggesting the dust opacity of AGB stars is thinner in the LMC and implying an effect of metallicity on reddening of the circumstellar envelope.

Smith & Lambert (1985, 1986, 1990) spectroscopied a sample of M, MS and S giants in infrared and near-infrared with high resolution and high S/N. Some of the MS and S stars show an excess of ^{12}C, a principle product of He-burning shell. and the ^{12}C enrichment is correlated with a more marked enrichment of the s-process elements. The MS and S stars also show a higher N abundance than the M giants. Such structure of chemical abundances is attributed to the expected deep mixing that occurs with the onset of the third dredge-up in the AGB phase. Derived from the abundance of Rb and and the absence of isotope ^{96}Zr whose synthesis is controlled by the branch in the s-process path at ^{95}Zr, the observed neutron densities are consistent with that predicted for low-mass AGB stars and inconsistent with that for intermediate-mass AGB stars(Lambert et al. 1995). The Mg isotope ratios require that the s-processing occur in low-mass AGB stars (Busso et al. 1995).

Radio line observations

The AGB stars are very rich in various molecular species due to the efficient shielding by the circumstellar dust of the molecules formed both in the stellar photosphere and in CSEs. A few tens species of molecules have been detected at radio wavelengths. The most popular molecular lines in observations of AGB stars are those from CO, HCN, SiO, H_2O, and OH molecules.

The rotational transitions in the vibrational ground state of ^{12}CO, very stable and the second most abundant molecule next to H_2 in CSEs, are generally the strongest thermal lines of AGB stars. In the catalogue (Loup et al. 1993) that compiled the observational results in CO(2-1) and CO(1-0) lines, 324 C-rich and O-rich AGB stars are reported being CO emitters. The expansion velocities of CSEs vary from 5 to 20 km s^{-1} in O-rich AGB stars and from 5 to 30 km s^{-1} in C-rich AGB stars according to the CO line width. Derived mass loss rates based on the CO line parameters range from $10^{-7}M_{\odot}yr^{-1}$ to 3 $\times 10^{-5}M_{\odot}yr^{-1}$. The isotopic ^{13}CO lines have also been detected though in fewer number reasonably resulted from its less abundance.

HCN, as the second most detectable molecule in C-rich CSEs, has been searched in a large number of AGB stars as well. Loup et al.(1993) collected the data on HCN(1-0) thermal line in about 120 AGB stars. Izumiura (1990) detected this line emission in 80 objects.

Maser emissions from OH, H_2O and SiO molecules are looked for and detected in hundreds or thousands of AGB stars.

OH maser emission was discovered as the first stellar maser 30 years ago and now has been detected in more than 1500 AGB stars or late-type stars(Benson et al., Lewis et al.) mainly at 1612MHz. Many of the OH maser lines appear in double-peak profile suggesting they are originated from the front and back expanding shell by far-IR radiative pumping. Interferometric mapping of the OH/IR star OH127.8 (Booth et al 1981) provided strong and direct confirmation of the "front-back" model. Additional support comes from the phase-lag measurements (Herman & Habing 1985). The interferometric observations also determine the radius of OH shell, with values just under $\sim 10^{16}$cm all the way to $\geq 10^{17}$cm. The CSEs expansion velocities derived from the front and back components mostly are between 10 km s^{-1} and 30 km s^{-1} (te Lintel Hekkert et al 1991).

The H_2O maser line emission of $6_{16} \rightarrow 5_{23}$ at 22GHz has been detected in about 400 AGB stars(Brand et al. 1994, Engels & Lewis 1996). The OH maser profiles are divided into type A and type B according to the maser velocity offsets from stellar radial velocity(Engels et al 1986). Type A masers appear close to the radial velocity and type B masers are double-peaked and centered at the radial velocity. Rotational collisional excitation mechanism was proposed (Deguchi 1977) and confirmed (Cooke & Elitzer 1985). Interferometric observations (Spencer et al. 1979, Johnston et al. 1985, Lane et al. 1987) showed that the maser region size varies with mass loss rate and ranges from 10^{15}cm to 10^{16}cm. This maser has been observed of the intensity variation by a large factor and correlated with visual light variation(Gomez Balboa & Lepine 1986). Besides this line, some other water lines are also detected as maser emission such as the 96.3GHz $5_{33} \rightarrow 4_{40}$, 232.7GHZ $6_{43} \rightarrow 5_{50}$(Menten & Melnick 1989) and 658GHz $1_{10} \rightarrow 1_{01}$ lines (Menten & Young 1995).

SiO masers

SiO maser emissions have been detected from several rotational transitions in different excited vibrational states in more than 400 late-type stars(Benson et al. 1990; Izumiura et al. 1995) since Kaifu et al.(1975) successfully observed the $v = 1, J = 2 - 1$ line emission in 12 OH/IR stars. The detected lines are rotational transitions obeying $\triangle v = 0, \triangle J = \pm 1$, from $J = 1 - 0$ to $J = 7 - 6$(Gray et al. 1995) in $v = 0, 1, 2, 3, 4$. The most observable and best studied lines are the $J = 1 - 0$ transition at a couple of vibrational states around 7mm, among which the v=1 and v=2 lines are found to appear simultaneously in most cases in light of the survey to the bulge direction(Jiang et al 1995). SiO maser spectra are usually multi-peaked and centered at stellar radial velocity(Jewell et al. 1991). The line profiles are found to be variable with a phase lag of about 0.1 to 0.2 to the IR variation (Martinez et al. 1988).

High resolution interferometry (Colomer et al. 1992) found that the observed spots of SiO maser emission are rather compact, typically $\sim$ 0.1 - 5 AU depending on stellar luminosity classes. The VLA mapping of SiO maser emitters reveal well-defined rings of maser emission at $\approx 2 \rightarrow 4$ stellar radii(Diamond et al. 1994). SiO maser spots are thus locating at $\sim 10^{13} \rightarrow 10^{14}$cm from stellar center, the innermost amid the detected masers from AGB stars. A polarization map of R Cas (McIntosh et al 1989) indicates that the SiO maser emission of different spots originates in separate cells, each one characterized by distinct radial velocity, linear polarization and polarization position angle.

The IR radiative pumping can lead to the required population inversion in the presence of a large velocity gradient (Kwan & Scoville 1974; Deguchi & Iguchi 1976) and so can a collisional excitation(Elitzur 1980). Both mechanisms can explain the coincidence of SiO maser velocity with stellar radial velocity. The radiative pumping can explain the correlation between maser variation and IR light variation and collisional pumping shows how masers occur at high-excited vibrational state. Neither can explain all the observational phenominea independently under present modelling constraints. Furthermore, neither can easily produce quantitatively the observed intensity ratio of the v=1 to v=2 lines.

Isotopic ^{29}SiO and ^{30}SiO maser emissions have been detected from a few rotational transitions in ground, first and second excited vibrational states in about 20 SiO maser sources (Cho et al. 1986; Alcolea & Bujarrabal 1992; Cho & Ukita 1995; Cho et al. 1996). The detected emitters are much fewer than the normal SiO sources due to that the ^{29}Si and ^{30}Si are about 20 and 30 times less abundant than ^{28}Si in the CSEs (Tsuji et al. 1994). The isotopic maser intensities also vary with the infrared continuum flux at 8μm. The isotopic masers differ from the normal ones. First the maser emissions occur from the transitions in ground vibrational state in which thermal emission is usually produced in ^{28}SiO (Bujarrabal et al. 1986). This ground-state maser invalidates the proposed modellings for normal SiO masers. Second the isotopic maser spectra exhibit usually only one peak instead of multi-spikes as normal ones(Alcolea & Bujarrabal 1992). The peak intensity is much weaker than that of normal SiO maser lines so that no interferometric mapping at isotopic maser lines has been performed yet.

I.3. Outline of the thesis

This thesis will concentrate on the observations of AGB stars in the outer disk of the Galaxy where the dark matter is suspected to exist from the flat rotation curve and less attention has been paid compared with the bulge and solar neighbourhood. Due to the high sensitivity at 43GHz of 45-m telescope system at Nobeyama Radio Observatory, a survey deep to 1Jy at 5 sigma level in SiO maser lines is carried out to about 250 stars in the second and third quadrants of the Galactic plane. Taking the advantage of the telescope system, the rotational transition J=1-0 line in three different vibrational states, ^{28}SiO v=1 and 2, ^{29}SiO v=0, is searched. This survey is the deepest and most complete in these SiO maser lines in the outer disk. Comparing with a survey of similar sensitivity and scale to the bulge direction infers the large-scale distribution of SiO maser populations of AGB stars. Follow-up optical and near infrared observations are also performed to a sub-sample of the SiO maser-survey sources. The near-infrared photometry observation was done by using a NICMOS3 detector attached to the 188cm telescope at Okayama Astrophysical Observatory and resulted in a high sensitivity too. The Kiso 105cm Schmidt telescope is used to identify some of the SiO maser-surveyed stars in the aspects of color and light variation as the basis of radio and near-infrared observations. Some sources are even taken low-resolution optical spectroscopy to clarify their spectral types. Combining all data in optical, near infrared, IRAS and SiO maser data, the thesis will give a scenario of AGB stars in the outer disk of the Galactic plane.

REFERENCES

Alcolea, J., & Bujarrabal, V. 1992, A&A 253, 475

Becker, S.A., Iben, I.Jr., 1979, ApJ 232, 831

Becker, S.A., Iben, I.Jr., 1980, ApJ 237, 111

Benson, P.J., Little-Marenin, I., Woods, T., Attridge, J., Blais, K., Rudolph, D., Rubiera, M., & Keefe, H. 1990, ApJS 74, 911

Booth, R., Kus, A., Norris, R., Porter, N., 1981, Nature 290, 382

Bujarrabal, V., Planesas, P., Gomez-Gonzalez, J., Martin-Pintardo, J., del Romero, A. 1986, A&A 162, 157

Bowen, G.H. 1988, ApJ 329, 299

Busso, M., Lambert, D., Beglio, L., Gallino, R., Raiteri, C., & Smith, V. 1995, ApJ 446, 775

Cho, S.H., Kaifu, N., Ukita, N., Morimoto, M., & Hayashi, M. 1986, Ap&SS 118, 237

Cho, S.H., & Ukita, N. 1995, PASJ 47, L1

Cho, S.H., Kaifu, N., Ukita, N. 1996, A&AS 115, 117

Colomer, F., Graham, D., Krichbaum, T., Ronnang, B., de Vicente, P., Witzel, A., Barcia, A., Baudry, A., Booth, R.S., Gomez-Gonzalez, J., Alcolea, J., Daigne, G. 1992, AA 254, L17

Cooke, B., Elitzur, M. 1985, ApJ 295, 175

Deguchi, S. 1977 PASJ 28, 307

Diamond, P.J., Kemball, A.J., Junor, W., Zensus, A., Benson, J., Dhawan, V. 1994, ApJL 430, 61

Elitzur, M. 1980, ApJ 240, 533

Engels, D., Schmid-Burgk, J., Walmsley, C. 1986, A&A 167, 129

Engels, D. & Lewis, B. 1996, AApS 116, 117

Epchtein, N., Le Bertre, T., Lepine, J., Santos, P., Matsuura, O. 1987, A&AS 71, 39

Feast, M.W., Glass, I.S., Whitelock, P.A. & Catchpole, R.M. 1989, MNRAS 241, 375

Fouqué, P., Le Bertre, T., Epchtein N., Guglielmo, F., Kerschbaum, F. 1992, A&AS 93, 151

Golmez Balboa, A., Lepine, J. 1986, A&A 159, 166

Gray, M., Ivison, R., Yates, J., Humphreys, E., Hall. P. & Field, D. 1995, MNRAS 277, L67

Gugliemo, F., Epchtein, N., Le Bertre, T., Fouqué, P., Hron, J., Kerschbaum, F. and Lépine 1993, A&AS 99, 31

Harmon, R. & Gilmore, G. 1988, MNRAS 235, 1025

Hartmann, L., MacGregor, K.B., 1980, ApJ 242, 260

Herman, J., Habing, H. 1985, AApS 59, 523

Herman, J., Burger, J.H., Penninx, W. 1986, AA 167, 247

Izumiura, 1990, thesis, Univ. of Tokyo

Izumiura, H., Catchpole, R., Deguchi, S., Hashimoto, O., Nakada, Y., Onaka, T., Ono, T., Sekiguchi, K., Ukita, N., & Yamamura, I. 1995a, ApJS 98, 271

Jewell, P.R., Snyder, L.E., Walmsley, C.M., Wilson, T.L., & Gensheimer, P.D. 1991, A&A 242, 211

Jiang, B.W. & Hu, J.Y. 1993, Chin. Astro. Astrophy. 17, 321

Jura, M. 1987, ApJ 313, 743

Kaifu, N., Buhl. D., Snyder, L. 1975, ApJ 195, 359

Lambert, D., Smith, V., Busso, M., Gallino, R., & Straniero, O. 1995, ApJ 450, 302

Kessler, M.F., 1996, ESA Bulletin, No.86

Kwan, J. & Scoville, N. 1974, ApJL 194, 97

Kwok, S. 1982, ApJ 258, 280

Kwok, S. 1993, ARA&A 31, 63

Loup, C., Forveille, T., Omont, A., & Paul, J.F. 1993, A&AS 99, 291

McIntosh, G., Predmore, C., Moran, J., Greenhill, L., Rodgers, A., Barvainis, R. 1989, ApJ 337, 934

Olnon, F.M., & Raimond, E. 1986, A&AS 65, 607

Martinez, A., Bujarrabal, V., Alcolea, J. 1988, A&AS 74, 273

Menten, K., Melnick, G. 1989, ApJ 341, L91

Menten, K., Young K. 1995, ApJ 450, L67

Noguchi, K., Sun, J. and Wang, G. 1991, PASJ 43, 275

Pijpers, F.P. & Hearn, A.G. 1989, AAp 209, 198

Reimers, D. 1975, in "Problems in stellar atmospheres and envelopes", Baschek, B., W.H.Kegel, G. Traving (eds), Springer, Berlin, p.229

Renzini, A. & Fusi, Pessi, F. 1988, ARA&A 26, 199

Renzini, A., Greggio, L. 1990, in "Bulges of Galaxies", B.J. Jarvis and D.M. Terndrup, eds., ESO Conf. and Workshops 35, p.47

Smith V. & Lambert, D. 1985, ApJ 294, 326

Smith V. & Lambert, D. 1986, ApJ 311, 843

Smith V. & Lambert, D. 1990, ApJS 72, 387

Tielens, A.G.G.M. 1983, ApJ 271, 702

Tsuji, T., Ohnaka, K., Hinkle, K., Ridgway, S. 1994. A&A 289, 469

Whitelock, P.A., Menzies, J., Feast, M., Marang. F., Carter, B., Roberts, G., Catchpole, R., & Chapman, J. 1994, MNRAS 267, 711

Whitelock, P., Feast, M., & Catchpole, R. 1991. MNRAS 250, 638

Wood, P.R. 1990, in "From Miras to Planetary Nebulae", Mennessier, M.O. and Omont, A.(eds.), Editions Frontieres, p.67

Wood P.R. 1983, ApJ

van der Veen W. & Habing, H.J. 1988, AA 195, 125

Chapter II

Survey in SiO maser lines (I)

This chapter has been published in
The Astrophysical Journal Supplement Series, 106:463-488, 1996 October
as
SiO maser sources in the outer disk of the Galaxy
co-authored by
S. Deguchi, I. Yamamura, Y. Nakada, S. Cho and T. Yamagata

ABSTRACT

The observations in the ^{28}SiO J=1-0 v=1, J=1-0 v=2 lines and the ^{29}SiO J=1-0, v=0 line were simultaneously made towards 181 color-selected IRAS sources in the outer disk of the Galaxy (at longitudes between 90° and 250°). The ^{28}SiO lines were detected in 63 sources (56 new) and the ^{29}SiO line in 11 sources (9 new). Most of the detections are optically variable stars, mainly Mira-type variables and a few semi-regular variables. The detection rate(35%) is much lower than that of the bulge survey performed by the same observational system, the 45m telescope at Nobeyama Radio Observatory. The lower detection rate of SiO maser emission is partly attributed to the increase of contaminations by stars with C-rich circumstellar envelope and young stellar objects in the outer disk sample. The kinematical implications of the observational results are also discussed. The luminosity distances to the SiO maser sources are estimated from their IRAS fluxes at 12 micron and colors. By combining the SiO radial velocity and the luminosity distance, the rotation curve of the outer Galactic disk is found to be slightly falling within the galactocentric distance between 8.5kpc and 12kpc. The sources located within 20° from the Galactic anticenter direction are used to check a peculiar motion of the local standard of rest.

II.1. Introduction

Since the discovery of SiO masers by Snyder & Buhl (1974), a lot of observational and theoretical works have been devoted to studying them. In the aspect of observation the ^{28}SiO and its isotopic maser lines have been searched for by some groups. Most observations were towards nearby stars such as Mira variables(cf. Cho et al. 1986, Jewell et al. 1991, Allen et al. 1989), semi-regular variables(Dickinson et al. 1986), symbiotic stars(Hall et al. 1987; Schwarz et al. 1995) an OH/IR stars (Lindqvist et al. 1991; Nyman et al. 1993). Nevertheless, the survey towards the Galactic bulge direction by Izumiura et al.(1994; 1995a; 1995b) could approach objects at a distance of 8.5 kpc or further, in which the sources are seldom associated with any known optical objects. In respect of theory, both radiative (Deguchi & Iguchi 1976) and collisional (Elitzur 1980) pumping mechanisms are proposed to interpret the SiO masers.

In spite of the abundant observations in SiO maser lines, little attention has been paid to stars in the outer disk of the Galaxy. Many InfraRed Astronomical Satellite(IRAS) Point Source Catalogue(PSC) (Beichman et al. 1985) sources in the outer disk have been observed in the CO and OH lines. Wouterloot & Brand(1989) detected CO(1-0) thermal emission in 1077 sources out of 1302 infrared sources whose IRAS colors are of young stellar objects. However there is less success when searching for OH maser emission in IRAS sources whose IRAS colors are of late-type stars. Lewis(1994) detected 1612MHz OH maser emission in fewer than 25 objects amid more than 250 sources using the Arecibo telescope so that the OH maser detection rate is a quarter of that in the inner Galaxy.

The purpose of this paper is to use SiO maser lines to investigate the IRAS sources in the outer disk of the Galaxy where the surveys in OH maser lines have not yet been made extensively. From radial velocities of SiO maser lines, we can study the Galactic kinematics of stars in this interesting region where the presence of dark matter is suspected from the flat rotation curve of the outer disk. In this paper, we report the results of an SiO maser line survey towards 181 color-selected IRAS sources distributed between 90° and 250° in the Galactic longitude.

II.2. Object selection, observation and data reduction

The main selection criteria of the sources in the outer Galactic part are almost identical to those in the bulge survey(Izumiura et al. 1994) for a convenient comparison. The Galactic latitudes of all the sources are as $|b| < 10°$ so that they are constrained in the outer stellar disk of the Galaxy, i.e. within 1kpc from the Galactic plane given a distance less than 6kpc. There are some minor differences in two observational runs made in May 15-19, 1994 and May 21, 22 and 26-29, 1995. In the 1994 May period, the criteria are (F_λ is the IRAS flux density at λ): (1) in the strip of $|l - 180°| < 10°$ where l is Galactic longitude, (2) IRAS color $C_{12}(\equiv \log_{10}(F_{25}/F_{12}))$ in the range [-0.4, 0.3], (3) F_{12} bigger than 3Jy. Seventy sources were observed in this semester and we intended to study the peculiar motion of local standard of rest(LSR). While in May 1995, we observed the sources in other parts of the outer disk as well as reachable at the site of the telescope. i.e. the Galactic longitude ranging from 90° to about 250° except between 170° and 190°. In addition, the IRAS variability index is bigger than

50 for selecting potential Mira-type variables and the qualities of IRAS fluxes at 12, 25 and 60μm are good (Beichman et al. 1988). The IRAS Low Resolution Spectra(LRS) class 4n type sources that may have C-rich circumstellar envelopes (CSE) (Olnon & Raimond 1986) are excluded. In this run, 111 sources were observed. In total 181 sources were searched in SiO maser lines. In case of not very good weathers, observations were more concentrated on closer IRAS LRS 2n sources with O-rich CSE. So the part of the sample with $F_{12} > 10$Jy is slightly biased to objects with O-rich CSE due to the casual selection of IRAS LRS classes, but the other part with $F_{12} < 10$Jy are not biased to have either C-rich or O-rich CSE.

The sample selected by above criteria can be consisted of two types of stars. The major is late-type stars with cold CSEs when $C_{12} < -0.4$ and the minor is possibly young stellar objects in star forming regions when $C_{12} > -0.4$. The IRAS PSC sources are divided into 10 groups with different IRAS colors based on the analysis of IRAS color-color diagram by van der Veen & Habing(1988) (VH). The sources in the sample with IRAS color C_{23} ($\equiv \log_{10}(F_{60}/F_{25})$) < -0.4 are grouped in VH IIIa and IIIb regions, the territory of variable stars with evolved circumstellar shells. When combining the constraints on IRAS variability index and flux at 12μm, these sources were certainly variable during the IRAS mission (Jiang et al. 1996). Therefore they are vary possibly variable late-type stars with cold circumstellar envelopes. Twenty more sources selected have IRAS color $C_{23} > -0.4$ as well as $C_{12} > 0.0$. They could be late-type stars while more possibly young stellar objects in star-forming regions(Harris et al. 1988). The bulge survey detected a number of IRAS sources of these colors (about 50%, see Jiang et al. 1995) in SiO maser lines. Thus the present survey includes the sources of such colors to compare the SiO detection rate with the bulge sample.

The observations were made with the 45m telescope at Nobeyama Radio Observatory. We used a cooled SIS receiver and an acousto-optical spectrometer(AOS) with eight high-resolution arrays AOS-H (the spectral resolution per two binned channels is 37kHz, 0.26 km s^{-1} at 43GHz) and four wide-band arrays AOS-W (the bandwidth 250MHz, i.e. 1740 km s^{-1} coverage in velocity at 43GHz). The rest frequencies were tuned to 43122.027MHz, 42820.539MHz, 42879.8MHz and 42851.970MHz for the ^{28}SiO v=1 J=1-0, ^{28}SiO v=2 J=1-0, ^{29}SiO v=0 J=1-0 (hereafter notations v=1, v=2, ^{29}SiO are used) and $H_{53}\alpha$ lines in order. The $H_{53}\alpha$ line was set purposely to observe a few strong HII regions for intensity calibration. At every frequency, two AOS-H arrays were used in order to enhance reliability of the observational result. The AOS-W arrays were set to centers at the v=1 and v=2 lines. The detection limit was usually better than 0.2K at 4σ level as the normal system temperature was around 200K (the conversion factor from antenna temperature to line intensity is about 3.6Jy/K) in spite of its variation from 200K to 500K depending mainly on the weather and elevation of the antenna. The Half Power Beam Width (HPBW) was about 40″. We checked the pointing every 3 hours or so by nearby strong SiO maser sources so that the pointing accuracy was around 2-8″. If the source has an optical counterpart or was identified by Jiang et al. (1996), its optical position was adopted. Otherwise we use the IRAS PSC (version 2) position whose uncertainty is much smaller than the HPBW of the telescope. All observations were made in the position-switching mode using a 5′ off position in the azimuth direction. The averages of rms for the sources without SiO detections are 0.054K and 0.056K for the v=1 and v=2 lines and these two averages are both 0.05K in the survey towards the bulge(Jiang et al. 1995). So the system condition is comparable to that in the bulge survey.

The raw data were processed by flagging out bad scans, making rms-weighted integrations and removing the first-order baseline. The signal is regarded as a detection when it is higher than 4σ of the noise level and its width is wider than two channels. For calculating the line parameters of detections, multiple-Gaussian fitting was performed by the NEWSTAR software developed by the staff at Nobeyama Radio Observatory. Because the line profiles are usually not simple, the multiple component fitting may not be unique. Our fitting procedure was thus made under two rules: the number of components should be as small as possible and the residuals should be smaller than 3σ to merge into the neighbouring noise. This policy should not generate any artificial component and should result in correct calculation of the integrated line intensity.

II.3. Results

In 1994, 15 sources were detected in the ^{28}SiO lines and one source, IRAS 05388+3200 was detected in the ^{29}SiO line. In 1995, 48 sources were detected in the ^{28}SiO lines and 10 of them were detected in the ^{29}SiO line. No source was detected in H53α line to the detection limit of about 0.8Jy. The wide velocity coverage of AOS-W prevented us from missing high velocity components. No high-velocity ($(|V_{\rm lsr}|) > 200$ km s^{-1}) emission component was found in any source. As a whole, 63 sources of 181 were detected in the ^{28}SiO J=1-0 v=1 and/or v=2 maser lines, 11 of which were detected in the ^{29}SiO J=1-0 v=0 line. Among the detections, IRAS 03206+6521, 05388+3200, 06500+0829, 21086+5238, NV Aur, IRC+60092 and R Cas (Benson et al. 1990) are already known ^{28}SiO maser sources, NV Aur and R Cas (Alcolea & Bujarrabal 1992) are known ^{29}SiO maser sources. Therefore we detected 56 new ^{28}SiO and 9 new ^{29}SiO maser sources in which IRAS 06500+0829 was also detected the ^{29}SiO line emission by Cho et al. (1996).

TABLE 1.1. Line parameters of Gaussian components of the v=1 and v=2 detections

	SiO v=1 J=1-0				SiO v=2 J=1-0			
IRASNAME	TA1 (K)	rms1 (K)	Vlsr1 (km/s)	FWHM1 (km/s)	TA2 (K)	rms2 (K)	Vlsr2 (km/s)	FWHM2 (km/s)
00127+5437	...	0.026	...	...	0.149	0.029	-91.788	1.983
00336+6744	0.136	0.034	-92.298	7.036	0.139	0.036	-90.267	2.206
	0.143		-90.973	0.700	...		...	...
00459+6749	0.597	0.060	-90.252	1.612	0.308	0.064	-90.177	2.512
	0.544		-87.591	2.831	0.239		-87.796	1.551
00534+6031	0.157	0.032	-100.604	1.102	0.106	0.029	-105.098	1.109
	...		...	...	0.148		-100.614	1.579
02433+6345	0.602	0.065	-58.526	2.608	0.383	0.070	-58.397	2.553
	0.965		-55.277	1.293	1.171		-55.392	1.334
	...		...	...	0.391		-52.455	1.691
02469+5646	0.254	0.062	-41.327	0.819	...	0.054	...	...
	0.345		-40.585	2.909	...		...	...
02470+5536	0.421	0.071	-38.966	1.858	0.539	0.073	-38.968	1.964
	0.436		-35.105	2.388	0.476		-34.903	1.754
03206+6521	...	0.044	...	...	0.283	0.048	-37.802	2.081
03469+5833	0.473	0.039	-74.130	1.181	0.342	0.039	-74.456	1.352
03513+4827	0.367	0.038	-69.043	2.835	0.285	0.040	-70.019	2.470
	0.369		-66.205	2.876	0.379		-66.433	2.170
	1.139		-63.722	1.571	0.818		-63.849	1.944
	0.318		-61.798	0.710	0.509		-56.338	2.518
	0.199		-56.294	3.297	0.243		-54.483	1.083
03572+5509	0.126	0.030	-37.546	0.719	...	0.029	...	...
04085+5347	...	0.045	...	...	0.361	0.037	-15.338	2.527
04209+4800	1.208	0.103	-16.766	1.510	1.075	0.057	-16.749	2.204
	0.288		-14.842	5.468	...		...	...
05031+3519	...	0.075	...	...	0.226	0.087	-36.993	0.838
	...		...	...	0.231		-35.462	1.669
05091+4639	0.116	0.027	12.676	1.239	...	0.032	...	...
05131+3039	0.408	0.043	8.274	1.789	0.089	0.044	10.104	7.663
	0.430		11.340	1.137	0.132		12.145	0.622
05146+2521	0.424	0.166	-1.292	2.660	0.385	0.173	-3.303	1.438
	...		...	...	0.559		-1.419	1.074
05284+1945	0.106	0.054	13.464	1.637	0.375	0.044	14.647	3.887
	0.247		14.240	1.250	...		...	...
05325+2351	0.273	0.085	8.861	3.086	0.109	0.086	8.522	2.385
	0.264		13.213	1.132	...		...	...
05354+2458	0.361	0.225	3.935	5.132	...	0.226	...	...
	1.510		4.117	0.799	...		...	...
	0.944		6.135	1.245	...		...	...
05367+3736	0.619	0.166	-37.879	0.775	4.013	0.169	-36.460	1.288
	4.201		-36.633	1.137	1.260		-33.457	1.858
05368+2841	0.644	0.074	-18.581	2.236	1.567	0.063	-19.041	1.422
	3.241		-16.970	0.969	1.629		-14.114	4.027
	1.420		-15.854	0.820	6.880		-11.830	1.941
	2.566		-14.765	1.179	0.791		-9.734	0.585
	5.863		-12.545	1.770	1.771		-8.809	1.710
	2.700		-11.161	1.020	...		...	...
	1.778		-9.278	1.904	...		...	...
05384+3854	0.457	0.063	5.989	1.637	0.278	0.061	6.307	1.199
	2.197		8.698	2.258	1.195		8.392	1.699
	2.002		8.841	0.566	0.784		10.683	1.148
	1.032		10.974	1.080	...		...	...
05423+2905	0.851	0.065	23.858	1.049	1.762	0.065	23.586	1.989

TABLE 1.1. (continued)

	SiO v=1 J=1-0				SiO v=2 J=1-0			
IRASNAME	TA1 (K)	rms1 (K)	Vlsr1 (km/s)	FWHM1 (km/s)	TA2 (K)	rms2 (K)	Vlsr2 (km/s)	FWHM2 (km/s)
	1.315		25.764	1.076	1.078		25.998	1.093
	0.579		27.116	0.906	0.501		27.184	3.353
	0.534		29.243	2.073	0.452		30.823	1.746
	1.035		30.416	2.297	...		...	...
05443+2707	0.355	0.069	-13.664	1.842	1.495	0.060	-12.542	1.652
	0.617		-12.532	0.753	0.614		-10.204	1.602
	0.739		-10.177	0.698	0.282		-6.845	3.442
	0.958		-9.701	3.427	...		...	...
05552+1720	0.215	0.039	42.246	3.793	0.240	0.043	40.810	2.650
	0.179		46.004	1.536	0.392		45.123	3.094
05559+3825	...	0.233	...	...	1.754	0.167	-32.476	0.714
	...		...	...	0.864		-31.490	2.095
06011+2829	2.493	0.073	13.038	3.268	0.570	0.068	11.842	3.827
	0.897		17.862	1.183	0.625		14.743	1.882
	1.835		19.804	1.835	0.645		18.300	1.623
	...		...	...	0.263		20.747	1.623
06170+3523	0.200	0.098	22.329	2.223	0.308	0.091	18.124	1.042
	0.105		26.331	2.688	0.365		21.812	1.972
	...		...	...	0.229		27.506	2.553
06193-0349	0.693	0.083	-10.534	1.332	3.826	0.071	-5.505	2.607
	2.836		-5.940	1.960	...		...	...
	1.630		-4.416	1.228	...		...	...
06329-0106	0.492	0.057	98.734	1.242	0.439	0.059	98.531	1.464
	0.338		100.413	1.373	0.378		100.892	1.955
	0.217		103.024	3.418	0.335		104.553	2.283
06346+1444	0.948	0.041	5.076	5.256	0.282	0.055	1.916	1.744
	0.523		6.227	0.856	0.191		6.571	5.027
	0.445		8.361	0.816	...		...	...
06398-0936	0.540	0.044	22.643	1.388	0.786	0.045	25.424	1.189
	1.241		25.352	1.527	0.456		27.174	1.704
	1.336		27.280	1.528	0.159		32.616	5.486
	0.512		29.320	1.007	...		...	...
	0.441		33.444	3.689	...		...	...
06550-1915	0.251	0.054	18.087	4.524	0.481	0.050	20.205	1.161
	0.204		24.604	1.880	0.221		21.233	6.894
06582-1512	0.284	0.039	65.697	1.198	0.210	0.039	65.683	1.604
	0.213		69.030	2.203	0.267		69.501	2.162
07019-1631	0.793	0.070	52.153	1.270	0.458	0.072	52.177	1.730
	0.289		55.034	1.177	0.495		54.995	1.910
07021-0852	0.319	0.041	76.962	1.425	0.302	0.040	76.943	1.619
07153-2411	0.291	0.073	59.996	1.197	0.481	0.074	62.036	1.260
	0.193		62.340	1.212	...		...	...
07197-1451	0.912	0.081	39.021	2.742	0.338	0.079	39.519	0.670
	0.924		41.994	0.959	...		...	...
	0.204		45.642	4.763	...		...	...
07200-1846	0.691	0.074	28.995	1.611	1.313	0.135	28.808	1.362
	0.757		31.512	1.222	0.678		31.402	2.921
07372-1036	0.780	0.118	29.738	1.968	0.621	0.125	32.553	1.095
	0.825		32.650	2.370	0.507		34.352	1.613
08084-1510	0.767	0.075	27.007	2.823	0.450	0.090	27.699	2.756
08100-2334	1.547	0.102	61.427	1.740	0.753	0.110	61.416	1.852
	0.558		68.017	4.081	0.754		67.932	4.769
20479+5336	0.199	0.043	-56.913	0.333	0.177	0.052	-57.674	0.959

TABLE 1.1. (continued)

	SiO v=1 J=1-0				SiO v=2 J=1-0			
IRASNAME	TA1 (K)	rms1 (K)	Vlsr1 (km/s)	FWHM1 (km/s)	TA2 (K)	rms2 (K)	Vlsr2 (km/s)	FWHM2 (km/s)
20523+5302	0.290	0.044	-67.438	1.359	0.102	0.045	-67.500	4.177
	0.299		-65.142	1.549	0.379		-64.974	1.968
21216+5536	0.227	0.044	-10.582	1.437	0.193	0.051	-12.018	0.945
	0.254		-8.408	2.458	0.254		-10.187	1.653
	...		...	...	0.204		-8.011	1.124
21341+5101	0.267	0.078	-4.125	9.139	1.051	0.068	-6.554	1.601
	0.515		1.446	1.299	0.376		1.830	2.754
21453+5959	0.434	0.068	-45.267	1.469	0.586	0.076	-44.802	1.523
	0.379		-43.602	0.682	0.329		-42.506	1.183
	0.432		-42.218	2.358	...		...	...
21509+6234	0.177	0.059	-69.070	2.516	0.393	0.055	-70.577	0.637
	0.136		-62.408	3.912	0.510		-69.647	2.343
21522+6018	0.324	0.074	19.833	1.188	1.322	0.069	20.058	1.490
	0.448		22.397	3.309	0.554		21.890	1.474
22394+5623	0.906	0.062	-26.424	2.253	0.875	0.060	-26.319	2.210
	...		...	...	0.255		-23.636	0.919
22466+6942	0.332	0.062	-48.217	0.909	0.185	0.060	-47.897	0.494

TABLE 1.2. Integrated line parameters of the v=1 and v=2 detections

	SiO v=1 J=1-0			SiO v=2 J=1-0			
IRASNAME	S1 (K*km/s)	Vcen1 (km/s)	FWHM1 (km/s)	S2 (K*km/s)	Vcen2 (km/s)	FWHM2 (km/s)	DATE yymmddhh
00127+5437	...	...	...	0.32	-91.79	1.98	95052806
00336+6744	1.13	-91.64	4.53	0.33	-90.27	2.21	95052608
00459+6749	2.68	-88.92	3.55	1.22	-88.99	3.22	95052207
00534+6031	0.19	-100.60	1.10	0.38	-102.86	3.59	95052608
02433+6345	3.02	-56.90	3.57	3.43	-55.43	5.09	95052108
02469+5646	1.30	-40.96	2.24	...	...	...	95052109
02470+5536	1.95	-37.04	4.05	2.03	-36.94	3.89	95052109
03206+6521	...	...	...	0.63	-37.80	2.08	95052210
03469+5833	0.60	-74.13	1.18	0.49	-74.46	1.35	95052709
03513+4827	5.11	-62.67	9.44	4.99	-62.25	9.54	95052709
03572+5509	0.10	-37.55	0.72	...	...	...	95052614
04085+5347	...	...	...	0.98	-15.34	2.53	95052213
04209+4800	3.64	-15.80	4.45	2.54	-16.75	2.20	95052213
05031+3519	...	...	...	0.62	-36.23	2.02	94051511
05091+4639	0.15	12.68	1.24	...	...	...	95052710
05131+3039	1.30	9.81	3.00	0.82	11.12	5.16	94051511
05146+2521	1.21	-1.29	2.66	1.23	-2.36	2.20	94051515
05284+1945	0.52	13.85	1.83	1.56	14.65	3.89	94051915
05325+2351	1.22	11.04	4.28	0.28	8.52	2.39	94051610
05354+2458	4.53	5.03	4.29	...	...	...	94051516
05367+3736	5.62	-37.26	1.58	8.04	-34.96	3.07	94051510
05368+2841	27.06	-13.93	6.72	27.43	-13.93	6.68	94051811
05384+3854	8.51	8.48	3.85	3.49	8.49	3.36	94051810
05423+2905	6.76	27.14	4.95	7.65	27.20	5.49	94051616
05443+2707	5.26	-11.68	4.62	4.73	-9.69	5.40	94051812
05552+1720	1.17	44.12	4.54	1.98	42.97	5.03	95052711
05559+3825	...	...	...	3.28	-31.98	1.90	94051512
06011+2829	13.46	16.42	5.93	5.17	16.29	7.18	94051811
06170+3523	0.78	24.33	4.46	1.74	22.82	6.49	94051612
06193-0349	9.08	-7.48	4.34	10.67	-5.51	2.61	95052813
06329-0106	1.94	100.88	4.47	2.30	101.54	4.88	95052813
06346+1444	6.20	6.72	4.68	1.55	4.24	5.71	95052713
06398-0936	7.31	28.04	7.94	2.76	29.02	6.93	95052814
06550-1915	1.63	21.35	6.46	2.23	20.72	4.54	95052814
06582-1512	0.87	67.36	3.37	0.98	67.59	3.79	95052815
07019-1631	1.44	53.59	2.66	1.86	53.59	3.23	95052815
07021-0852	0.49	76.96	1.43	0.52	76.94	1.62	95052815
07153-2411	0.62	61.17	2.38	0.65	62.04	1.26	95052913
07197-1451	4.66	42.33	7.06	0.24	39.52	0.67	95052911
07200-1846	2.18	30.25	2.67	4.03	30.10	3.44	95052913
07372-1036	3.73	31.19	3.62	1.60	33.45	2.25	95052915
08084-1510	2.32	27.01	2.82	1.33	27.70	2.76	95052915
08100-2334	5.32	64.72	6.21	5.34	64.67	6.57	95052916
20479+5336	0.07	-56.91	0.33	0.18	-57.67	0.96	95052604
20523+5302	0.92	-66.29	2.60	1.25	-66.24	4.34	95052103
21216+5536	1.02	-9.49	3.03	0.89	-10.01	3.04	95052104
21341+5101	3.33	-1.34	8.00	2.91	-2.36	6.37	95052204
21453+5959	2.05	-43.74	3.44	1.37	-43.65	2.50	95052205
21509+6234	1.05	-65.74	6.54	1.55	-70.11	1.96	95052205
21522+6018	2.00	21.11	3.53	2.98	20.97	2.40	95052207
22394+5623	2.18	-26.42	2.25	2.32	-24.98	2.91	95052105
22466+6942	0.32	-48.22	0.91	0.10	-47.90	0.49	95052106

TABLE 1.3. Infrared properties of the v=1 and v=2 detections

IRASNAME	l(o)	b(o)	F12(Jy)	C_{12}	C_{23}	Var	LRS	Id	Molecules(reference)
00127+5437	117.7	-7.6	55.970	-0.15	-0.86	3	29	0	OH-(9,10)
00336+6744	121.5	5.2	6.373	-0.20	-0.77	65		1	
00459+6749	122.7	5.2	8.069	-0.28	-0.77	80		1	
00534+6031	123.5	-2.1	4.691	-0.20	-0.46	98		1	
02433+6345	135.2	3.9	20.080	-0.08	-0.85	99	29	1	OH-(10)
02469+5646	138.7	-2.2	90.580	-0.06	-0.72	69	28	1	OH-(2)
02470+5536	139.2	-3.2	29.280	-0.20	-0.92	76		1	
03206+6521	138.0	7.3	95.760	0.14	-0.55	98	34	0	OH+(1),CO+(7)
03469+5833	144.5	3.6	7.343	-0.26	-0.72	99		1	
03513+4827	151.3	-3.9	18.650	-0.26	-0.74	65	15	1	
03572+5509	147.7	1.8	45.330	-0.12	-0.81	96	29	1	
04085+5347	149.9	1.9	29.530	-0.26	-0.78	99	27	1	OH-(9),CO+(7,13)
04209+4800	155.3	-0.9	24.870	-0.11	-0.77	99	27	1	OH-(9,10)
05031+3519	170.0	-3.2	11.510	-0.34	-0.77	98	14	1	OH-(12)
05091+4639	161.6	4.4	17.210	-0.17	-0.77	99	27	1	OH-(10)
05131+3039	175.0	-4.3	11.860	-0.39	-0.80	38	15	1	OH-(6)
05146+2521	179.6	-7.1	19.960	-0.22	-0.87	99	29	1	OH-(4,10)
05284+1945	186.1	-7.6	4.174	0.33	-0.43	99			OH+(1,5)
05325+2351	183.1	-4.6	25.510	-0.34	-0.72	3		1	
05354+2458	182.5	-3.4	104.200	-0.25	-0.70	0	22	1	
05367+3736	172.0	3.6	154.000	-0.28	-0.84	99	25	1	OH+(12)
05368+2841	179.5	-1.2	31.350	-0.32	-0.65	98	15	1	OH-(12),H2O-(12)
05384+3854	171.1	4.6	61.430	-0.40	-0.69	38	15	1	OH-(12)
05423+2905	179.8	0.1	49.810	-0.10	-0.57	99	29	1	OH+(5)
05443+2707	181.8	-0.6	19.680	-0.33	-0.83	69		1	
05552+1720	191.4	-3.4	8.673	-0.10	-0.72	99		1	OH+(4)
05559+3825	173.2	7.3	117.800	-0.23	-0.87	99	27	1	OH-(12),H2O-(12),CO-(11)
06011+2829	182.5	3.3	67.900	-0.29	-0.75	93	28	1	OH-(4),H20-(12)
06170+3523	177.9	9.5	22.840	-0.20	-0.91	99	28	1	OH-(4,10)
06193-0349	213.0	-8.3	86.070	-0.15	-0.64	99	27	1	OH-(12),H2O-(12),CO+(11)
06329-0106	212.1	-4.1	32.430	-0.09	-0.88	99	29		OH-(1)
06346+1444	198.3	3.6	16.100	-0.19	-0.68	98	28	1	OH-(5)
06398-0936	220.5	-6.4	31.520	-0.17	-0.89	99	29		OH-(1)
06550-1915	230.9	-7.5	8.005	-0.30	-0.75	93	29		
06582-1512	227.6	-4.9	21.020	-0.25	-0.84	99	29		
07019-1631	229.2	-4.7	20.670	-0.27	-0.69	99	28	1	
07021-0852	222.4	-1.2	122.100	-0.24	-0.85	99	29	1	H2O-(12)
07153-2411	237.5	-5.5	35.290	-0.13	-0.82	99	27		
07197-1451	229.7	-0.2	19.460	-0.28	-0.74	83	27	1	OH-(1),H2O-(12)
07200-1846	233.2	-2.0	21.580	-0.15	-0.88	95	29		OH+(1),CO+(7)
07372-1036	228.0	5.6	10.790	-0.25	-0.72	99	29	1	
08084-1510	235.9	9.8	36.720	-0.22	-0.78	99	29	1	OH-(1,12),H2O-(12)
08100-2334	243.2	5.6	10.840	-0.12	-0.77	99	28	1	
20479+5336	91.8	6.3	5.085	-0.02	-0.81	99		0	OH-(1)
20523+5302	91.8	5.4	11.070	-0.09	-0.70	97		1	OH-(1)
21216+5536	96.6	4.0	11.410	-0.19	-0.69	51	29	1	OH-(1.10)
21341+5101	94.8	-0.6	24.830	-0.27	-0.77	98	26	1	OH-(10)
21453+5959	101.9	5.1	24.380	-0.11	-0.69	98	23	1	
21509+6234	104.0	6.7	23.990	-0.22	-0.72	96	27	1	
21522+6018	102.7	4.8	13.290	-0.28	-0.78	94	14	1	
22394+5623	105.7	-1.8	6.833	-0.26	-0.67	63		1	
22466+6942	112.7	9.6	16.180	-0.19	-0.79	91	29	1	OH+(1)

References for Table 1.3.

1. te Lintel et al., 1990; 2. Le Sequeren et al., 1992; 3. Eder et al., 1988; 4. Lewis et al., 1990; 5. Chengalur et al., 1993; 6. Lewis, 1994; 7. Loup et al., 1993; 8. Wouterlout et al., 1989; 9. Sivagnanam et al., 1990; 10. Galt et al., 1989; 11. Nyman et al., 1993; 12. Benson et al., 1990; 13. Kastner et al., 1993

TABLE 2.1. Line parameters of Gaussian components of the v=1 and v=2 detections

	SiO v=1 J=1-0				SiO v=2 J=1-0			
IRASNAME	TA1 (K)	rms1 (K)	Vlsr1 (km/s)	FWHM1 (km/s)	TA2 (K)	rms2 (K)	Vlsr2 (km/s)	FWHM2 (km/s)
01217+6049	4.563	0.066	-12.411	2.223	3.808	0.075	-12.669	1.578
	1.598		-8.221	2.663	0.610		-10.062	1.650
	...		...	...	0.881		-7.200	2.101
	...		...	...	0.558		-4.982	1.105
05388+3200	4.599	0.083	2.075	2.397	6.289	0.093	4.220	0.325
	49.254		4.689	1.456	28.448		4.639	1.412
	9.029		6.766	1.469	6.690		6.795	1.955
	1.672		10.613	5.050	3.125		11.622	1.949
06241+1025	0.276	0.031	-15.563	1.313	0.539	0.027	-13.679	1.159
	0.717		-13.655	1.313	0.249		-12.975	3.787
	0.354		-11.440	1.768	0.104		-8.555	2.050
	0.261		-9.642	3.915	...		...	...
06500+0829	6.272	0.043	-11.157	0.620	0.690	0.046	-15.081	2.617
	5.769		-10.258	0.820	13.871		-10.796	2.644
	13.630		-10.554	3.489	6.623		-7.498	1.310
	2.850		-6.115	2.776	1.448		-5.722	1.115
21086+5238	2.193	0.059	-17.529	1.895	1.007	0.064	-18.119	1.751
	4.880		-13.283	1.534	6.639		-13.045	1.430
	6.212		-11.868	1.176	6.344		-11.585	0.957
	6.831		-10.217	2.114	7.303		-9.678	1.872
	2.177		-10.650	7.141	2.248		-9.307	8.387
21456+6422	0.476	0.074	-49.238	0.113	0.445	0.081	-50.406	1.150
	4.855		-45.755	3.563	9.825		-46.791	0.955
	2.268		-41.206	1.735	6.199		-45.349	1.311
	1.904		-39.896	0.674	1.715		-45.609	7.301
	1.082		-38.591	3.108	0.787		-37.515	2.405
21563+5630	3.439	0.065	-12.794	1.754	1.291	0.079	-13.572	1.523
	6.611		-11.285	1.407	4.152		-11.376	1.411
	0.381		-8.713	0.724	1.076		-9.390	1.066
	4.168		-5.939	2.124	7.717		-5.519	2.570
	3.405		-4.733	3.318	2.071		-2.917	2.905
22103+5120	0.482	0.060	-57.003	1.025	0.680	0.048	-54.416	3.506
	1.545		-54.166	2.776	1.732		-50.289	2.162
	2.155		-50.370	1.937	0.926		-46.392	3.813
	0.950		-45.447	4.055	0.462		-40.363	3.251
	0.554		-40.620	2.465	...		...	...
NVAur	9.604	0.108	1.041	1.896	4.938	0.124	-0.583	1.629
	0.648		5.594	1.522	12.634		1.320	1.371
IRC+60092	4.459	0.115	10.887	0.902	3.606	0.122	10.758	1.407
	7.899		12.282	1.028	2.808		12.449	0.570
	8.006		12.628	3.367	14.001		12.967	2.587
RCas	9.253	0.120	23.296	1.179	53.670	0.136	23.373	0.979
	34.340		25.311	1.330	38.517		24.986	1.084
	30.782		26.356	0.793	16.852		26.272	0.715
	27.797		27.919	2.940	55.177		27.844	3.333
	6.254		31.378	1.329	9.693		31.808	1.369

TABLE 2.2. Integrated line parameters of the ^{29}SiO detections

	^{28}SiO v=1 J=1-0			^{28}SiO v=2 J=1-0			^{29}SiO v=0 J=1-0					
IRASNAME	S1 K*km/s	Vcen1 km/s	FW1 km/s	S2 K*km/s	Vcen2 km/s	FW2 km/s	S3 K*km/s	Ta3 K	rms3 K	V3 km/s	FW3 km/s	DATE yymmd
01217+6049	15.41	-10.32	4.54	10.15	-8.83	5.18	0.35	0.51	0.065	-12.34	0.64	950521
05388+3200	111.76	6.34	7.99	65.68	7.92	4.84	2.51	1.98	0.090	4.22	1.18	940518
06241+1025	3.16	-12.60	5.57	1.91	-11.12	4.17	0.37	0.25	0.031	-14.36	1.39	950527
06500+0829	68.57	-8.64	4.22	52.19	-10.40	6.55	2.12	1.23	0.042	-10.96	1.61	950522
21086+5238	52.36	-14.09	7.96	53.34	-13.71	9.47	0.56	0.46	0.060	-12.28	1.14	950521
21456+6422	27.75	-43.91	6.93	34.71	-43.96	8.22	0.44	0.69	0.076	-45.28	0.60	950522
21563+5630	38.26	-8.76	6.57	37.26	-8.24	7.54	1.02	0.56	0.069	-12.11	1.70	950526
22103+5120	15.17	-48.81	9.94	11.94	-47.39	10.41	0.28	0.34	0.052	-51.15	0.75	950526
NVAur	20.54	3.32	3.99	27.14	0.37	2.45	1.68	0.97	0.115	0.73	1.63	950526
IRC+60092	41.84	11.76	3.01	45.90	11.86	3.10	1.57	0.64	0.109	11.03	2.31	950522
RCas	183.00	27.34	5.30	324.77	27.59	5.39	2.44	1.89	0.117	24.71	1.21	950521

TABLE 2.3. Infrared properties of the v=1 and v=2 detections

IRASNAME	l(o)	b(o)	F12(Jy)	C_{12}	C_{23}	Var	LRS	Id	Molecules(reference)
01217+6049	127.0	-1.5	52.310	-0.22	-0.62	58	23	1	
05388+3200	177.0	1.0	115.500	-0.32	-0.69	99	23	1	OH-(6)
06241+1025	200.9	-0.6	37.120	-0.26	-0.84	99	29	1	
06500+0829	205.6	4.1	601.300	-0.22	-0.53	99	28	1	OH+(4),H2O+(12),CO+(7)
21086+5238	93.1	3.3	54.320	-0.28	-0.69	94	14	1	OH-(12),H2O(-)
21456+6422	104.7	8.5	175.300	-0.21	-0.82	91	28	1	CO-(11)
21563+5630	100.8	1.5	84.300	-0.21	-0.66	99	26	1	OH-(12),H2O-(12)
22103+5120	99.4	-3.9	15.780	-0.20	-0.73	92	29	1	OH+(9)
NV Aur	156.4	7.8	226.90	0.08	-0.58	99	24	1	OH+(1,10),CO+(7)
IRC+60092	133.6	4.5	481.20	-0.19	-0.84	14		1	OH-(12).H2O+(12),CO+(7)
R Cas	114.6	-10.6	1341.00	-0.38	-0.73	12	24	1	OH+(12).H2O+(12),CO+(7),HCN+(7)

TABLE 3. Infrared properties and observation parameters of the non-detections

IRASname	l	b	F_{12}	C_{12}	C_{23}	var	lrs	Id	rms1	rms2	DATE	Molecules(reference)
00070+6503	118.6	2.8	4.203	0.22	1.21	97		0	0.032	0.036	95052806	OH-(10),CO+(8)
00554+6524	123.7	2.8	4.574	0.29	1.11	95		0	0.071	0.079	95052908	CO+(8)
00589+5743	124.3	-4.8	4.284	-0.23	-0.73	59		1	0.060	0.075	95052208	
01036+5924	124.9	-3.1	3.693	0.10	1.32	77		0	0.032	0.038	95052609	CO+(8)
01557+5759	131.8	-3.5	5.236	-0.24	-0.60	71		0	0.027	0.032	95052707	
02117+5559	134.4	-4.8	7.399	-0.04	-0.86	78		1	0.061	0.069	95052107	
02173+6322	132.7	2.5	9.849	-0.07	-0.59	99		0	0.034	0.038	95052611	
02272+6327	133.7	2.9	8.261	-0.29	-0.62	95		1	0.033	0.035	95052610	
02408+5458	138.6	-4.2	11.700	0.25	-0.46	83		0	0.052	0.063	95052108	OH-(1)
02535+5555	139.9	-2.6	11.850	-0.26	-0.59	93	15	0	0.032	0.037	95052611	
02570+6028	138.2	1.7	4.823	0.23	0.98	99		0	0.033	0.039	95052808	
03022+5409	141.8	-3.5	11.160	-0.17	-0.87	72	29	1	0.066	0.076	95052209	
03078+6046	139.2	2.6	13.640	0.05	-0.53	69	13	0	0.033	0.037	95052612	OH-(2)
03093+4313	148.4	-12.4	14.110	-0.15	-0.99	0	29	0	0.029	0.032	95052808	OH-(10)
03096+5936	139.9	1.7	16.330	-0.21	-0.54	99	14	1	0.039	0.053	95052209	CO+(7,13)
03201+5459	143.6	-1.5	13.770	-0.43	0.19	29	32	0	0.032	0.038	95052809	OH-(10),H2O-(12)
03313+6058	141.5	4.3	30.870	0.15	-0.46	50	22	0	0.038	0.040	95052211	OH-(2,10),CO+(7),HCN+(
03353+5550	144.9	0.5	3.721	0.22	1.26	53		0	0.032	0.040	95052810	CO+(8)
03371+4932	148.8	-4.5	5.420	-0.27	-0.62	92		0	0.038	0.052	95052210	
03434+5818	144.3	3.1	4.199	-0.11	-0.61	82		0	0.032	0.040	95052708	
03478+6349	141.3	7.7	14.350	-0.29	-0.65	73	16	1	0.029	0.034	95052613	
03525+5711	145.9	3.0	7.132	-0.21	-0.70	99		1	0.036	0.039	95052212	
04254+5255	152.3	3.1	3.124	-0.15	-0.44	97		0	0.030	0.040	95052709	
04256+4435	158.3	-2.7	14.260	-0.24	-0.59	99		0	0.031	0.035	95052615	
04264+3853	162.6	-6.5	11.530	-0.09	-0.72	97	29	1	0.035	0.037	95052614	
04344+3231	168.4	-9.6	18.120	-0.37	-0.75	14	15		0.446	0.467	94051914	OH-(6),H2O-(12)
04402+3426	167.7	-7.5	3.394	-0.23	-0.65	75		1	0.032	0.032	95052213	OH-(4)
04469+3020	171.8	-9.0	5.192	-0.34	-0.65	99			0.076	0.134	94051514	
04470+3002	172.1	-9.2	5.950	-0.12	-0.73	99		1	0.032	0.036	95052214	
04486+3042	171.8	-8.5	3.769	0.24	0.04	51		1	0.117	0.141	95052910	OH+(12),H2O-(12)
04491+3825	165.8	-3.5	16.600	-0.33	-0.50	15	16		0.066	0.056	94051910	
04525+3028	172.5	-8.0	27.160	0.25	0.34	79	69	1	0.088	0.097	95052911	OH-(12),H2O-(12)
04555+2946	173.5	-7.9	10.250	0.00	0.03	3		1	0.101	0.109	94051510	OH-(12)
05159+2442	180.3	-7.2	13.080	-0.32	-0.50	9	16		0.054	0.053	94051615	
05176+3502	172.0	-1.0	21.000	-0.26	-0.34	3	15	1	0.052	0.064	94051810	OH-(6),H2O-(12)
05184+4208	166.3	3.2	17.020	-0.15	-0.92	37	29		0.062	0.058	94051909	
05192+3849	169.1	1.4	12.130	-0.39	-0.67	0	14	1	0.059	0.055	94051910	H2O-(12)
05204+3227	174.4	-2.0	23.010	-0.17	-0.89	99			0.056	0.056	94051515	OH-(5)
05235+3651	171.2	1.0	17.590	-0.35	-0.80	5		1	0.076	0.084	94051612	OH-(12)
05236+3200	175.2	-1.7	17.380	-0.31	-0.74	25	16	1	0.088	0.099	94051611	H2O-(12)
05242+2303	182.7	-6.6	20.950	-0.32	-0.74	59	24		0.166	0.176	94051515	
05255+3222	175.1	-1.2	10.130	-0.29	-0.64	0			0.071	0.071	94051816	
05273+2019	185.4	-7.5	5.242	-0.17	-0.60	99			0.031	0.031	94051914	OH-(4)
05290+4126	168.0	4.4	10.760	-0.40	-0.87	22			0.060	0.065	94051910	
05345+3157	176.5	0.2	12.260	0.19	1.25	0	31		0.067	0.062	94051610	CO+(8)
05346+2106	185.7	-5.6	8.299	-0.33	-0.51	39	16		0.054	0.069	94051813	
05374+3153	176.9	0.7	43.490	-0.28	-0.65	6	43	1	0.068	0.073	94051516	OH-(12),H2O-(12)
05378+2804	180.2	-1.3	63.490	-0.28	-0.79	0	15		0.066	0.058	94051615	
05382+3547	173.7	2.9	8.121	0.24	1.15	10			0.100	0.106	94051611	CO+(8)
05390+1448	191.6	-8.1	34.810	-0.26	-1.01	6	25		0.056	0.057	94051912	
05405+3240	176.6	1.6	196.000	-0.19	-0.57	99	42	1	0.054	0.050	94051616	OH-(5,12)
05408+4249	168.0	7.0	16.170	-0.39	-0.69	92	18		0.056	0.060	94051911	
05424+4414	166.9	8.0	19.510	-0.31	-0.67	99	15		0.060	0.057	94051911	
05438+2337	184.7	-2.5	16.470	-0.32	-0.67	99			0.065	0.059	94051813	
05440+4311	167.9	7.7	47.220	-0.25	-0.80	99	44	1	0.072	0.078	94051911	OH-(12),H2O-(12)
05447+1321	193.6	-7.6	21.100	-0.27	-0.60	98	43		0.056	0.059	94051912	OH-(4)

TABLE 3. (continued)

IRASname	l	b	F_{12}	C_{12}	C_{23}	var	lrs	Id	rms1	rms2	DATE	Molecules(reference)
05452+2001	187.9	-4.1	15.740	-0.21	-0.69	99	15	1	0.034	0.040	95052715	OH-(5)
05461+1903	188.9	-4.4	9.481	-0.36	-0.43	51			0.064	0.058	94051814	
05484+3521	175.1	4.4	8.001	-0.29	-0.55	99		1	0.032	0.040	95052715	OH-(4)
05495+2520	183.9	-0.5	14.030	-0.35	-0.65	94	15		0.071	0.032	94051616	
05508+3930	171.8	6.9	33.340	-0.36	-0.83	9	16		0.099	0.073	94051810	
05510+2747	182.0	1.0	4.519	-0.22	-0.72	5			0.059	0.058	94051814	OH-(4)
05533+3022	180.0	2.8	16.090	-0.12	-0.42	2	22		0.058	0.060	94051811	OH-(6,10)
05551+2305	186.5	-0.5	7.209	-0.12	-0.88	18			0.035	0.032	94051914	OH-(5)
05580+2224	187.4	-0.3	15.960	-0.21	-0.53	25	15		0.044	0.045	94051615	
05582+3450	176.6	5.9	14.760	-0.16	-0.81	24			0.060	0.063	94051816	OH-(4)
06034+1354	195.4	-3.4	12.430	0.08	-0.55	93		1	0.032	0.038	95052712	OH-(5)
06062+2632	184.7	3.3	6.729	-0.33	-0.57	15			0.068	0.070	94051812	
06069+2142	189.0	1.1	7.740	0.25	0.16	79			0.060	0.056	94051916	
06088+1909	191.5	0.3	60.200	-0.37	-0.56	99	43		0.060	0.058	94051912	
06088+2152	189.1	1.6	96.080	-0.37	-0.83	3	28		0.065	0.060	94051814	OH+(12)
06092+2255	188.2	2.2	78.200	-0.22	-0.66	5	23	1	0.070	0.035	94051816	OH-(4),H2O-(12)
06101+2039	190.3	1.3	14.510	-0.26	-0.76	14	14		0.060	0.058	94051912	OH-(5)
06104+1833	192.2	0.3	26.010	-0.36	-0.70	41		1	0.055	0.050	94051912	H2O-(12)
06139+3313	179.6	8.0	106.500	-0.30	-0.78	2	22		0.083	0.064	94051811	
06156+2321	188.5	3.7	4.534	0.16	-0.08	-1			0.058	0.061	94051916	
06157+3120	181.5	7.5	27.710	-0.39	-0.73	72	15		0.076	0.073	94051612	
06158+2333	188.4	3.8	11.960	-0.35	-0.53	70			0.060	0.060	94051813	
06181+0406	205.8	-4.9	35.280	-0.04	-0.63	99	23	0	0.027	0.031	95052215	OH-(2,4)
06242+2830	184.9	7.8	17.770	-0.20	-0.66	99	14		0.077	0.063	94051812	OH-(4)
06278+2729	186.1	8.0	161.000	-0.33	-0.88	5	27		0.067	0.058	94051815	
06278+2329	189.7	6.2	6.759	-0.25	-0.50	26			0.064	0.062	94051816	OH-(4)
06283+1028	201.3	0.3	35.000	0.29	0.22	85	50	1	0.047	0.044	95052812	OH-(12),H2O-(12)
06308+2819	185.7	9.0	13.250	-0.38	-0.80	0	16		0.148	0.160	94051513	
06319-0501	215.5	-6.1	51.210	0.10	-0.38	95	32		0.054	0.061	95052912	OH+(1),H2O+(12),CO-(11
06341+2109	192.5	6.5	23.090	-0.37	-0.74	0			0.055	0.058	94051913	
06345+2739	186.7	9.4	7.595	-0.40	-0.86	12			0.070	0.062	94051813	
06364+0450	207.3	-0.5	6.633	-0.27	-0.57	95		1	0.041	0.046	95052216	OH-(4)
06447+0817	205.1	2.9	21.250	-0.28	-0.65	88		1	0.029	0.032	95052713	OH-(5)
06448+1639	197.7	6.7	5.756	-0.30	-0.58	97		1	0.031	0.037	95052714	
06582+1507	200.5	8.9	38.670	0.16	-0.51	96	22	0	0.032	0.040	95052813	OH-(1,2,4),CO+(7),HCN+(
07085-0018	215.5	4.2	36.530	-0.29	-0.59	99	22		0.060	0.062	95052912	
07300-2140	236.8	-1.3	16.200	-0.17	-0.76	51	29		0.098	0.101	95052914	OH-(1)
07376-2827	243.6	-3.1	17.690	0.02	-0.88	99	29		0.162	0.166	95052914	OH-(1)
21046+5110	91.6	2.7	7.183	0.21	1.12	99		0	0.031	0.035	95052703	CO+(8)
21122+4900	90.9	0.4	14.430	0.06	-0.53	93	13	0	0.045	0.059	95052203	
21269+5030	93.6	-0.2	4.459	-0.07	-0.39	96		0	0.035	0.044	95052104	
21290+4919	93.0	-1.3	5.375	-0.20	-0.63	93		0	0.032	0.038	95052702	
21297+5251	95.5	1.2	7.985	-0.30	-0.70	91		0	0.055	0.056	95052604	
21377+5042	95.0	-1.2	94.490	-0.20	-0.95	99	15	1	0.043	0.050	95052105	
21381+5000	94.6	-1.8	114.200	0.28	0.23	78	32	0	0.054	0.056	95052204	OH+(12),H2O+(12)
21415+5025	95.3	-1.8	8.293	-0.21	-0.63	93		1	0.086	0.095	95052205	OH-(1)
21533+5844	101.9	3.5	7.298	-0.22	-0.65	93		0	0.038	0.042	95052605	OH-(1)
22045+6306	105.6	6.2	11.690	0.06	-0.63	97		0	0.039	0.046	95052606	OH-(1)
22112+5322	100.7	-2.3	14.500	-0.28	-0.71	62	25	1	0.036	0.041	95052607	
22130+5634	102.7	0.2	10.960	0.08	-0.47	99		0	0.042	0.047	95052607	CO+(7),HCN+(7)
22147+5948	104.7	2.8	3.418	0.22	1.25	99		0	0.031	0.034	95052802	CO+(8)
22224+5736	104.4	0.4	3.215	0.17	1.32	92		0	0.031	0.036	95052803	CO+(8)
22394+6930	112.0	9.7	5.606	-0.26	-0.71	90		1	0.038	0.043	95052106	
22451+6154	109.0	2.7	5.910	0.14	1.21	99		0	0.032	0.037	95052804	CO+(8)
23030+5719	109.1	-2.4	14.430	-0.25	-0.73	93		0	0.032	0.037	95052704	
23183+6151	112.5	1.1	8.106	-0.27	-0.48	97		0	0.032	0.041	95052704	

We divide the objects into three groups: (1) 52 sources which were detected only in the v=1 and/or v=2 lines, (2) 11 sources which were detected in the ^{29}SiO line and (3) 118 sources which were not detected in any SiO maser lines. Table 1, table 2 and table 3 are for the three groups respectively. In table 1.1 are listed the IRAS PSC name and line parameters of each Gaussian component of the v=1 and v=2 lines, antenna temperature, rms of the noise level, velocity in LSR and full width at half maximum (FWHM). In table 1.2 are listed integrated line intensity, central velocity, FWHM and date of observation in the form of YYMMDDHH. If a line is composed of more than one Gaussian component, the central velocity is the midpoint of the reddest and bluest components and the line width is taken as the width between the half maxima of the reddest and the bluest components. We listed in table 1.3 their other related parameters as Galactic longitude, Galactic latitude, F_{12}, color indexes C_{12} and C_{23}, IRAS variability index, IRAS LRS class, status of optical identification (1: identified, 0: unidentified) and observational results in other molecules(+: detection, -: non-detection, reference code in the bracket) which will be discussed in succeeding sections. Table 2.1, 2.2 and 2.3 are organized in the same way as table 1.1. 1.2 and 1.3 while they are for the 11 sources of group 2. Table 3 is for the sources of group 3 where the columns are the same as those in table 1 and 2. The SiO maser spectra of group 1 sources are shown in Fig.II.1. In Fig.II.2 we present the spectra of group 2 sources. Because the ^{29}SiO lines are much weaker than the v=1 and v=2 lines, the scale of ^{29}SiO line is multiplied by ten times of its original value. All the spectra in Fig.II.1 and Fig.II.2 are only informative part of the whole AOS-H spectra, which are centered at the signal and 100 km s^{-1} wide. The distribution of these sources in the Galaxy is shown in Fig.II.3, where a filled circle denotes a group 1 source, a filled square denotes a group 2 source and an open circle denotes a group 3 source.

II.4. Discussion

II.4.1. Features of SiO lines

^{28}SiO lines

The ^{28}SiO lines usually have multiple peaks as can be seen from Fig.II.1. When the line is strong, it is always composed of more than one Gaussian component(see Table 1.1). This phenomena is exhibited clearly in the spectra of sources which were detected in the ^{29}SiO line (Fig.II.2) and are usually stronger than those without ^{29}SiO detection. They show $\geq$

TABLE 3. (continued)

IRASname	l	b	F_{12}	C_{12}	C_{23}	var	lrs	Id	rms1	rms2	DATE	Molecules(reference)
23361+6437	115.3	3.1	4.075	0.03	-0.54	74		0	0.028	0.032	95052804	OH-(1)
23389+6529	115.8	3.9	10.180	-0.22	-0.57	79		0	0.033	0.039	95052705	
23507+6230	116.3	0.7	9.288	0.22	1.05	96	14	0	0.031	0.036	95052805	CO+(8)
23516+6430	116.9	2.6	41.600	-0.12	-0.56	75	14	0	0.031	0.040	95052705	
23592+6228	117.3	0.4	23.180	-0.16	-0.58	79	14	0	0.026	0.029	95052706	

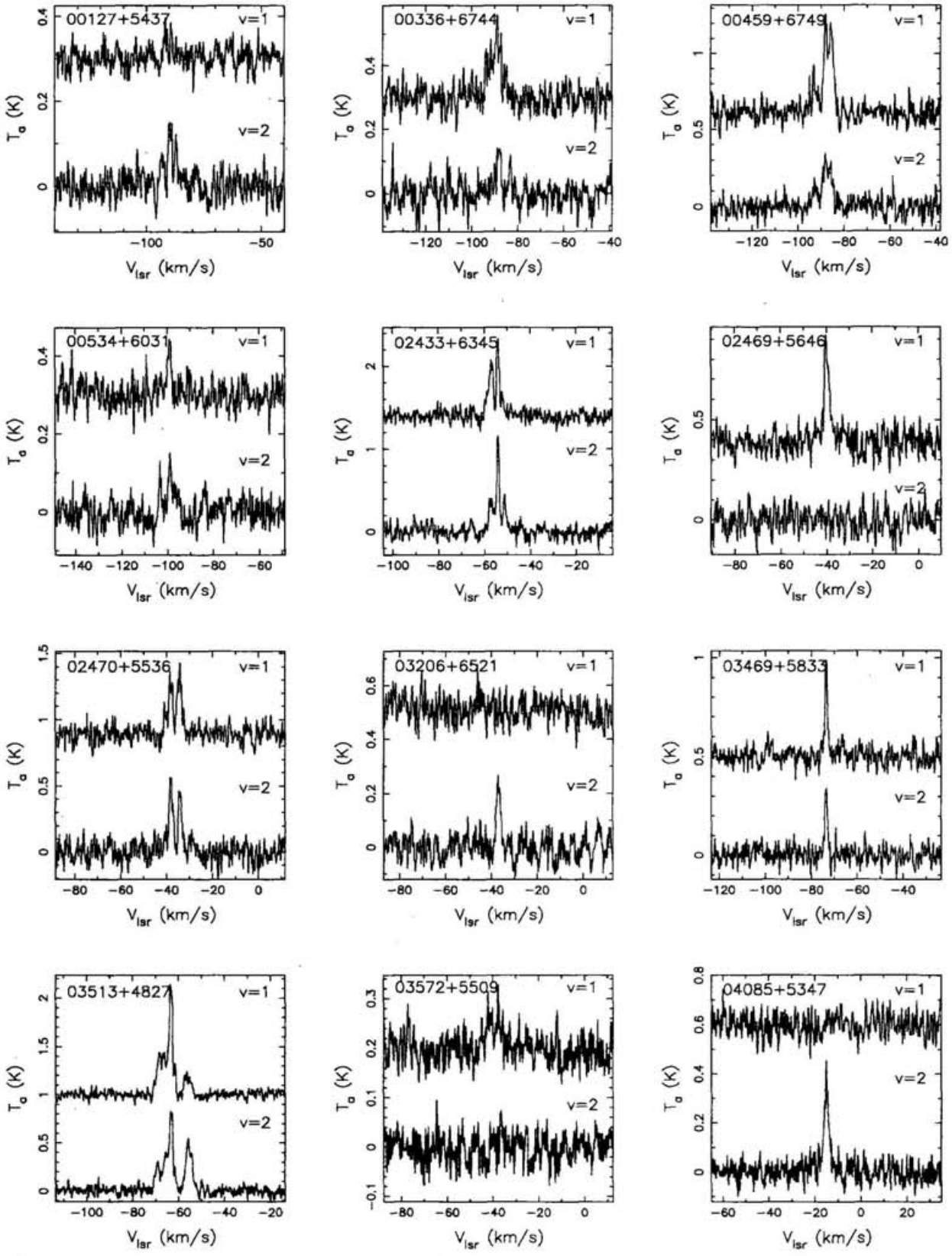

Fig.II.1.(a)

Fig. II.1.— Spectra of 52 ^{28}SiO maser detections.

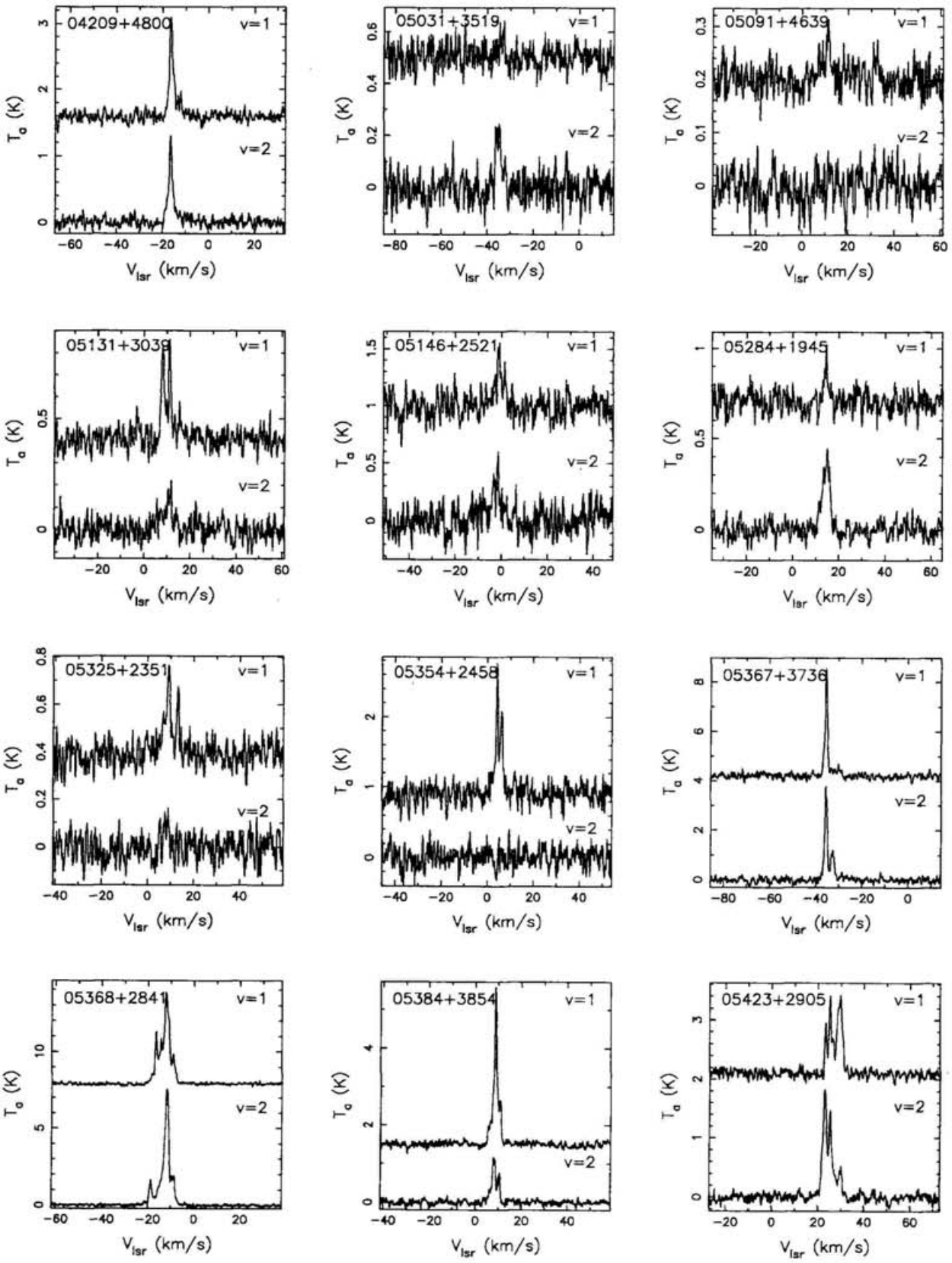
04209+4800
v=1
v=2
05031+3519
05091+4639
05131+3039
05146+2521
05284+1945
05325+2351
05354+2458
05367+3736
05368+2841
05384+3854
05423+2905
T_a (K)
V_lsr (km/s)

Fig.II.1.(b)

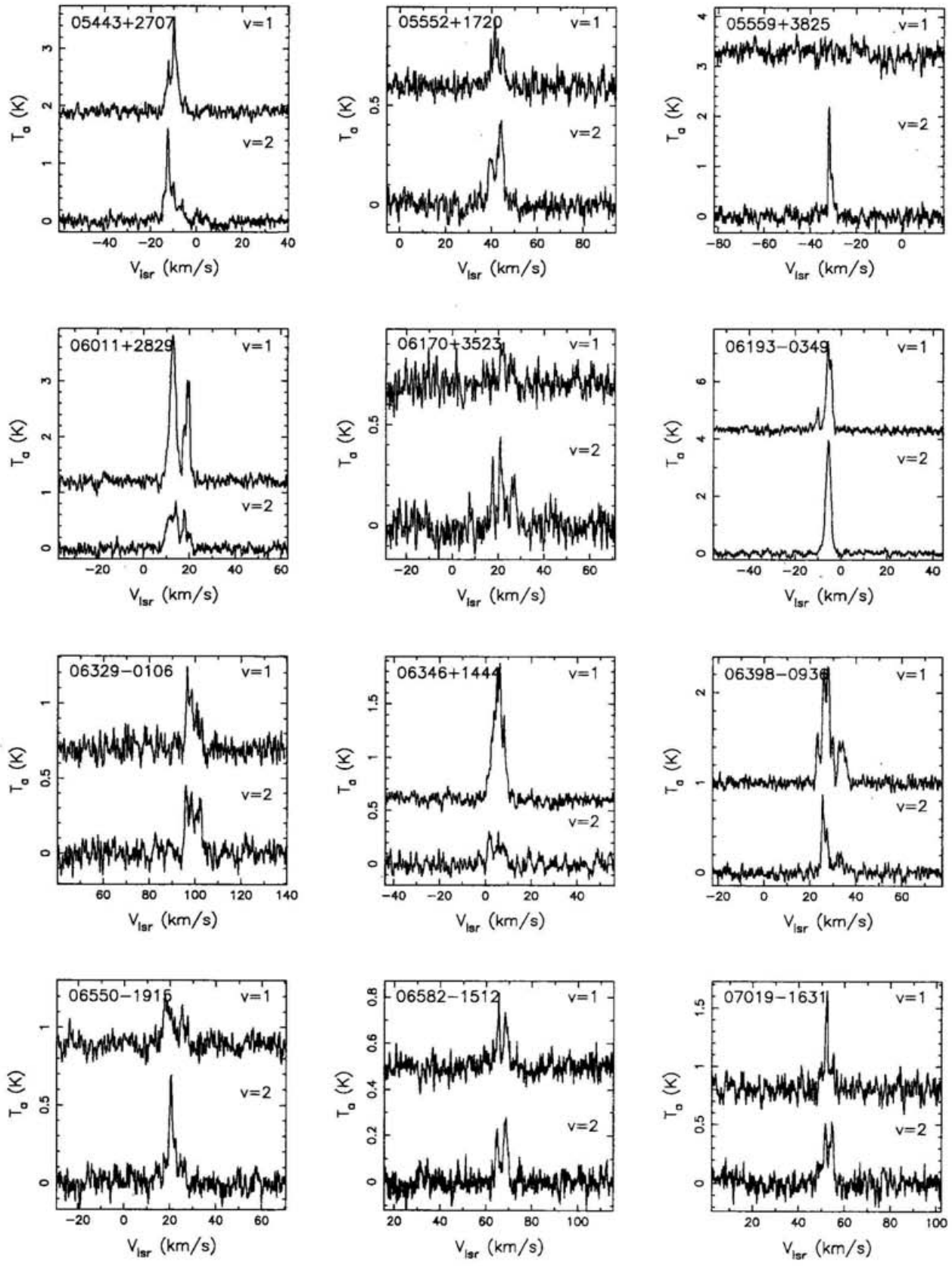
05443+2707
v=1
v=2
05552+1720
v=1
v=2
05559+3825
v=1
v=2
06011+2829
v=1
v=2
06170+3523
v=1
v=2
06193−0349
v=1
v=2
06329−0106
v=1
v=2
06346+1444
v=1
v=2
06398−0936
v=1
v=2
06550−1915
v=1
v=2
06582−1512
v=1
v=2
07019−1631
v=1
v=2
T_a (K)
V_lsr (km/s)

Fig.II.1.(c)

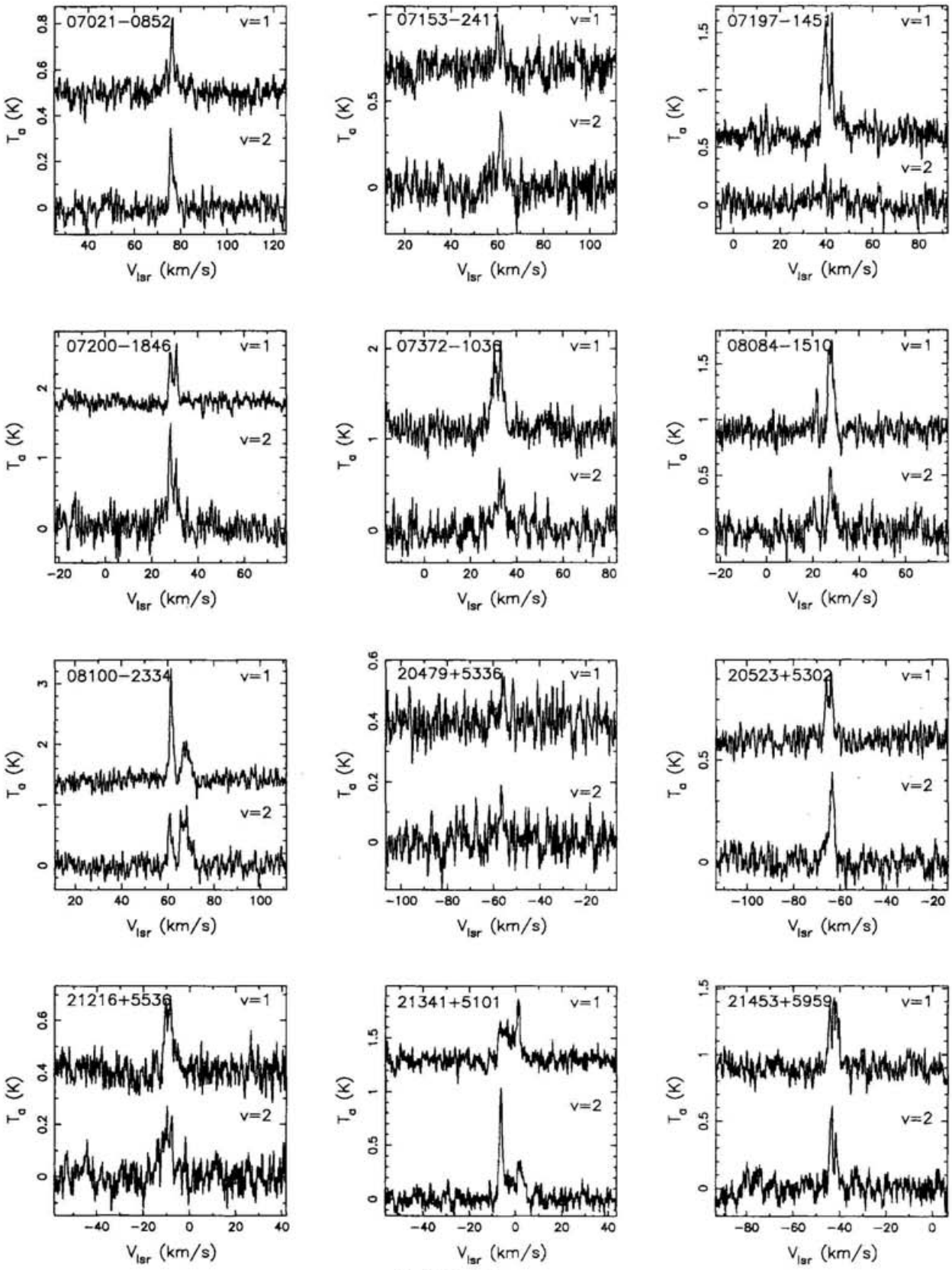
07021−0852
v=1
v=2
07153−241
07197−145
07200−1846
07372−1036
08084−1510
08100−2334
20479+5336
20523+5302
21216+5536
21341+5101
21453+5959
T_a (K)
V_lsr (km/s)

Fig.II.1.(d)

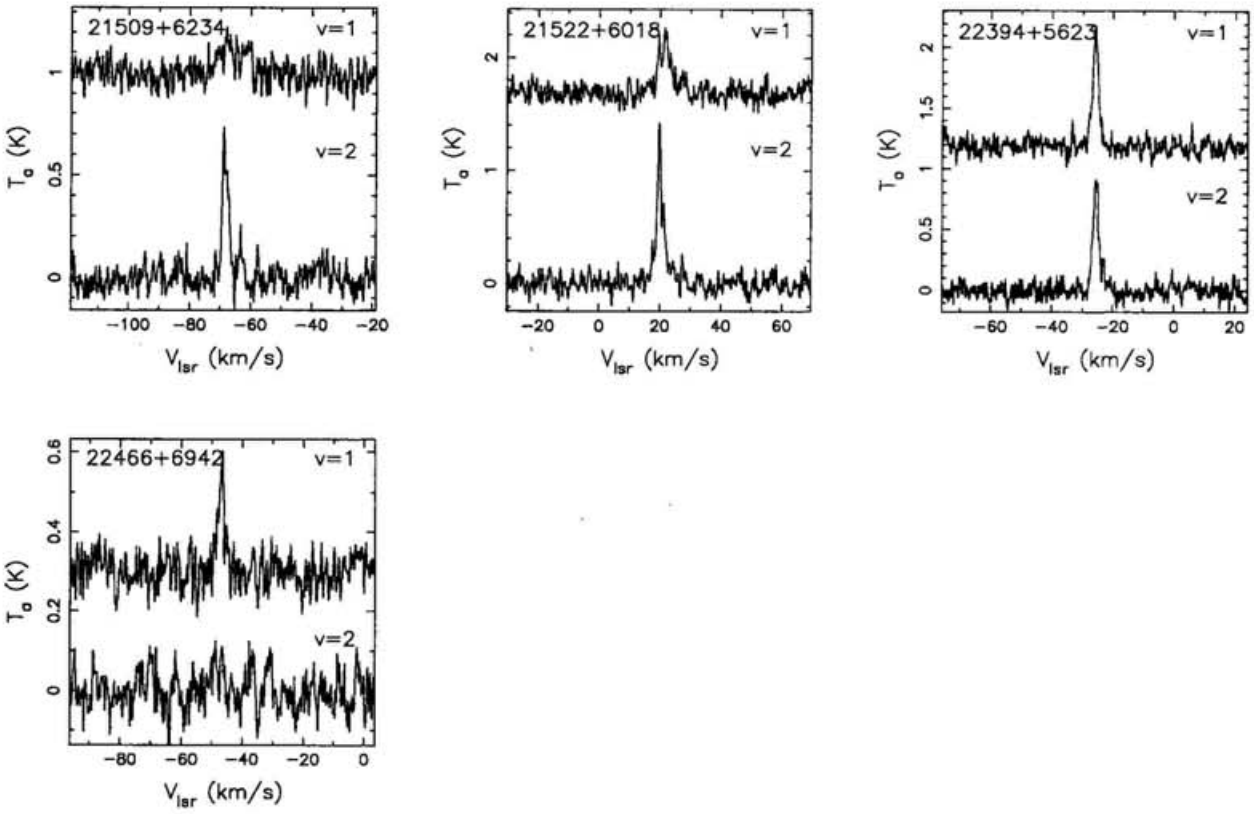

Fig.II.1.(e)

4 Gaussian components. The width of one component is mostly narrower than 3 km s^{-1} though occasionally as wide as 6-7 km s^{-1}, while no component is broader than 10 km s^{-1} (see table 1.1 and 2.1). The line profiles comply with their maser nature.

The profiles of the v=1 and v=2 lines are similar in respect that once one SiO maser component is found in either line, the corresponding component can almost, although not always, also be found in the other line at the same velocity and with similar line width. But the intensities are hardly the same for the components at the same velocity in these two lines, which accounts for the above "not always". It sometimes happens that one component is strong in the v=1 line while another component is strong in the v=2 line like in the spectra of IRAS 21341+5101. But sometimes the SiO maser emission is only detected in one line. There are four sources which were detected only in the v=1 line and five sources which were detected only in the v=2 line. Here are two extreme instances: IRAS 05354+2458 was detected only in the v=1 line, i.e. the v=1 line is at least 6 times as strong as the v=2 line; IRAS 05559+3825 was detected only in the v=2 line, i.e. the v=1 line is at most as one-sixth strong as the v=2 line. Although the non-detection in one of the two lines can be due to either no emission or weakness, we tend to believe it is caused by weakness of the line because these two lines were always both detected in strong SiO sources such as those with the ^{29}SiO detections. The interferometric images of SiO maser sources revealed that the SiO masers come from several discrete clumps(cf. Diamond et al. 1994). The fact that

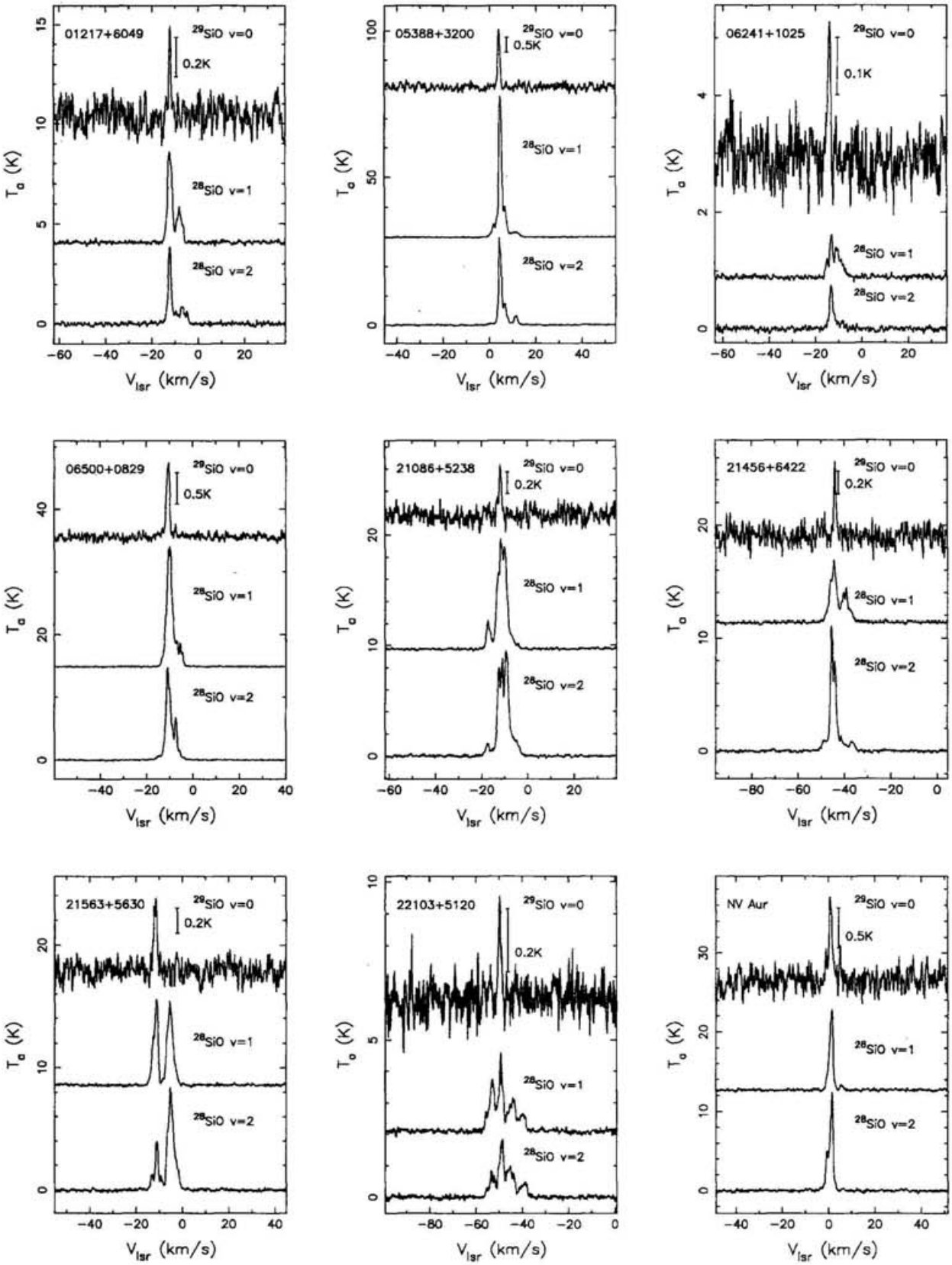

Fig.II.2.(a)

Fig. II.2.— Spectra of 11 ^{29}SiO detections, the amplified scale of the ^{29}SiO line is labelled beside the emission line.

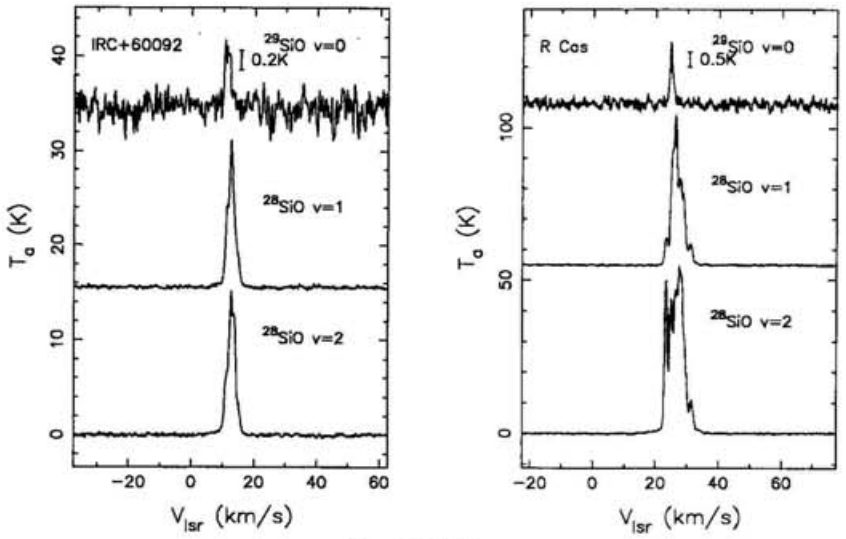

Fig.II.2.(b)

the intensity ratios of the components vary in one source indicates that the SiO line intensity may be much influenced by the local density and temperature besides the global physical conditions of stellar envelope. Of 193 SiO maser sources detected in the survey towards the Galactic bulge, 188 sources were detected SiO maser emission in both lines and 5 sources detected only in the v=2 line (Jiang et al. 1995). According to the observations towards the Galactic bulge and the outer disk, the v=1 and v=2 line emissions occur mostly, if not always, at the same time, i.e. the conditions to excite them, such as density, temperature and velocity gradient (depending on the models), almost overlap.

^{29}*SiO lines*

Because the rare isotopic substitutions, ^{29}SiO and ^{30}SiO, are 20 and 30 times less abundant than ^{28}SiO (Penzias 1981), previous searches for their masers have been made only in strong ^{28}SiO sources. Until now, the ^{29}SiO J=2-1 and J=1-0 transitions in vibrational ground state are successfully observed in some objects (cf. Deguchi et al. 1983; Nguyen-Q-Rieu et al. 1988) and the J=1-0 transition in first excited vibrational state is detected only in TX Cam by Cho & Ukita(1995). The most extensive observations in ^{29}SiO and ^{30}SiO maser lines were made by Alcolea & Bujarrabal(1992) in 38 bright ^{28}SiO sources resulting in 14 detections in Miras, supergiants and semi-regular variables. Taking advantage of the wide band coverage (600MHz) of the receiver attached to the 45m telescope, we searched for the ^{29}SiO v=0 J=1-0 maser emission in all the 181 sources simultaneously with the vibrationally excited ^{28}SiO maser emissions.

Although previous searches for ^{29}SiO line emission were done in strong ^{28}SiO maser sources, most of them failed. We observed the vibrational ground-state ^{29}SiO line in the sources which had hardly been observed in any SiO maser lines before so that the ^{29}SiO maser emission was searched in much fainter sources in terms of ^{28}SiO line intensity. The intrinsically ^{29}SiO

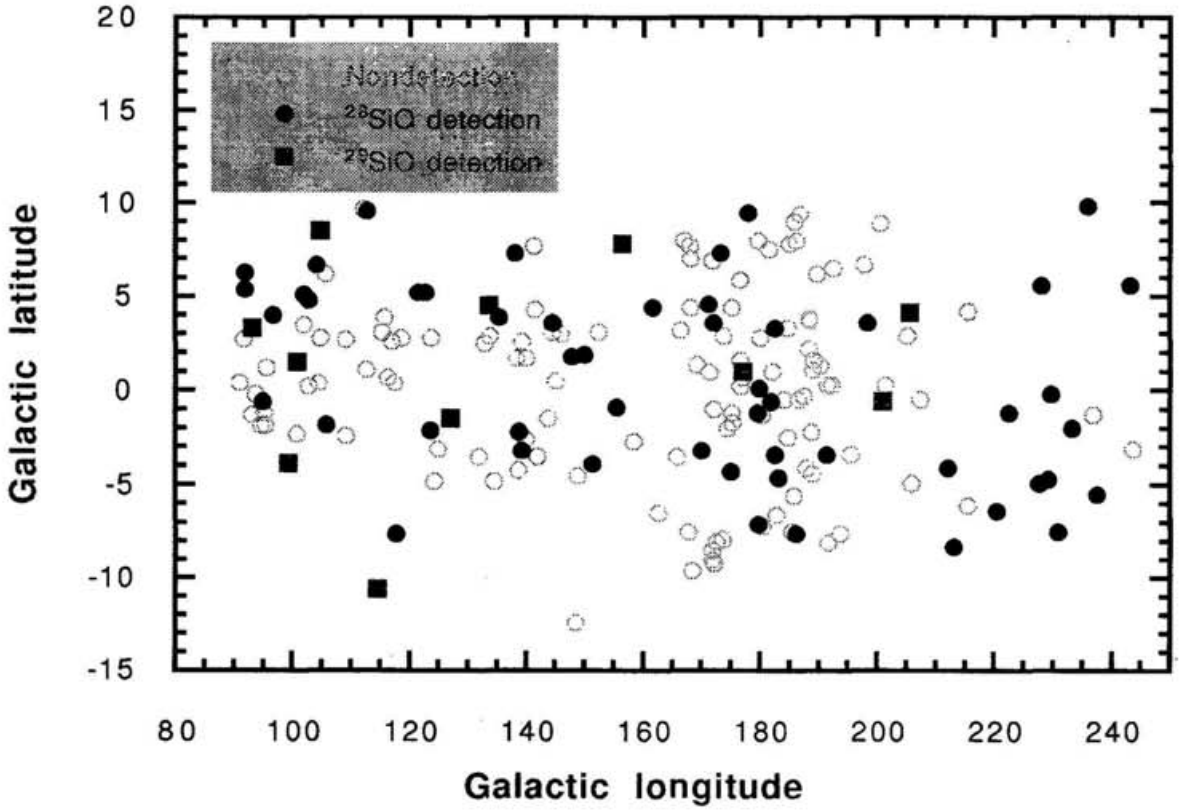

Fig. II.3.— Distribution in the Galactic plane of all the observed sources, non-detections (open circles), ^{28}SiO maser detections (filled circles) and and ^{29}SiO detections (filled boxes).

bright sources should be detected.

Different from the ^{28}SiO lines, the v=0 ^{29}SiO lines have only one component with FWHM narrower than 3 km s^{-1} (see Fig.II.2). The velocity of ^{29}SiO line peak coincides very well within 1km s^{-1} with that of the strongest peak of the v=1 ^{28}SiO line and occasionally shifts a little from that of the strongest peak of the v=2 line. Both radiative and collisional pumping models for the vibrationally excited ^{28}SiO masers (Deguchi & Iguchi 1976; Elitzuer 1980) predict that the excitation of v=2 maser line needs higher density or temperature than the v=1 line does. If the components of ^{28}SiO maser lines originate from different clumps in stellar envelopes, the coincidence of ^{29}SiO line peak with the strongest v=1 ^{28}SiO line peak may indicate that the ^{29}SiO maser may not necessarily be generated in a very dense clump where the v=2 line be stronger than the v=1 line. But the dependence of the ^{29}SiO line intensity on stellar properties is not clear and there has not been any good model for ^{29}SiO maser emission or vibrational ground-state SiO maser emission.

All the ^{29}SiO maser sources are ^{28}SiO maser sources with peak intensities stronger than 0.8K. The intensity ratios of the ^{29}SiO line to the ^{28}SiO v=1 line vary from 1/4 through 1/30 in terms of peak intensity and from 1/10 through 1/100 in terms of integrated intensity. The weakest ^{28}SiO maser source detected in ^{29}SiO line is IRAS 06241+1025 whose peak intensities are 0.8K and 0.2K for the v=1 ^{28}SiO and v=0 ^{29}SiO lines, respectively. Fig.II.4 shows the correlation of the integrated intensity between the v=1 ^{28}SiO and ^{29}SiO lines. The best linear fit is:

$$\log(S3) = 0.58(\pm 0.17) \times \log(S1) - 0.93(\pm 0.27) \qquad \text{(II.1)}$$

where S1 and S3 are the integrated intensities of v=1 ^{28}SiO and ^{29}SiO lines. The correlation of the peak intensities is also shown in Fig.II.4 and the best fit line is at the very similar slope to that of the integrated intensities.

II.4.2. Detections and non-detections

In this survey, 63 sources were detected and 118 sources were not detected in SiO maser lines. This section discusses the optical, infrared properties and observations made in other molecular lines of the SiO detected and un-detected sources.

Optical identification

Although many sources in the observed sample are not associated with optical stars in catalogues, the addition of the identification in V and I bands by CCD images by Jiang et al.(1996) brings about 127 objects with optical counterparts. Fifty-three of the 63 SiO maser sources have optical counterparts. Except two of them have not been checked optical variability, 50 of the other 51 sources are optically variable. The only exception is IRAS 06241+1025 that has not been found optical variation with amplitude bigger than 0.2mag (Jiang et al. 1996) and should be variable in the IRAS mission since the IRAS variability index (Beichman et al. 1985) is 99. On the basis of the SIMBAD database, there are 17 Mira variables, three semi-regular variables IRAS 02469+5646, 03572+5509 and 05354+2458 and one S-type star IRAS 07197-1451. Although at present we do not know the type of the other variable stars identified by Jiang et al.(1996), they are mainly late-type variables such

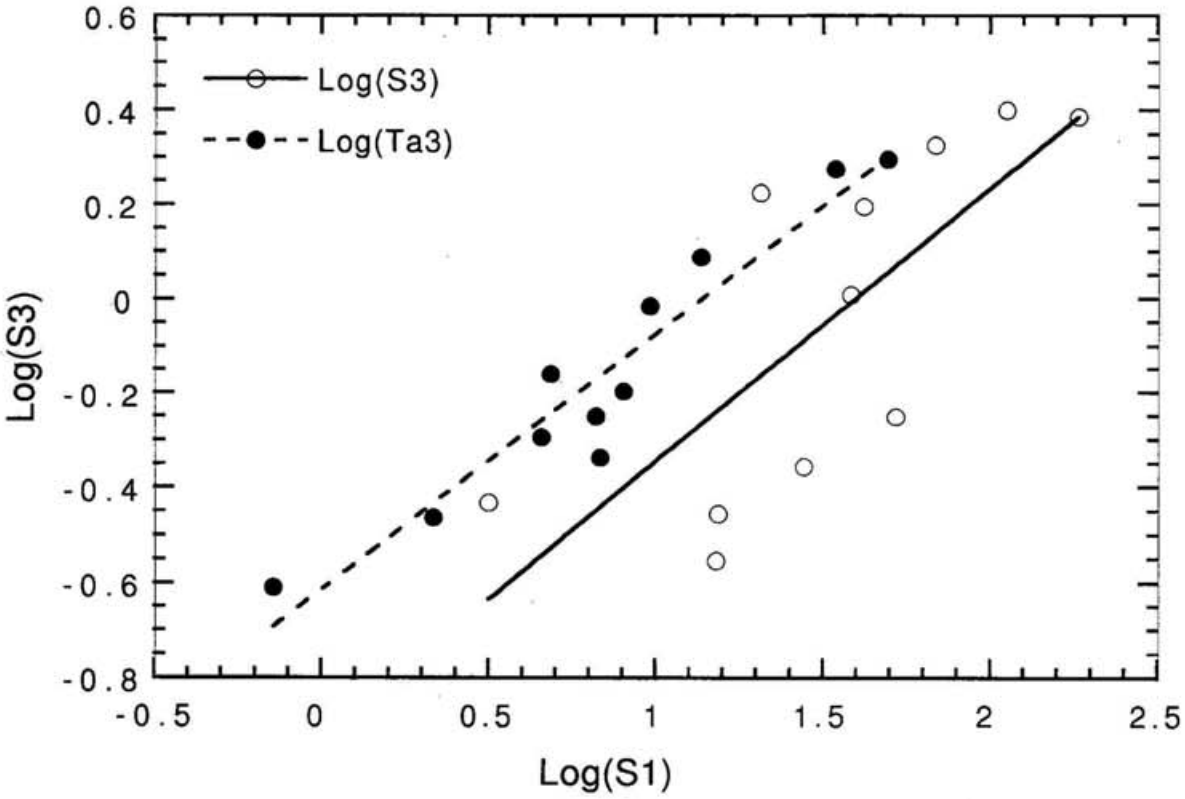

Fig. II.4.— Correlations of intensities between ^{29}SiO and v=1 ^{28}SiO lines, where S3(K km/s) and S1(K km/s) are the integrated intensities of the ^{29}SiO and v=1 ^{28}SiO lines, respectively, and Ta3(K) and Ta1(K) are the peak intensity of ^{29}SiO and the peak intensity of corresponding component of the v=1 ^{28}SiO line, respectively. The best fits are shown as solid and dashed lines.

as Miras and semi-regular variables with amplitude bigger than 0.2mag. Besides 53 sources which are associated with optical stars, there are three SiO maser sources for which we could not find any optical counterparts brighter than 19 mag at I band: IRAS 00127+5437, 03206+6521 and 20479+5336. Even there are 7 more sources which we do not know their optical features, most of the SiO maser sources are optically visible and may be late-type variables.

Among the 118 non-detections, 33 sources have optical counterparts. They seem to be a mixture of various types of objects including early-type stars. M-type and C-type stars. There are 38 sources for which optical counterparts have not yet been found (Jiang et al. 1996). These sources have optically thick shells and might be very evolved stars or young stellar objects in star forming regions. Since we are not sure of the nature of the 39 optically unidentified sources and no optical data are available for the other 47 sources, additional information of these SiO non-detections is necessary to clarify their nature.

IRAS LRS classes

The IRAS LRS spectrum is a good tool to classify the CSEs of the objects because it covers the range from 7μm to 23μm within which the silicate feature at 10μm of O-rich stars and SiC molecular feature at 11μm of C-rich stars can occur(Olnon & Raimond 1986). The histogram of the SiO observational results with IRAS LRS classes is shown in Fig.II.5. Fifty of the 63 SiO detections were taken of IRAS LRS spectrum. They involve seven 1n sources without clear spectral feature, one 3n source with silicate absorption feature and forty-two 2n sources with silicate emission feature. So most of the SiO detections not only have O-rich circumstellar envelope but also are optically thin at 9.7μm. On the other hand, 57 of the 118 SiO non-detections whose IRAS LRS spectra are known span almost all the IRAS LRS classes through 1n, 2n, 3n, 4n, 5n and 6n. In view of the spectra, they consist of various objects such as O-rich, C-rich stars and planetary nebulae. 18 of them are classified as IRAS LRS 2n sources showing weak, moderate or strong silicate emission features. Considering this phenomenon, together with the fact that some of the SiO non-detections are M-type stars, indicates that some of the sources which were not detected with SiO emission have an O-rich envelope. Perhaps some of the non-detections are caused by the time variation of SiO masers (Nyman et al. 1986).

IRAS colors

The locations of sources in the IRAS color-color diagram are shown in Fig.II.6. If we divide the color-color diagram into three regions as in the optical identification (Jiang et al. 1996), the detection rates are 41%(60/147), 21%(3/14) and 0%(0/20) in area I, II and III respectively. None of the objects in area III was detected with SiO maser emission. Because some of these objects appear in optical nebulosity (Jiang et al. 1996) and their IRAS colors are quite similar to that of young stellar objects(YSOs) as $C_{12} > 0.0$ and $C_{23} > -0.4$ (Harris et al. 1988; Weintraub 1990), the major SiO non-detections in area III can be YSOs. Besides area III, non-detections are also abundantly distributed in area II where the objects have a cold circumstellar envelope and are perhaps more evolved than objects in area I (Bedijn

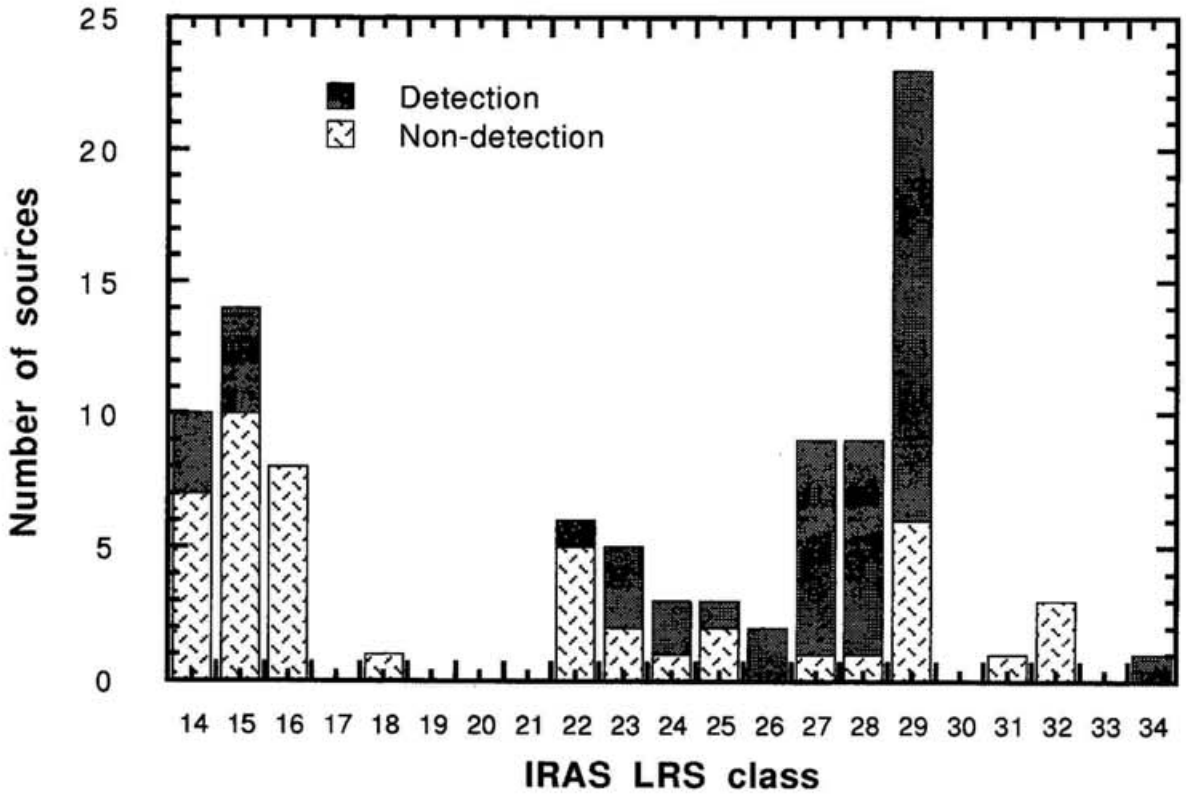

Fig. II.5.— SiO maser detections and nondetections versus the IRAS LRS classes.

1987). Except for three sources in area II, all the other 60 SiO detections are in area I with $C_{12} < 0.0$. A rough estimation of mass loss rate according to the formula by van der Veen (1989) results that the sources bluer than 0.0 in C_{12} have mass loss rates less than $5.6 \times 10^{-6} M_{\odot} yr^{-1}$ (assuming the luminosity of $8000 L_{\odot}$ and the expansion velocity of 15 km s^{-1}). Because an AGB star experiences accelerated mass loss to reach $\geq 10^{-5} M_{\odot} yr^{-1}$ at the end of AGB phase(Kwok 1993), these SiO maser sources are still in the relatively young AGB phase.

Observations in other molecular lines

A number of sources in the sample have been previously observed in other molecular lines. We cross-identified such sources as observed in OH maser, H_2O maser, CO thermal and HCN maser lines and listed the observational results in table 1.3 and 2.3. The catalogues of OH maser sources are taken from the survey at Arecibo(Eder et al. 1988; Lewis et al. 1990; Chengalur et al. 1993; Lewis 1994), at Dwingeloo, Effelsberg and Parkes (te Lintel Hekkert et al. 1991) and at Nancay (Le Squeren et al. 1992). The lists of CO and HCN sources are mainly from the catalogue compiled by Loup et al.(1993) and a small part of the CO data are from Wouterlout & Brand (1989). Benson's catalogue (Benson et al. 1990) is used as a complete collection of observational results in OH, H_2O and SiO maser lines made before 1990. Several other papers are referenced for OH and CO observations as can be seen in table 1.3.

Thirty-nine of the SiO detections were searched for OH masers resulting in 11 detections. Forty-five of the SiO non-detections were observed in OH maser lines and 4 of them are OH maser sources[1]. The search for H_2O masers was successful in 3 of the 14 sources with SiO detections and 2 of the 14 sources without SiO detections. The detection of OH and H_2O masers which only appear in O-rich stars means that there are four objects with O-rich CSE that were not detected in SiO maser lines, IRAS 04486+3042, 06088+2152, 06319-0501 and 21381+5000. In total 15 sources of our sample are detected in the OH and H_2O masers lines in 84 searched.

The CO(J=1-0) thermal line emission has been searched for in 10 of our SiO detections and detected in 8 sources, in 16 SiO non-detections and detected in 15 sources. The CO detections in the present sample can be divided into two groups, one with broad CO profile (line width bigger than 10 km s^{-1}) which are from the CSE of late-type stars and found in both SiO detections and non-detections, the other with narrow CO profile (line width smaller than 5 km s^{-1}) which are from molecular clouds, possibly foreground and background clouds as well as the source itself, and are found only in eleven of the SiO non-detections. Among the SiO non-detections, HCN maser emission has been seen in 3 sources, IRAS 03313+6058, 06582+1507 and 22130+5634 which are possibly C-rich objects.

Based on the optical, middle-infrared, far-infrared and molecular line features of the sources, we conclude that most of the SiO maser sources are optically visible and variable and they are losing mass to have a cold circumstellar envelope. Meanwhile we are not sure of the

[1]The anonymous referee informed us 4 new OH detections at Arecibo: IRAS 04402+3426, 04470+3002, 05345+3157 and 05378+2804.

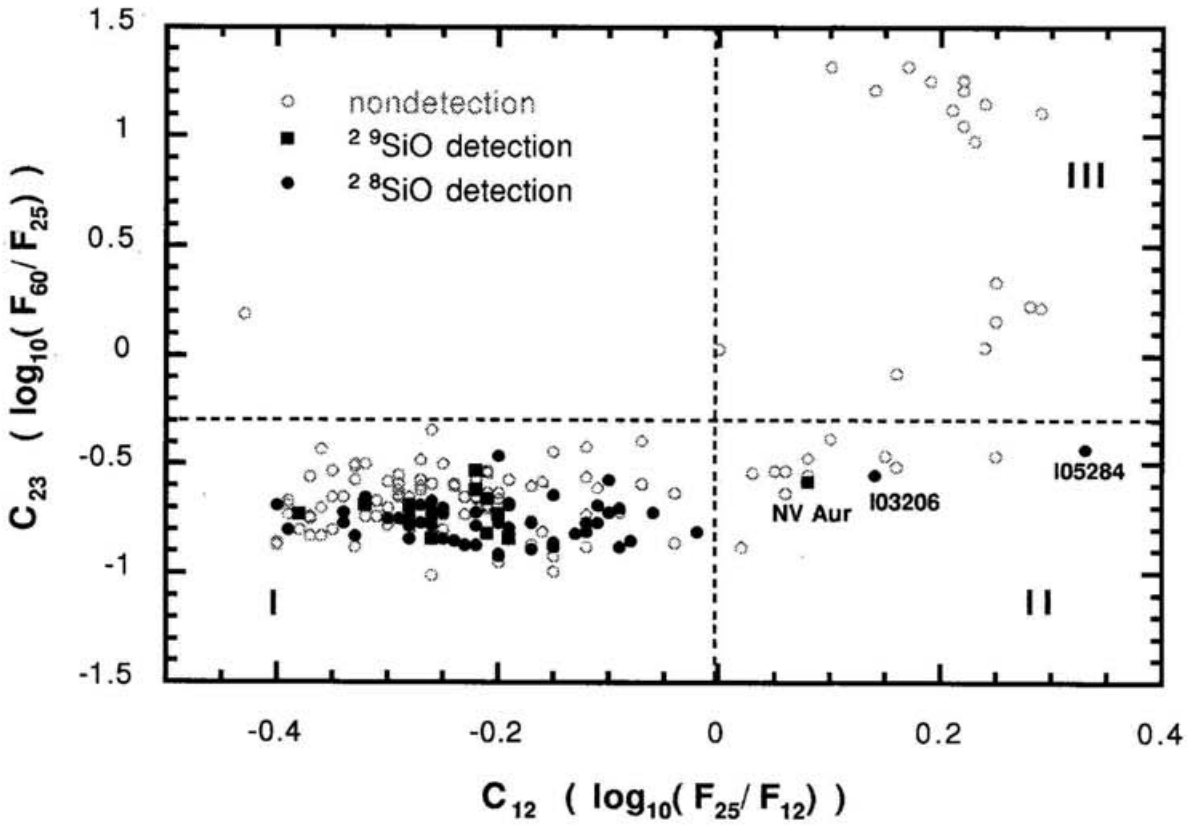

Fig. II.6.— IRAS color-color diagram, an open circle denotes a non-detection, a filled circle denotes a ^{28}SiO maser detection and a filled box denotes a ^{29}SiO detection. The three sources with $C_{12} > 0.0$ are labelled with their names.

nature of many SiO non-detections but some of them, particularly those with $C_{12} > 0$ and $C_{23} > -0.4$, may be YSOs in star forming region, while others may be C-rich stars or very evolved objects, and some could be O-rich stars without detection of SiO maser emission.

II.4.3. Comparison with the bulge survey sample

The survey in the outer disk resulted in a 35%(63/181) detection rate. This value is much lower than that of the survey towards the bulge direction even though the distances to sources are smaller on average. Because the same observing system was used in the two surveys as described in Section 2, the lower detection rate can not be attributed to the difference in observational sensitivity. Instead it may very possibly be due to that the outer disk sample includes many objects which are intrinsically not SiO maser sources. Because the sources with $F_{12} > 10Jy$ were observed somewhat randomly in both the bulge and outer disk surveys, it would be more objective to compare only the group of sources with $F_{12} < 10Jy$. The detection rate in the sources with $F_{12} < 10Jy$ is 16.7%(9/54) in the outer disk, which is less than half in the inner disk (35.9%) and one-fourth in the bulge (68.2%)(see Jiang et al. 1995). There should also be kept in mind that the lower limit of F_{12} is 3Jy in present survey sample while 1Jy in the bulge survey sample. If the distance effect is taken into account, the difference in detection rates between the bulge and the outer disk surveys is even more notable.

The SiO non-detection can be caused by the contamination from several types of objects: (1) YSOs, (2) C-rich objects, (3) post-AGB stars, (4) O-rich late-type stars without SiO maser emission and (5) the weakness of apparent intensity of SiO maser due to distance and/or time variation of SiO masers. Before studying the un-detected sources in details, we can not tell quantitatively how many percentage of the non-detections should be allocated to the above five factors individually. We try to figure out qualitatively the factors for the different detection rates between the outer disk and the bulge.

Because the bulge survey searched many distant and faint sources for which neither optical data nor IRAS LRS spectra are available, their IRAS colors turn to be important indicators of their natures. In Fig.II.7, all the sources searched in this survey and bulge survey are plotted in the IRAS color-color diagram where circles are for this survey, triangles for the bulge survey, filled for detection and open for non-detection. Since no limitation of flux quality is set for F_{60} in the bulge survey, some sources in the bulge direction might be shifted up in C_{23} because of the contribution of infrared cirrus to 60μm (Ivezić & Elitzur 1995). So the feature in the rectangle in Fig.II.7 emerged by the bulge sources could be caused by the pollution from cirrus. There is a clear branch stood out only by the outer disk objects with $C_{12} > 0$ and $C_{23} > -0.4$, typical colors of YSOs. Therefore more contamination from YSOs in the outer disk should account for some part of the low detection rate in this survey.

There are very few C-rich stars in the bulge (Blanco & Terndrup 1989) and no object is found to have CO/HCN line emissions in the bulge sample (Jiang et al. 1995). We can not attribute the bulge SiO non-detection to the contamination by C-rich objects. But in the outer disk non-detection group, two are optical C-rich stars and four more were detected in CO and/or HCN lines which suggest a possible C-rich nature. The contamination from C-rich objects must also be higher in the outer disk than that in the bulge sample.

In the five types of objects mentioned above, we can not easily find clear differences of

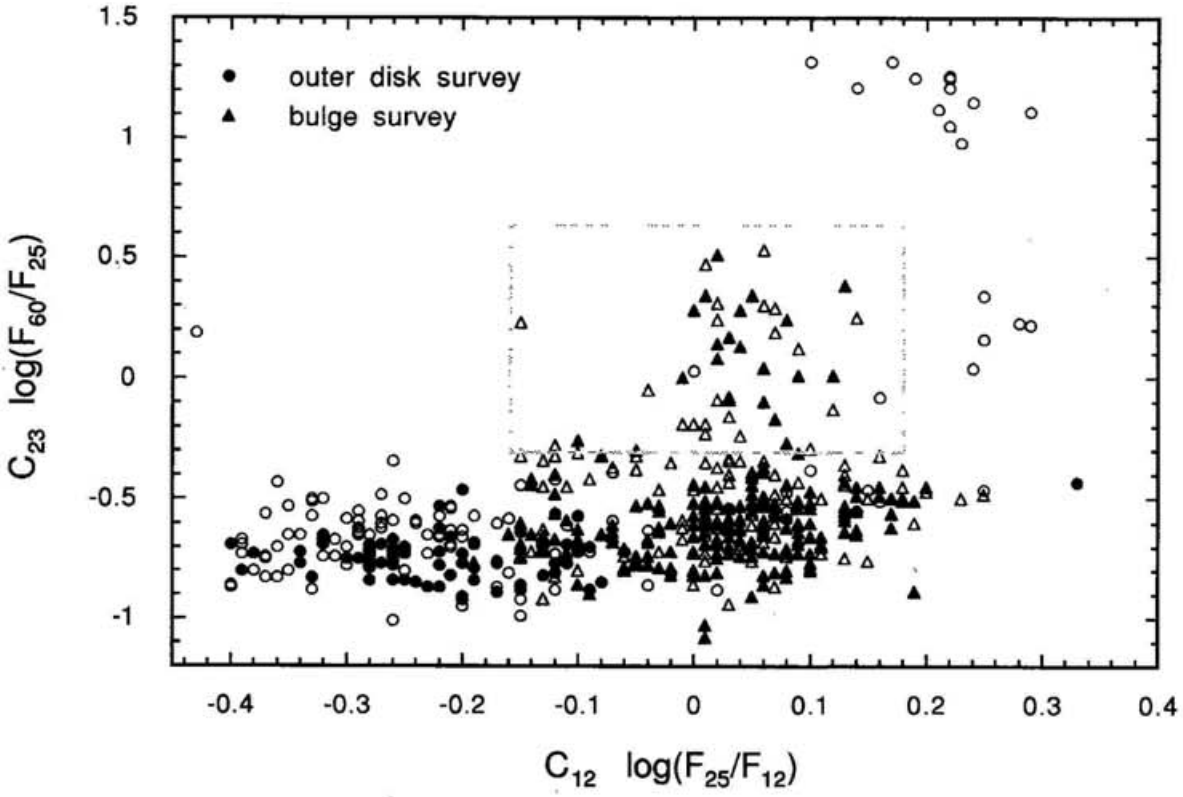

Fig. II.7.— IRAS color-color diagram of the sources in this survey and the bulge survey. The filled and open circles denote SiO detections and non-detections in this survey, the filled and open triangles denote SiO detections and non-detections in the bulge survey.

contamination in the later three types between the bulge and outer disk samples. There could be some other reasons. For example, the SiO masers in the bulge sources might be more luminous than in the outer disk as the bulge sources are metal-rich (Frogel 1988) and most of them are LPVs (Harmon & Gilmore 1988).

II.4.4. Galactic kinematics

By comparing the SiO velocity with the center velocity of double-peaked OH masers(Jewell et al. 1991; Jiang et al. 1995), the SiO maser velocity is proved to be stellar velocity. Therefore, we can use the SiO velocity as the stellar radial velocity to study Galactic kinematics.

Kinematic distance

According to the relation between radial velocity and kinematical distance in the outer Galaxy, one is able to extract the distance from stellar radial velocity. The SiO velocities change systematically along Galactic longitude as shown in Fig.II.8. The solid lines are calculated from the slightly rising rotation curve,

$$\Theta/\Theta_0 = 1.0074 \times (R/R_0)^{0.0382} + 0.00698 \qquad \text{(II.2)}$$

(Burton, 1988) derived to CO observational data, where Θ_0 (220 km s^{-1}) is the solar rotational velocity and R_0 (8.5 kpc) is the distance of the sun to the Galactic center. The sources extend to about 20kpc away from the Galactic center according to this diagram. But if the kinematical distance is correct, the implied luminosities of the sources are then often larger than $10^4 L_\odot$. Since the SiO detections are very possibly late-type variables, the luminosities obtained from the kinematic distances are overestimated, i.e. the kinematic distances are bigger than luminosity distances. This phenomenon is also found in C-rich stars (Epchtein et al. 1990). These may be caused by the velocity dispersion of stars. It can be seen that some sources in the second quadrant have positive V_{lsr} in scale of about 30 km s^{-1} in Fig.II.8.

Luminosity distance and rotation curve

So far there is not enough data to get accurate distances of these objects while we are measuring the periods of light variation of the optically identified SiO maser sources. Nevertheless, the luminosity distance can be estimated from IRAS fluxes and colors by bolometric correction method if the luminosity is known (Jiang & Hu 1993). First, the apparent bolometric flux F_{bol} is calculated from F_{12} and the bolometric corrections BC_{12} for O-rich groups stars based on IRAS color C_{12} (van der Veen & Breukers 1989):

$$F_{bol} = BC_{12} \times (\nu F_\nu)_{12} \qquad \text{(II.3)}$$

where

$$BC_{12} = 0.7 + 2.9e^{-3.0\times2.5\times C_{12}} + 0.9e^{0.7\times2.5\times C_{12}}. \qquad \text{(II.4)}$$

The distance D is then calculated,

$$D = \sqrt{L/(4\pi F_{bol})} \qquad \text{(II.5)}$$

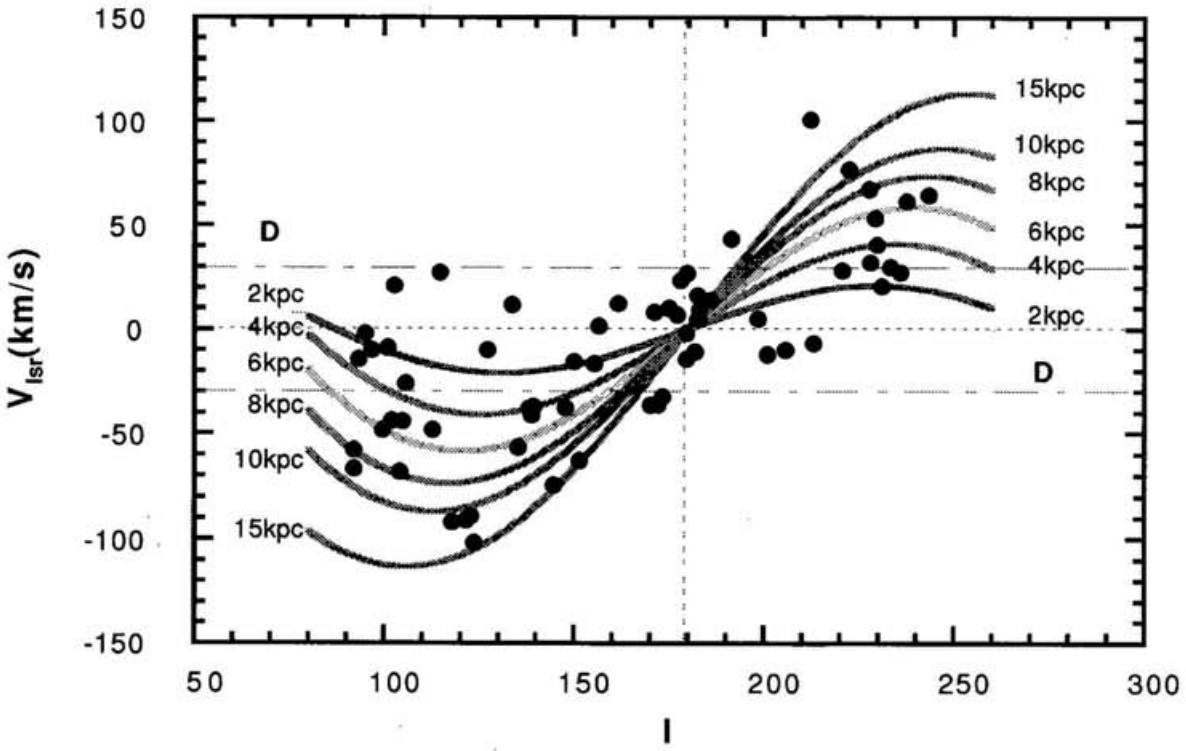

Fig. II.8.— Galactic longitude l vs. the velocity relative to the local standard of rest $V_{\rm lsr}$ diagram. The solid lines are calculated from the rotation curve derived by Burton(1988).

where L is stellar luminosity and we assume L=8000$L_\odot$ in calculating the distances.

The rotational velocity is calculated from V_{lsr} by extracting the rotational velocity 220 km s^{-1} of the local standard of rest and assuming the radial velocity is the projection of circular rotation velocity in the radial direction. But we exclude the sources within 10° from Galactic anticenter direction where small deviation from circular rotation brings about significant error in rotational velocity. Fig.II.9 shows the locations of the sources in the diagram of rotational velocity versus galactocentric distance R. The least-square linear fitting results in a falling tendency of the rotation curve internal to the distance scale $1.3R_0$:

$$V_{rot} = 220.0 kms^{-1} - 21.7(\pm 5.7) kms^{-1} kpc^{-1} \times (R - R_0) kpc \qquad (II.6)$$

where R_0 equals 8.5kpc. Besides, the adopted value of luminosity 8000$L_\odot$ might be higher than the average of M-type stars. The curve will be drawn down more if the luminosity is 3000$L_\odot$, as marked by two open circles and arrows in Fig.II.9. More accurate determinations of both luminosity and distance will alleviate the uncertainty. The local falling of rotation curve at the outside of solar circle can also be seen in the rotation curve from the CO data by Brand & Blitz(1993). From the rotation curve, the Oort's constants are reduced: A= $23.8 \pm 2.9 kms^{-1} kpc^{-1}$, B = $-2.1 \pm 2.9 kms^{-1} kpc^{-1}$. These two values are slightly different from previous values (Kerr & Lynden-Bell 1986), because this result suffers very much from the distance uncertainty of the sources.

Peculiar motion of the Local Standard of Rest

We especially tried to detect SiO maser emission in the sources within 20° from the Galactic anti-center direction (l=180°, b=0°) in the 1994 May observing session to check the peculiar motion of the local standard of rest to the Galactic center. The local standard of rest (LSR) is defined as a system of nearby stars (within a few kpc) from which the average solar peculiar motion is subtracted (see Kuijken 1992 for a recent review). It is moving with a velocity of 220 km s^{-1} around the Galactic center (Kerr & Lynden-Bell 1986). However, it is argued that, in addition to the Galactic rotation, the system may have a motion toward or away from the Galactic center with a velocity of about 10-15 km s^{-1}. The direction of this motion has been a source of controversy (see Blitz & Spergel 1991; based on the HI observations, they concluded that LSR is moving away from the galactic center). Izumiura et al.(1994; 1995a; 1995b) recently found that the linear fit rotation curve of the bulge SiO maser sources is significantly negative (about 20 km s^{-1}) at l=0° so that the local standard of rest is moving toward the galactic center. Metzger & Schechter (1994) observed 178 carbon stars toward the Galactic anti-center and obtained the velocity of the local standard of rest with respect to the distant carbon stars at 6.6 ± 1.7 km s^{-1}. These observations support that LSR is moving toward the galactic center.

To check this possibility of the LSR motion toward the galactic center, we have plotted in Fig.II.10 the residual radial velocity (after subtracting the Galactic rotation), V_{lsr} - V_{exp}, with distance from the galactic center, R, for 17 detected sources within 20 degree from the Galactic anti-center. The rotation curve given in section 4.4.1 (equation 2) is adopted to calculate the radial velocity expected from the Galactic rotation, V_{exp}. The V_{exp} of sources with $|l - 180°| < 20°$ has a maximum of about 75 km s^{-1} so that the uncertainty of the

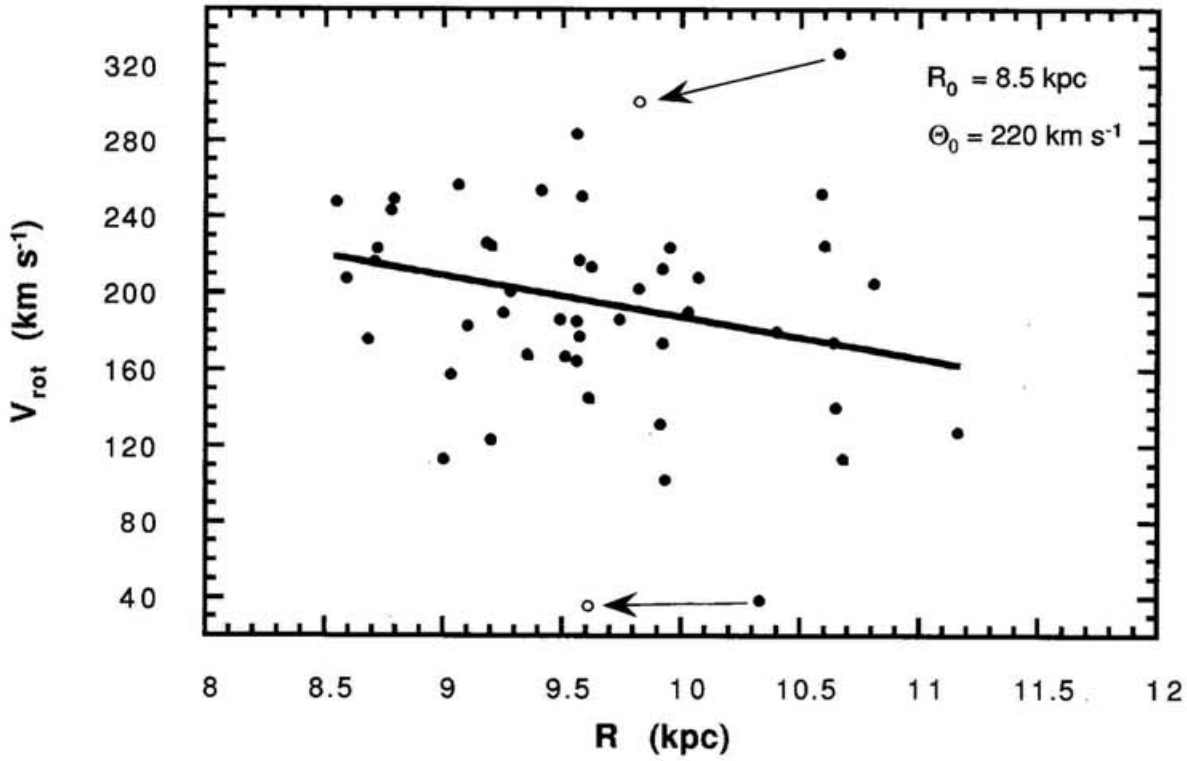

Fig. II.9.— Rotation curve from luminosity-distance and SiO radial velocity. The luminosity of all the detections is assumed identical as $8000L_{\odot}$ and R is the galactocentric distance. The sources in $|l - 180°| < 10°$ are excluded, R_0=8.5kpc and $\Theta_0 = 220$ km s^{-1}. The two arrows and the two open circles indicate the change tendency of V_{rot} and R when the luminosity is $3000L_{\odot}$.

distance to the source does not cause large errors in the residual velocity. The deviation from zero is mainly due to the random motion of stars on the Galactic rotational motion.

However, the 17 detected SiO maser sources are insufficient to determine the systematic motion of the local standard of rest. We added 8 OH 1612 MHz sources in this direction which have been detected by te Lintel-Hekkert et al. (1990) and Lewis et al.(1990, 1994): IRAS 04130+3918, 04269+3550, 05131+4530, 05274+3345, 05342+2744, 05423+2905, 05506+2414, and 05528+2010. The best fit curve to the residual velocities is then V_{lsr}-V_{exp} = (0.42±1.77 km s^{-1} kpc^{-1}) (R_0=8.5 kpc). There is a slight tendency that the average stellar velocity is positive at large galactocentric distance. However, even with these additional OH sources, the result is not statistically significant and a peculiar motion of the local standard of rest towards the galactic center is not confirmed.

II.5. Summary

The observations in the ^{28}SiO J=1-0 v=1 and v=2 maser lines, ^{29}SiO J=1-0 v=0 maser line were made towards 181 IRAS sources in the outer disk of the Galaxy. Sixty-three (56 new) sources were detected in the ^{28}SiO lines and 11 (9 new) in the ^{29}SiO line. Most SiO maser sources are optical variables. On the properties of SiO masers, we do not find any clear difference between the bulge group and the outer disk group. But the detection rates of these two samples, although chosen by similar criteria and observed by the same system, are drastically different that in the outer disk the detection rate is less than one quarter of that in the bulge among the sources with F_{12} <10JY. The difference may be caused by more contaminations from C-rich objects and YSOs in this color-selected sample in the outer disk.

Based on the velocity derived from the SiO maser lines, we found that the rotation curve shows slightly falling tendency between 8.5kpc and 12kpc. By using the data of sources in the Galactic anti-center direction, the peculiar motion of LSR towards the Galactic center is checked although not confirmed. Because of insufficient number of objects and limiting distance, these results on Galactic kinematics suffer some uncertainty.

The authors thank the staff member of the 45m group at Nobeyama Radio Observatory to help the observation. They also thank Dr. H. Izumiura for helpful discussion. One of the authors B.W.J. thanks Drs. S. Ichikawa and M. Fitzpatrick for providing the software package to read FITS format data. This research made use of the SIMBAD database, operated at CDS, Strasbourg, France. B.W.J. is supported by Japanese Government Scholarship. With the agreement of the editor, Table 1.1, Table 2.1 and Table 3 will be published on the AAS CD-ROM.

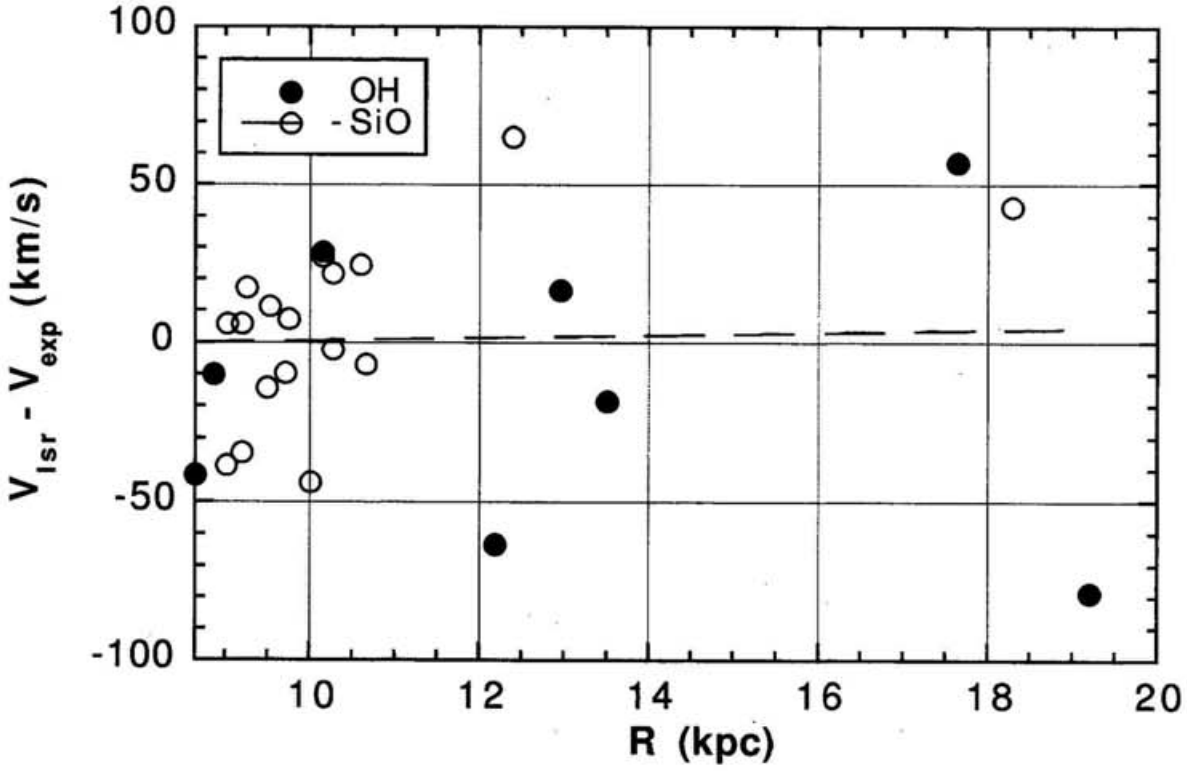

Fig. II.10.— Residual velocity vs. the galactocentric distance. The ordinate is the observed V_{lsr} minus V_{exp}, expected velocity from rotation curve.

REFERENCES

Alcolea, J., & Bujarrabal, V. 1992, A&A 253, 475

Allen, D.A., Hall, P.J., Norris, R.P., Troup, E.R., Wark, R.M., & Wright, A.E. 1989, MNRAS 236, 363

Bedijn, P.J. 1987, A&A 186, 136

Beichman, C.A., Neugebauer, G., Habing, H.J., Clegg, P.E., & Chester, T.J. 1985, IRAS Catalogues and Atlases Explanatory Supplement, US Government Printing Office, Washingon DC

Benson, P.J., Little-Marenin, I., Woods, T., Attridge, J., Blais, K., Rudolph, D., Rubiera, M., & Keefe, H. 1990, ApJS 74, 911

Blanco, V.M., & Terndrup, D.M. 1989, AJ 98, 843

Blitz, L., & Spergel, D. 1991, ApJ 370, 205

Brand, J., & Blitz, L. 1993, A&A 275, 78

Burton, W.B.1988, in 'Galactic and extragalactic radio astronomy', eds. Verschuur G.L. and Kellermann K.I., p.295, Springer-Verlag

Chengalur, J.N., Lewis, B.M., Eder, J., & Terzian, Y., 1993, ApJS 89, 189

Cho, S.H., & Ukita, N. 1995, PASJ 47, L1

Cho, S.H., Kaifu, N., Ukita, N., Morimoto, M., & Hayashi, M. 1986, Ap&SS 118, 237

Cho, S.H., Kaifu, N., & Ukita, N. 1996, A&AS 115, 1

Deguchi, S., Good, J., Fan, Y., Mao, X.J., Wang, D., & Ukita, N. 1983, ApJ 264, L65

Deguchi, S., & Iguchi, T. 1976, PASJ 28, 307

Diamond, P.J., Kemball, A.J., Junor, W., Zensus, A., Benson, J., & Dhawan, V. 1994, ApJ 430, L61

Dickinson, D.F., Turner, B.E., Jewell, P.R., & Benson, P.J. 1986, AJ 92, 627

Eder, J., Lewis, B.M., & Terzian, Y. 1988, ApJS 66, 183

Elitzur, M. 1980, ApJ 240, 533

Epchtein, N., Le Bertre, T., & Lépine, J.R.D. 1990, A&A 227, 82

Frogel, J.A. 1988, ARA&A 26, 51

Galt, J.A., Kwok, S., & Frankow, J. 1989, AJ 98, 2182

Hall, P.J., Wark, R.M., & Wright, A.E. 1987, PASP 7, 50

Harmon, R., & Gilmore, G. 1988, MNRAS 235, 1025

Harris, S., Clegg, P., & Hughes, J. 1988, MNRAS 235, 442

Ivezić, Ž, & Elitzur, M. 1995, ApJ 445, 415

Izumiura, H., Catchpole, R., Deguchi, S., Hashimoto, O., Nakada, Y., Onaka, T., Ono, T., Sekiguchi, K., Ukita, N., & Yamamura, I. 1995a, ApJS 98, 271

Izumiura, H., Deguchi, S., Hashimoto, O., Nakada, Y., Onaka, T., Ono, T., Ukita, N., & Yamamura, I. 1994, ApJ 437, 419

Izumiura, H., Deguchi, S., Hashimoto, O., Nakada, Y., Onaka, T., Ono, T., Ukita, N., & Yamamura, I. 1995b, ApJ 453, 837

Jewell, P.R., Snyder, L.E., Walmsley, C.M., Wilson, T.L., & Gensheimer, P.D. 1991, A&A 242, 211

Jiang, B.W., Deguchi, S., Izumiura, H., Nakada, Y., & Yamamura, I. 1995, PASJ 47, 815

Jiang, B.W., Deguchi, S., & Nakada, Y. 1996, AJ 111, 231

Jiang, B., & Hu, J.Y. 1993, Chin. Astron. Astrophy. 17, 321

Kastner J., Forveille, T., Zuckerman, B., & Omont, A. 1993, A&A 275, 163

Kerr, F.J., & Linden-Bell, D. 1986, MNRAS 221, 1023

Kuijken, K., & Tremain, S. 1991, in "Dynamics of disk galaxies", p 71, Ed. Sundelius, B. (Göteborg Univ., Göteborg)

Kwok, S. 1993, ARA&A 31, 63

Le Squeren, A.M., Sivagnanam, P., Dennefeld, M., & David, P. 1992, A&A 254, 133

Lewis, B.M. 1994, ApJS 93, 549

Lewis, B.M., Eder, J., & Terzian, Y. 1990, ApJ 362, 634

Lindqvist, M., Ukita, N., Winnberg, A., & Johansson, L.E.B. 1991, A&A 250, 431

Loup, C., Forveille, T., Omont, A., & Paul, J.F. 1993, A&AS 99, 291

Metzger M., & Schechter, P. 1994, ApJ 420, 177

Nguyen-Q-Rieu, Deguchi, S., Izumiura, H., Kaifu, N., Ohishi, M., Suzuki, H. & Ukita N. 1988, ApJ 330, 374

Nyman, L.-A., Booth, R.S., Carlstrom, U., Habing, H.J., Heske, A., Sahai, R., Stark, R., van der Veen, & Winnberg, A. 1992, A&AS 93, 121

Nyman, L.-A., Hall, P.J., & Le Bertre, T.L. 1993, A&A 280, 551

Nyman ,L-A, Johansson, L.E.B., & Booth, R.S. 1986, A&A 160, 352

Olnon, F.M., & Raimond, E. 1986, A&AS 65, 607

Penzias, A.A. 1981, ApJ 249, 513

Schwarz, H.E., Nyman, L.-A., Seaquist, E.R., & Ivison, R.J. 1995, A&A 303, 833

Sivagnanam, P., Braz, M.A., Le Squeren, A.M., & Tranminh, F. 1990, A&A 233, 112

Snyder, L.E., & Buhl, D. 1974, ApJ 189, L31

te Lintel Hekkert, P., Caswell, J.L., Habing, H.J., Haynes, R.F., & Norris, R.P. 1990, A&AS 90, 327

van der Veen, W.E.C.J. 1989, A&A 210, 127

van der Veen, W.E.C.J., & Breukers, R.J.L.H. 1989, A&A 212, 133

van der Veen, W.E.C.J., & Habing, H.J. 1988, A&A 194, 125 (VH)

Weinberg, W.D. 1992, ApJ 384, 81

Weintraub, D.A. 1990, ApJS 74, 575

Whitelock, P., Feast, M., & Catchpole, R. 1991, MNRAS 248, 276

Whitelock, P., Menzies, J., Feast, M., Marang, F., Carter, B., Roberts, G., Catchpole, R., & Chapman, J. 1994, MNRAS 267, 711

Wouterloot, J.G.A., & Brand, J. 1989, A&AS 80, 149

Chapter III

Survey in SiO maser lines (II)

ABSTRACT

The observation in the J=1-0, v=1 and v=2 ^{28}SiO and v=0 ^{29}SiO maser lines was made to 97 outer disk stars and 19 inner disk stars that are of typical IRAS colors of AGB stars. By using the 45m telescope system at Nobeyama, 21 new ^{28}SiO and 1 new ^{29}SiO maser sources were found at the detection limit of about 1 Jy at 5 sigma level. Collecting all the observational data in SiO J=1-0 maser lines by the 45m telescope system, a comparison is made between the outer disk, inner disk and bulge samples. The samples themselves align a sequence of IRAS color, flux at 12μm and variability index. The detection rates are 66%, 45% and 31% respectively in the bulge, inner disk and outer disk. A more detailed analysis shows consistency with the conclusion from Chapter V, i.e. the proportion of C-rich stars increases with Galactocentric distance in the observed sample of late-type stars with cold circumstellar envelopes.

III.1. Introduction

The observation in SiO maser lines around 43GHz have been performed to a great deal of color-selected IRAS PSC sources in the Galactic bulge, inner disk and outer disk by using the 45m telescope system at Nobeyama Radio Observatory. Such observations are the deepest at this frequency thanks to that the 45m telescope system deserves an antenna of large diameter and a receiver of high sensitivity. In 1991, 1992 and 1993, 313 sources in the direction of bulge were observed. In 1994, 1995 and 1996, 244 sources in the outer disk and 23 sources in the inner disk were observed. The observational results from 1991 through 1995 have been reported in separate papers (Izumiura et al. 1994, 1995a and 1995b, Jiang et al. 1995, 1996), here we first report the results of the 1996 observations. Then the statistical comparison will also be done between the bulge, inner disk and outer disk groups, since all these observations were carried out by the same observational system and sources were selected under quite similar selection criteria.

III.2. The 1996 May observation

On May 10-14 and 16-19, 1996, mainly two groups of objects were observed. The major group is in the outer disk and the minor one in the inner disk. The selection criteria are quite similar for these two groups. They are listed in Table 1. Because of time limitation, the inner disk sources are also restricted to have no association in any catalogue in light of the IRAS PSC database together with the criteria listed in Table 1. In the study of IRAS PSC sources with infrared excess, people found that the IRAS colors are different for various objects such as young stellar objects, late-type stars and galaxies. The selected IRAS colors C_{12} ($logF_{25}/F_{12}$ F_λ is the flux density at λ), and C_{23} ($logF_{60}/F_{25}$ are set to pick up the stars in late stage of evolution and with cold circumstellar envelope(CSE). The limitation on IRAS flux density at 12μm makes that the sources are not very close to the sun and may be at a distance further than 4kpc if the star is an M-type star with cold CSE. Among the 97 sources in the outer disk, 15 had been observed in 1995 or 1994 and 5 of them were already detected SiO maser emission. Some of the non-detections were observed again and no new detections were found. In addition to the objects in the samples, 6 sources that could not been detected SiO maser emission in previous observations were observed again and 7 more sources beyond the selection criteria were also observed.

The observational details had been described in Chapter II so that only a few important parameters are briefed here. The 45m telescope system at Nobeyama Radio Observatory with SIS receiver S40 was used and AOS spectrometers were attuned at SiO maser lines ^{28}SiO J=1-0, v=1 and v=2, ^{29}SiO J=1-0 v=0. The velocity resolution is about 0.26km/s and the detection sensitivity is about 0.28K ($\sim$ 1Jy) at 5 sigma level.

The observational results are summarized in Table 2. Amid the 97 sources in the outer disk, 8 new ^{28}SiO sources and 1 new ^{29}SiO source were detected in 82 searched. Out of the 19 sources in the inner disk, 8 new ^{28}SiO sources were detected. In the other 13 sources, 5 were newly detected among which IRAS 04264+3853, 04402+3426 and 22394+6930 were not detected in 1995 (Chapter II). Totally 21 new ^{28}SiO and 1 new ^{29}SiO maser source were found in 114 searched.

The SiO maser spectra of newly detected stars are displayed in Fig. III.1 and Fig. III.2 respectively for the ^{28}SiO and ^{29}SiO lines. The related parameters of SiO maser lines are summarized in Table 3.1 and 3.2. The other infrared properties such as IRAS colors and Galactic positions are listed in Table 4 for all the observed objects. The same convention as in Chapter II is applied to the tables for naming the columns.

TABLE 1. Selection criteria of the 1996 May observed sources

	outer disk	inner disk
Galactic longitude	115° – 155°	55° – 70°
Galactic latitude	[-10°, 10°]	
IRAS color	$C_{12} \subset$ [-0.4, 0.4]	
	$C_{23} \leq$ -0.4	
IRAS flux density	$F_{12} <$ 15Jy	
Qualities of IRAS fluxes	333 at 12,25 and 60 μm	
No. of sources	97	19

TABLE 2. Number of detections

	outer disk	inner disk	miscellaneous
^{28}SiO	13/97	8/19	5/13
^{29}SiO	1/97	0/19	0/13

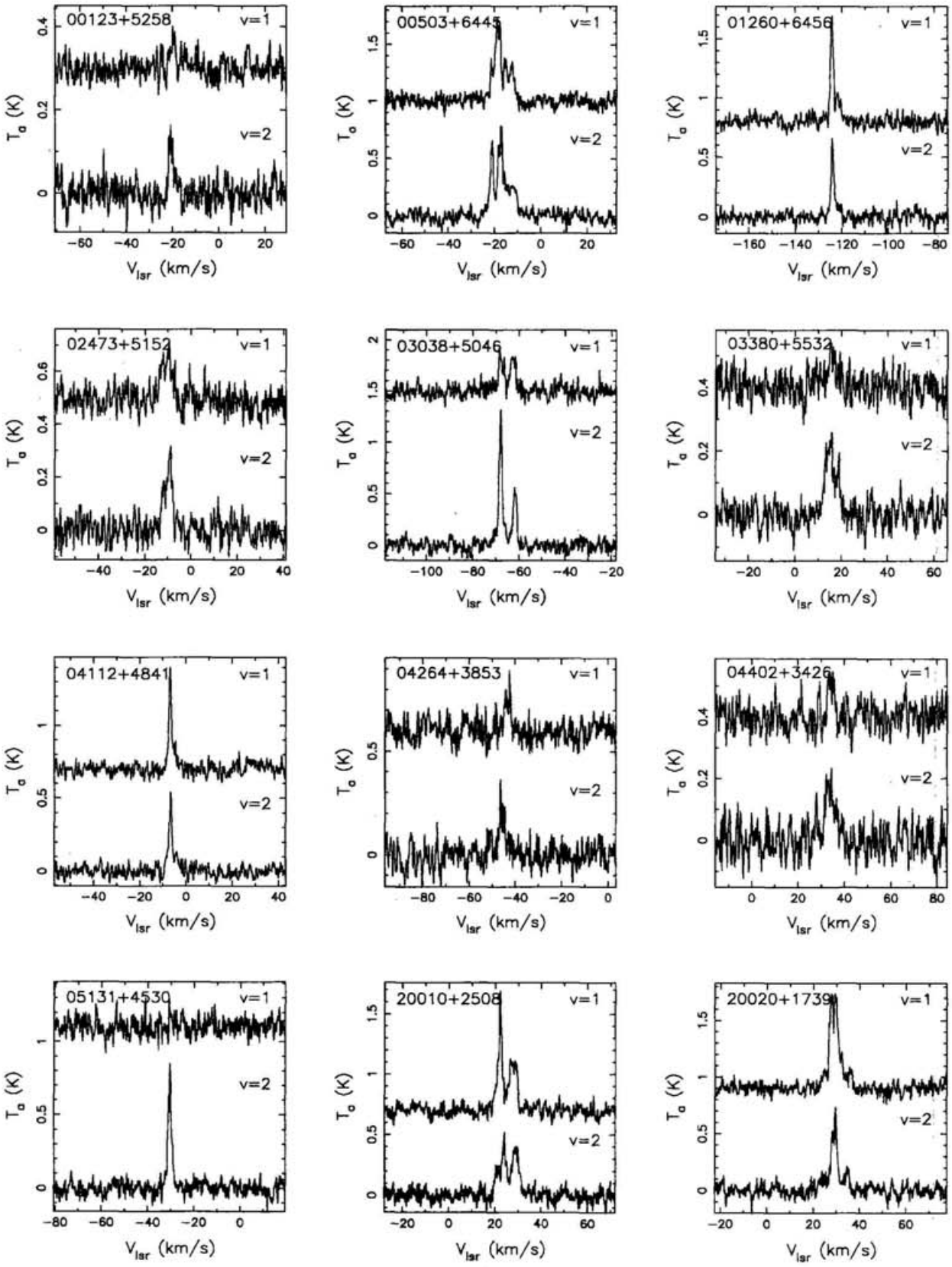

Fig. III.1.(a)

Fig. III.1.— Spectra of 21 ^{28}SiO new detections.

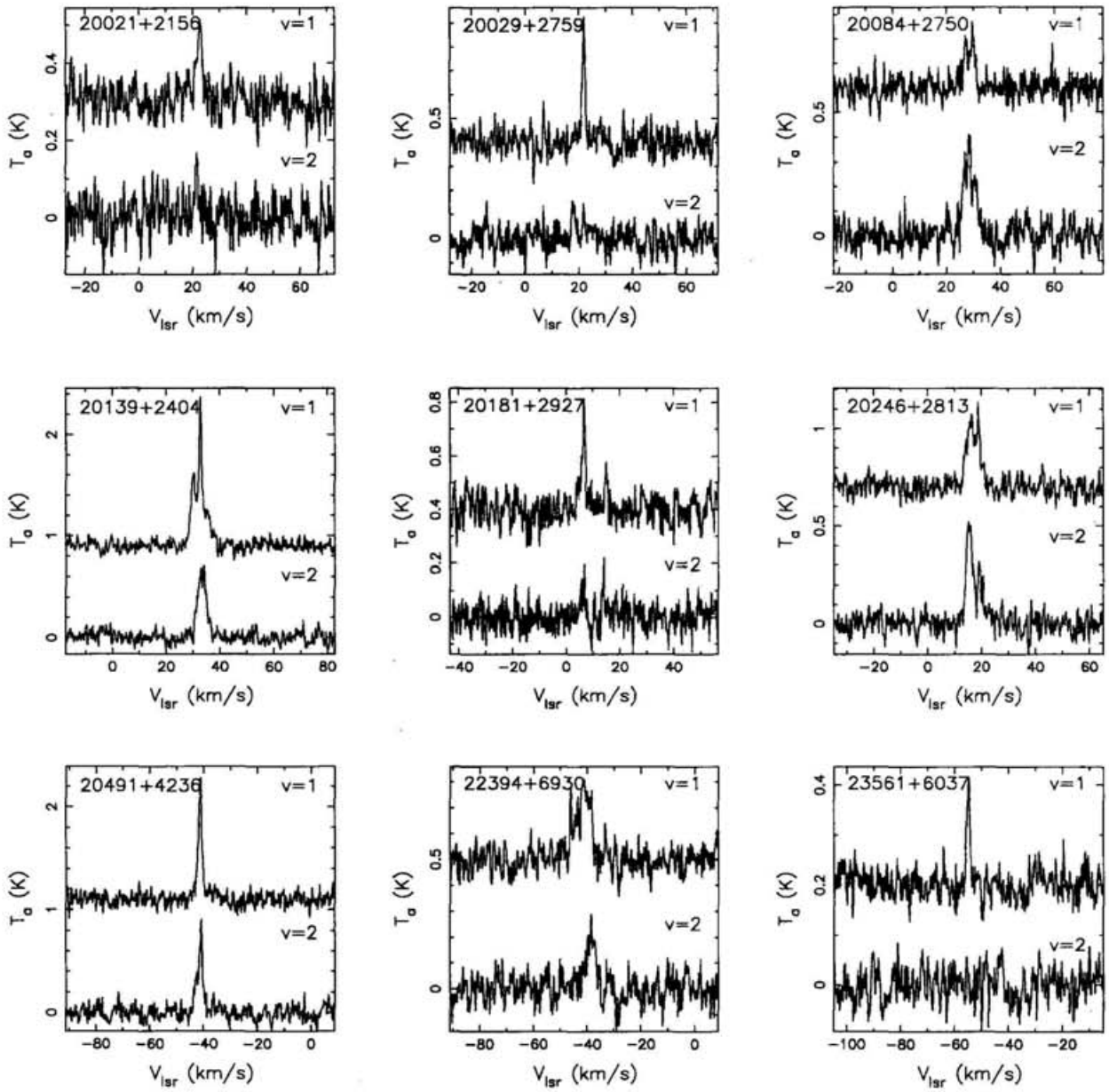
20021+2156
v=1
v=2
20029+2759
v=1
v=2
20084+2750
v=1
v=2
20139+2404
v=1
v=2
20181+2927
v=1
v=2
20246+2813
v=1
v=2
20491+4236
v=1
v=2
22394+6930
v=1
v=2
23561+6037
v=1
v=2
T_a (K)
V_lsr (km/s)

Fig. III.1.(b)

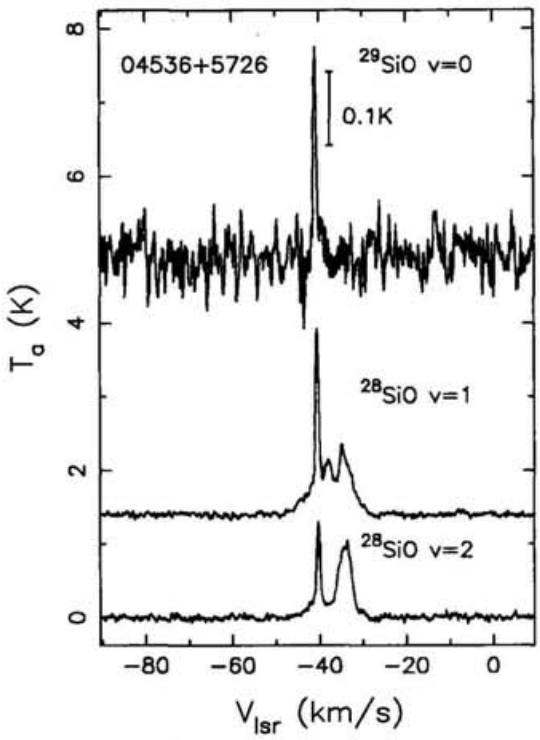

Fig. III.2.— Spectra of the unique ^{29}SiO new detection, the scale of the ^{29}SiO line is labelled beside the emission line.

TABLE 3.1. Line parameters of Gaussian components of the ^{28}SiO detections

	SiO v=1 J=1-0				SiO v=2 J=1-0			
IRASNAME	TA1 (K)	rms1 (K)	Vlsr1 (km/s)	FWHM1 (km/s)	TA2 (K)	rms2 (K)	Vlsr2 (km/s)	FWHM2 (km/s)
00123+5258	0.092	0.025	-18.837	1.353	0.128	0.028	-20.185	2.345
00503+6445	0.619	0.043	-17.684	4.126	0.620	0.045	-20.775	1.635
	0.282		-14.056	1.242	0.689		-16.839	2.975
	0.307		-11.415	2.576	0.253		-11.773	5.175
01260+6456	0.882	0.045	-125.877	1.401	0.558	0.042	-126.010	1.062
	0.214		-123.106	2.703	0.148		-125.164	4.758
02473+5152	0.108	0.043	-11.675	1.926	0.191	0.040	-11.092	2.081
	0.154		-8.576	3.951	0.285		-8.195	2.358
03038+5046	0.412	0.061	-68.663	1.248	1.238	0.047	-68.553	1.681
	0.285		-66.841	1.103	0.553		-62.225	1.902
	0.340		-62.817	2.741	...		...	...
03380+5532	0.131	0.042	16.989	2.253	0.236	0.040	16.307	4.397
	...		...	...	0.150		20.427	1.471
04112+4841	0.667	0.035	-5.672	1.257	0.415	0.036	-5.678	1.076
	0.145		-3.655	2.102	0.126		-4.788	5.591
04264+3853	0.199	0.049	-43.875	1.448	0.261	0.054	-46.500	0.500
	0.275		-42.149	0.810	0.150		-45.589	3.680
04402+3426	0.141	0.042	34.740	2.893	0.172	0.049	34.686	5.782
04536+5726	0.339	0.027	-41.095	6.255	0.243	0.028	-40.266	5.660
	2.232		-40.128	0.926	1.176		-40.153	0.857
	0.503		-37.759	1.873	1.033		-33.847	3.537
	0.792		-33.775	4.522	...		...	...
05131+4530	...	0.058	...	...	0.768	0.045	-31.188	1.540
	...		...	...	0.173		-29.744	0.918
20010+2508	0.248	0.044	21.338	2.314	0.227	0.046	21.410	2.401
	0.796		23.011	1.442	0.451		24.368	2.001
	0.415		28.407	4.190	0.382		29.371	3.846
20020+1739	0.114	0.045	24.998	2.179	0.147	0.049	29.241	10.347
	0.339		28.186	1.468	0.396		28.669	0.937
	0.714		30.135	4.406	0.547		30.135	1.279
	0.150		36.768	2.338	0.155		35.496	1.180
20021+2156	0.232	0.041	23.426	1.479	...	0.046	...	...
20029+2759	0.496	0.047	22.465	1.314	...	0.048	...	...
20084+2750	0.207	0.047	27.767	1.345	0.276	0.048	27.148	2.028
	0.220		30.415	2.174	0.358		28.914	1.150
	...		...	...	0.234		31.168	2.471
20139+2404	0.439	0.048	30.797	1.715	0.642	0.052	34.025	3.931
	1.004		33.606	0.823	...		...	...
	0.464		33.869	6.271	...		...	...
20181+2927	0.424	0.049	6.835	1.097	...	0.051	...	...
	0.159		15.210	1.185	...		...	...
20246+2813	0.320	0.040	16.977	5.357	0.517	0.046	15.607	2.674
	0.225		19.538	0.795	0.247		19.683	2.937
20491+4236	0.605	0.060	-42.327	2.427	0.375	0.062	-43.809	1.825
	0.582		-42.048	0.736	0.806		-42.012	1.256
22394+6930	0.257	0.044	-42.460	7.061	0.215	0.048	-39.746	3.977
23561+6037	0.231	0.027	-54.907	1.202	...	0.030	...	...

TABLE 3.2. Integrated line parameters of the ^{28}SiO detections

	SiO v=1 J=1-0			SiO v=2 J=1-0			
IRASNAME	S1 (K*km/s)	Vcen1 (km/s)	FWHM1 (km/s)	S2 (K*km/s)	Vcen2 (km/s)	FWHM2 (km/s)	DATE yymmddhh
00123+5258	0.13	-18.84	1.35	0.32	-20.18	2.34	96051710
00503+6445	3.95	-14.55	6.49	4.68	-16.27	7.91	96051810
01260+6456	1.94	-124.49	3.44	1.39	-125.59	3.33	96051712
02473+5152	0.87	-10.13	4.49	1.14	-9.64	3.67	96051612
03038+5046	1.88	-65.74	4.92	3.35	-65.39	4.96	96051213
03380+5532	0.32	16.99	2.25	1.35	18.37	4.99	96051614
04112+4841	1.22	-4.66	2.69	1.23	-5.23	3.78	96051814
04264+3853	0.55	-43.01	1.99	0.73	-46.04	2.55	96051314
04402+3426	0.44	34.74	2.89	1.06	34.69	5.78	96051315
04536+5726	9.32	-37.44	9.05	6.46	-37.06	7.81	96051315
05131+4530	...	...	...	1.44	-30.47	1.95	96051215
20010+2508	3.70	24.87	6.79	3.12	25.39	7.10	96051706
20020+1739	4.54	30.88	8.14	2.97	32.37	8.89	96051807
20021+2156	0.37	23.43	1.48	...	...	...	96051906
20029+2759	0.70	22.47	1.31	...	...	...	96051707
20084+2750	0.81	29.09	3.08	1.66	29.16	4.26	96051707
20139+2404	4.80	32.33	5.53	2.70	34.03	3.93	96051808
20181+2927	0.70	11.02	5.33	...	...	...	96051708
20246+2813	2.03	18.26	4.36	2.26	17.65	4.84	96051908
20491+4236	2.03	-42.19	1.72	1.82	-42.91	2.44	96051909
22394+6930	1.94	-42.46	7.06	0.91	-39.75	3.98	96051809
23561+6037	0.30	-54.91	1.20	...	...	...	96051409

TABLE 4. Infrared properties of all observed sources

IRASNAME	l(o)	b(o)	F12(Jy)	C_{12}	C_{23}	LRS	var
00027+6952	119.01	7.64	6.75	-0.22	-0.73		0
00036+6117	117.58	-0.84	7.22	-0.24	-0.60		1
00123+5258	117.42	-9.23	7.11	-0.32	-0.64		2
00131+6925	119.84	7.05	5.78	-0.30	-0.70		8
00161+5820	118.69	-3.98	11.45	-0.33	-0.77	16	7
00180+6414	119.64	1.84	13.31	-0.35	-0.78	15	57
00243+6316	120.23	0.81	10.69	-0.31	-0.72		5
00246+6837	120.77	6.13	6.69	-0.31	-0.65		45
00361+6515	121.65	2.70	9.65	-0.15	-0.46		47
00425+6820	122.40	5.76	7.17	0.01	-0.59		5
00461+6439	122.69	2.07	5.87	-0.31	-0.54		5
00464+6430	122.73	1.91	5.48	-0.25	-0.50		5
00470+6448	122.79	2.20	10.30	-0.06	-0.45		15
00503+6445	123.14	2.16	14.36	-0.31	-0.86		0
00513+6317	123.27	0.69	8.81	-0.29	-0.71	13	2
00555+5353	123.97	-8.70	10.30	-0.19	-0.66		25
00589+5743	124.33	-4.85	4.28	-0.23	-0.73		59
00593+5836	124.36	-3.97	5.51	-0.27	-0.68		7
01065+6452	124.86	2.34	12.46	-0.20	-0.56		4
01097+6154	125.44	-0.59	13.99	-0.27	-0.73		3
01102+6153	125.51	-0.60	7.53	-0.31	-0.59		63
01108+6059	125.64	-1.50	11.86	-0.31	-0.62		0
01129+6352	125.63	1.40	9.94	-0.33	-0.65		17
01176+6710	125.78	4.72	5.71	-0.33	-0.66		8
01217+6049	126.98	-1.53	52.31	-0.22	-0.62	23	58
01260+6456	126.91	2.62	6.20	-0.08	-0.73		20
01296+6813	126.78	5.92	5.83	-0.21	-0.80		5
01301+6118	127.92	-0.91	6.30	-0.20	-0.52		4
01327+6503	127.60	2.85	11.86	-0.30	-0.68	16	10
01344+6232	128.21	0.40	11.17	-0.24	-0.51	16	5
01386+7010	127.22	7.98	6.09	-0.40	-0.72		88
01435+6007	129.75	-1.76	6.28	-0.32	-0.55		6
01441+6026	129.76	-1.43	11.59	-0.15	-0.53		25
01550+5901	131.41	-2.50	8.93	-0.35	-0.69	14	8
01583+5508	132.87	-6.13	7.66	-0.23	-0.80		5
02016+5802	132.51	-3.22	6.64	-0.32	-0.71		16
02047+5901	132.62	-2.15	14.75	-0.22	-0.83	27	9
02117+5559	134.44	-4.77	7.40	-0.04	-0.86		78
02155+6410	132.25	3.14	2.30	0.03	-0.44		14
02157+5843	134.07	-2.00	10.37	-0.16	-0.52	14	6
02167+5926	133.95	-1.29	12.04	-0.14	-0.59	50	3
02172+6752	131.19	6.69	3.80	-0.28	-0.56		35
02174+5655	134.88	-3.62	11.17	-0.37	-0.63	50	12
02181+5738	134.73	-2.93	12.79	-0.13	-0.60	15	5
02245+5823	135.26	-1.92	7.00	-0.11	-0.88		17
02252+6630	132.40	5.68	6.89	-0.27	-0.65		0
02272+6327	133.73	2.91	8.26	-0.29	-0.62		95
02289+5404	137.42	-5.70	9.98	-0.21	-0.82		8
02294+6411	133.66	3.69	6.49	-0.17	-0.76		0
02321+6312	134.33	2.89	7.61	-0.34	-0.53		95
02367+5155	139.36	-7.23	13.93	-0.30	-0.88		2
02408+5458	138.65	-4.20	11.70	0.25	-0.46		83
02467+5432	139.61	-4.22	4.68	-0.21	-0.70		2
02473+5152	140.86	-6.58	12.21	-0.35	-0.72	15	10
02570+5602	140.24	-2.22	5.69	-0.27	-0.50		28
03022+5409	141.79	-3.52	11.16	-0.17	-0.87	29	72

TABLE 4. (continued)

IRASNAME	l(o)	b(o)	F12(Jy)	C_{12}	C_{23}	LRS	var
03038+5046	143.68	-6.35	10.36	-0.37	-0.85		96
03151+5446	143.10	-2.03	6.66	-0.25	-0.69		19
03205+5223	145.06	-3.62	5.47	-0.39	-0.50		99
03316+5745	143.35	1.72	7.22	-0.26	-0.58		0
03317+6300	140.31	6.00	12.09	-0.32	-0.86	24	22
03347+6503	139.36	7.85	6.90	-0.34	-0.70		2
03380+5532	145.37	0.45	8.92	-0.22	-0.69		7
03409+6159	141.77	5.82	9.44	-0.22	-0.70		2
03466+4834	150.66	-4.27	7.20	-0.34	-0.82		7
03525+5711	145.92	2.98	7.13	-0.21	-0.70		99
03549+5602	146.92	2.31	3.88	-0.09	-0.74		38
04004+5547	147.67	2.62	10.72	-0.22	-0.84		5
04026+4737	153.32	-3.28	5.75	-0.20	-0.67		4
04050+4734	153.66	-3.04	3.80	-0.29	-0.40		13
04071+5215	150.76	0.64	9.78	-0.33	-0.65	14	96
04079+5135	151.29	0.24	6.54	-0.35	-0.59		8
04091+5054	151.90	-0.14	6.23	-0.07	-0.63		3
04112+4841	153.66	-1.52	7.50	-0.37	-0.63		2
04130+3918	160.41	-8.09	53.59	-0.51	-0.65	43	98
04166+5719	148.26	5.26	8.25	-0.17	-0.48		42
04264+3853	162.55	-6.53	11.53	-0.09	-0.72	29	97
04269+3550	164.86	-8.55	2.83	0.54	0.33		0
04402+3426	167.73	-7.46	3.39	-0.23	-0.65		75
04470+3002	172.08	-9.18	5.95	-0.12	-0.73		99
04536+5726	151.52	9.05	13.56	-0.34	-0.74	14	80
05131+4530	162.95	4.33	27.80	0.24	-0.52	42	99
05274+3345	174.20	-0.08	6.89	1.00	0.81		0
05342+2744	180.03	-2.15	3.85	0.57	0.08		0
05506+2414	184.96	-0.85	14.93	0.63	0.21		0
06099+1800	192.60	-0.05	107.20	0.54	0.93		0
20005+1635	56.10	-7.47	5.53	-0.12	-0.71		99
20010+2508	63.45	-3.03	9.12	-0.37	-0.75		37
20020+1739	57.22	-7.22	8.51	-0.21	-0.81		99
20021+2156	60.86	-4.95	11.56	-0.32	-0.82		99
20029+2759	66.08	-1.87	6.94	-0.23	-0.56		47
20046+2954	67.90	-1.15	11.47	-0.20	-0.73		99
20053+2958	68.03	-1.23	11.50	-0.10	-0.65	14	99
20084+2750	66.62	-2.98	9.73	-0.09	-0.71	14	99
20121+1756	58.74	-9.08	4.47	-0.29	-0.59		5
20127+2957	68.90	-2.58	10.53	-0.28	-0.81		99
20137+2838	67.93	-3.49	4.46	0.32	-0.62		94
20139+2404	64.15	-6.08	12.33	-0.24	-0.80	27	99
20178+2832	68.37	-4.30	10.92	-0.25	-0.85		59
20181+2927	69.16	-3.83	5.95	-0.23	-0.71		71
20190+2423	65.06	-6.86	7.83	-0.22	-0.65		99
20246+2813	68.97	-5.71	13.56	-0.07	-0.85		99
20285+2411	66.15	-8.75	4.17	-0.36	-0.45		15
20287+2719	68.74	-6.96	7.20	-0.14	-0.81		99
20304+2241	65.18	-9.98	3.47	-0.21	-0.67		6
20491+4236	83.42	-0.89	54.81	0.10	-0.65	43	99
20523+5302	91.76	5.40	11.07	-0.09	-0.70		97
20567+4727	87.98	1.23	17.09	-0.19	-0.80	25	64
21149+4634	89.43	-1.65	13.85	-0.17	-0.72		0
21415+5025	95.28	-1.83	8.29	-0.21	-0.63		93
22045+6306	105.60	6.20	11.69	0.06	-0.63		97
22112+5322	100.72	-2.28	14.50	-0.28	-0.71	25	62

III.3. Comparison in samples and detection rate

Though there have been a lot of observations in SiO maser lines, to compare the results is difficult because of the difference in observational system. By the Nobeyama 45m telescope system that is the most sensitive around 43GHz, more than 500 sources in the outer disk, inner disk and bulge have been searched in the SiO J=1-0 v=1 and v=2 lines at the limit of about 1Jy at 5 sigma level, the deepest survey until now. Therefore we can compare the observational results objectively in the sense that no bias effect is induced by the system difference.

With the Galactic latitude $|b| < 10°$, the observed sources are divided into three groups as in the Galactic bulge, inner disk and outer disk. The 244 sources in the second and third quadrants belong to the outer disk group and the 22 sources with Galactic longitude $30 < l < 90$ belong to the inner disk group without any argument. However in the survey to the bulge direction, whether an object belongs to the inner disk or to the bulge group is not direct. Their memberships are judged in such ways as calculating distance from light variation period or luminosity function, depending on available observational data of individual sources. The details of assigning the membership of these sources are described by Izumiura et al.(1995a,b) and the result is that 201 stars belong to the bulge group and 112 to the inner disk group. Therefore in all the 579 sources observed by using the 45m antenna of Nobeyama Radio Observatory, 201, 134 and 244 sources belong to the bulge, inner disk and outer disk respectively.

III.3.1. Samples

The basic and possibly most important selection criterion of the samples is the IRAS colors as there is little other systematic observations to these optically thick sources in addition to IRAS. The IRAS color C_{12} is always within the range [-0.4, 0.4], typical of a late-type star with cold CSE of about 600K to 200K. The IRAS color C_{23} should be used with combination of C_{12} to clarify the nature of sources. But in the survey to the bulge direction, no limitation was set to IRAS color C_{23} or quality of flux at 60μm. Some of the sources have IRAS color $C_{23} > -0.4$ and would be suspected as young stellar objects other than late-type stars. But because the pollution from infrared cirrus to 60μm flux is serious in the Galactic plane to the bulge direction(Ivezić & Elitzur 1995), their apparent values of C_{23} are redder than the

TABLE 4. (continued)

IRASNAME	l(o)	b(o)	F12(Jy)	C_{12}	C_{23}	LRS	var
22367+5537	105.05	-2.30	10.17	-0.22	-0.72		81
22394+6930	112.03	9.71	5.61	-0.26	-0.71		90
23280+7107	116.48	9.56	10.14	-0.35	-0.72		0
23361+6437	115.29	3.13	4.07	0.03	-0.54		74
23431+6204	115.38	0.45	7.08	-0.19	-0.63		7
23457+6045	115.35	-0.91	9.57	-0.26	-0.64		0
23561+6037	116.55	-1.32	8.01	-0.32	-0.49		17

intrinsic. A careful investigation furthermore indicates that the quality of F_{60} is unreliable for most of such sources with $C_{23} > -0.4$. The apparent colors of young stellar objects can be regarded as forged. So the sources in the bulge survey are almost late-type stars though there could be a few young stellar objects. In the other surveys of the outer and inner disks, C_{23} is set to be < -0.4 to exclude young stellar objects so that only late-type stars are left in the observations. Therefore in general the samples are consisted of late-type stars with cold CSEs.

Besides the IRAS colors, the selection criteria also concern F_{12} and IRAS variability Var. Var is an index between 0 and 99 to judge the possibility for a source being variable from the IRAS multi-times measurements. The survey to the bulge direction looked for the sources with $F_{12} > 1$Jy and the other observations for the sources with $F_{12} > 3$Jy. The Var is set as > 50 only for the 1995 surveyed outer disk sources and free for all the other observations. In the final executed observations, there were trifle deviations from the criteria.

In order to know the general features of the outer disk, inner disk and bulge groups, the mean values and standard deviations of C_{12}, F_{12} and Var are listed in Table 5.1.

As shown in Table 5.1, the outer disk, inner disk and bulge samples align a reddening sequence of color C_{12}. Since there is no correction to the colors for interstellar extinction which follow the same sequence of seriousness, the effect of interstellar reddening should be estimated to figure out if the color sequence is intrinsic. The SiO maser survey to the bulge direction objects tried to avoid the area of $|b| < 3°$ of serious extinction. According to the estimation by Frogel(1988), the extinction at K band $A_K = 0.17$mag at b=3°. Then based on the extinction law(Mathis 1990), $A_{12\mu m} = 0.04$mag and $A_{25\mu m} = 0.02$mag. The color reddening is only 0.01 at C_{12}, much less than the difference presented by the bulge and outer disk sample. The color sequence is then mostly intrinsic. Bedijn(1987) showed that for a given model C_{12} depends only on the optical depth in the infrared. Bedijn(1988) explained the IRAS color sequence of stars with cold CSEs is that of accelerated mass loss with time, i.e. the redder stars have larger mass loss rate and in later stage of evolution. This means that the bulge sample has the thickest CSE and is in the latest stage of evolution among the three groups as a general tendency. Besides the evolutionary effect on the IRAS colors, metallicity may also play a role. It's suspected that the metals would redden the stars(Habing 1996). Observations showed that the Long Period Variable stars in the MCs are not so red in IRAS colors as those in the Galactic bulge with the same period, i.e. luminosity or mass.

TABLE 5.1. Mean value & standard deviation of C_{12}, F_{12} and Var

	bulge	inner disk	outer disk
C_{12}	0.033±0.075	-0.022±0.127	-0.217±0.140
F_{12}	5.553±2.453	13.235±21.091	32.606±101.65
Var	79.871±32.568	75.015±35.033	53.779±41.168

Though the metallicity gradient in the Galaxy is not clearly quantitatively established, the declining tendency with Galactocentric distance is however seen in several works. The study of globular clusters found a slope $\sim \triangle[Fe/H]/R_{gc} = -0.091$(Friel 1995).

The bulge sample is the faintest in the flux density F_{12} averagely. This is expected from the distance effect. Because the sources in the bulge are about 8kpc or further away where an M-type star with 300K CSE is < 4.4Jy strong at 12μm(Nakada et al. 1993). While in the inner disk and outer disk samples, many sources are nearby and their average distances are shorter than 8kpc. Furthermore, because of inclusion of some very bright objects like R Cas in the outer disk sample, the standard deviation gets very big. As the inner disk sample looked for some sources beyond the bulge(Jiang et al. 1995). the average F_{12} is fainter than that of the outer disk sample. If F_{12} can be taken as a distance indicator in the limited color range i.e. the same kind of objects, the outer disk sample is the closest and the bulge sample is the furthest.

The average IRAS variability index Var is almost the same for the bulge and the inner disk samples and somewhat smaller for the outer disk sample even though the 1995 outer disk survey only looked the sources with $Var > 50$. In present selected range of F_{12}, the sources with $Var > 50$ were variable at 12μm within the IRAS photometric accuracy(Chapter II). Most of stars in the bulge and inner disk samples are variable and there is quite a fraction in the outer disk sample being non-variable. The IRAS survey strategy produced more confirmed observations in some regions than the others at time intervals suitable for detecting variability and some spurious indications of variability in regions of high source density(Beichman 1988). However, the SiO-surveyed regions are not IRAS-biased. So it could be true that there is more proportion of variables in the bulge and inner disk samples than in the outer disk sample.

For the sources in which SiO maser emissions were detected , the above three parameters, C_{12}, F_{12} and var are compared again and shown in Table 5.2.

There is little difference in C_{12} between SiO maser sources and the sample in every given group. As is shown in Fig. III.3, the bulge SiO maser sources have mainly $C_{12} < 0.0$, the outer disk SiO maser sources mainly have $C_{12} > 0.0$ and the inner disk is intermediate. Regarding of F_{12}, except the bulge SiO maser sources that differ little from the sample, the disk SiO maser sources are averagely brighter than the samples. That means there are many nearby and not so many distant SiO maser sources in the disk which possibly due to that the nearby SiO maser sources are apparently bright and thus easily detectable. The variability

TABLE 5.2. Average C_{12}, F_{12} and Var of SiO maser sources

	bulge	inner disk	outer disk
C_{12}	0.03±0.08	-0.00±0.11	-0.20±0.24
F_{12}	5.60±2.52	16.58±21.59	67.00±174
Var	84±29	84±28	77±33

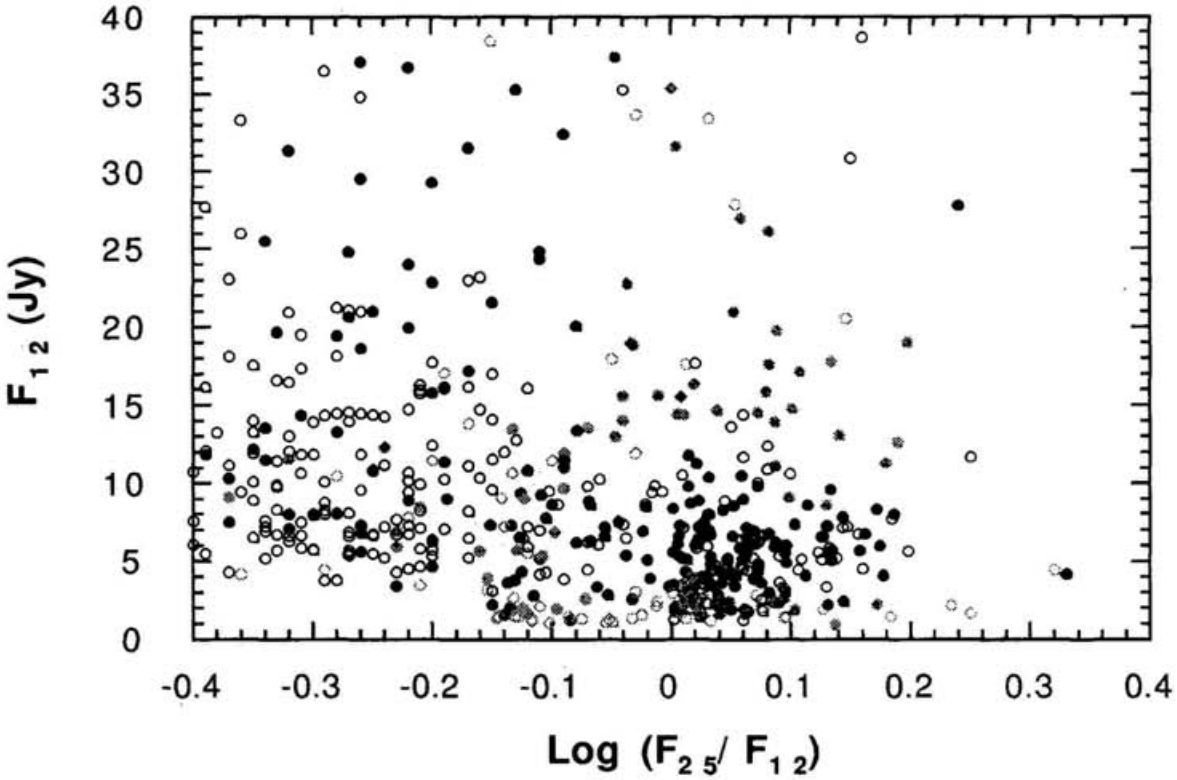

Fig. III.3.— Flux at 12 μm and color C_{12} of the observed sources. The red is for the bulge object, the purple is for the inner disk object and the blue for the outer disk object. Filled circles are SiO detections and open ones SiO non-detections.

index is the same in the inner disk and bulge groups. The outer disk SiO maser group has a little lower average variability index but much higher than the sample itself.

III.3.2. Detection rate

It has been noticed that the SiO maser detection rate in the outer disk is much lower than that in the bulge survey (Chapter II). The difference is mainly attributed to the more inclusion of C-rich stars in the outer disk sample based on the analysis of near-infrared observational data (Chapter II). Here I will brief the change in detection rate after including the 1996 May observational data. In Table 6.1, the numbers of SiO detections and non-detections in the bulge, inner disk and outer disk are shown for all the stars observed in the bulge survey and the outer disk survey.

Since no new data is collected for the bulge source, the detection rate remains 66%, the same as analyzed by Jiang et al. (1995). The detection rate in the inner disk is 51%, a little bit lower than 54% from the sample to the bulge direction. There could be some errors to assign the membership of the stars in the bulge direction, e.g. to mistake the bulge stars as inner disk stars since the method to separate the bulge and disk stars is not very certain.

There could be another possibility that there is a slightly decreasing detection rate with increasing Galactic longitude even in the inner disk. As the 1996 May observation of the stars with Galactic longitude between 55° and 70° yielded 42%, about 12% lower than the disk sources in the bulge direction. According to the analysis in Chapter V, the basic reason is that the stars with $55° < l < 70°$ are averagely further from the Galactic center and have lower metallicity and thus more proportion of C-rich stars. The detection rate in the outer disk is now 31%, also lower than 39%, the result shown in Chapter II. This is also expected since the 1996 observation only looked for the stars with $F_{12} < 15$ Jy, i.e. further than 4kpc or so where there are more C-rich stars and resulted in only 13% detections, much lower than previous average detection rate.

If we take the F_{12} as a distance indicator as these objects more or less belong to the same type of stars and should have similar luminosity, then the variation of detection rate with Galactocentric distance is given in Table 6.2. It seems there is no definite tendency that the highest detection rate happens in the inner disk part with $F_{12} > 15$Jy. But if we take the distance-to-us effect into account, it's easy to find the decreasing tendency of detection rate with the Galactocentric distance. For example, the inner disk group and outer disk group with $F_{12} > 15$Jy have different population of SiO maser stars, 70% and 52% respectively, even their average distances to us are supposed to be the same. This is also the case of inner and outer disk groups with $F_{12} < 15$Jy. The bulge group is the furthest but deserves the highest detection rate. This result is in agreement with the explanation of low detection rate in the outer disk by the difference of proportion of C-rich stars with metallicity or with Galactocentric distance as in Chapter V.

III.4. Summary

The survey in SiO maser line transitions J=1-0, v=1 and v=2 and isotopic ^{29}SiO J=1-0 v=1 line is carried out by using the 45m telescope system at Nobeyama Radio Observatory from 1994 through 1996. This survey is concentrated on the IRAS PSC sources with typical colors of AGB stars surrounded by a cold circumstellar envelope, the same as the survey towards the bulge direction. Combining these two survey data, totally 579 stars, among which 201, 134 and 244 in the bulge, inner disk and outer disk respectively, are searched for SiO maser emission at a sensitivity limit of about 1Jy at 5 sigma level. Comparison between the bulge, inner disk and outer disk sample found that they consist a sequence of IRAS color

TABLE 6.1. Detection rates for all the stars observed

	bulge	inner disk	outer disk
Detections	133	69	76
Non-detections	68	65	168
Total	201	134	244

C_{12}, variability and flux at 12μm. They are a sequence of SiO maser population as a possible consequence of Galactic metallicity gradient.

TABLE 6.2. Change of detection rate with the Galactocentric distance

Bulge	Inner disk		Outer disk	
	F_{12} <15Jy	F_{12} >15Jy	F_{12} >15Jy	F_{12} <15Jy
66%	45%	70%	52%	18%

REFERENCES

Bedijn, P.J. 1987, AA 186, 136

Bedijn, P.J. 1988, AA 205, 105

Beichman, C.A., Neugebauer, G., Habing, H.J., Clegg, P.E., & Chester, T.J. 1988, IRAS Catalogues and Atlases Explanatory Supplement, US Government Printing Office, Washingon DC

Friel, E.D. 1995 Ann. Rev. Astro. Astrophy. 33, 381

Frogel, J.A. 1988, Ann.Rev.Astr.Astrophy. 26, 51

Habing, H.J. 1996, Astron.Astrophy.Review 7, 97

Ivezić, Ž, & Elitzur, M. 1995, ApJ 445, 415

Izumiura, H., Catchpole, R., Deguchi, S., Hashimoto, O., Nakada, Y., Onaka, T., Ono, T., Sekiguchi, K., Ukita, N., & Yamamura, I. 1995a, ApJS 98, 271

Izumiura, H., Deguchi, S., Hashimoto, O., Nakada, Y., Onaka, T., Ono, T., Ukita, N., & Yamamura, I. 1994, ApJ 437, 419

Izumiura, H., Deguchi, S., Hashimoto, O., Nakada, Y., Onaka, T., Ono, T., Ukita, N., & Yamamura, I. 1995b, ApJ 453, 837

Jiang, B.W., Deguchi, S., Izumiura, H., Nakada, Y., & Yamamura, I. 1995, PASJ 47, 815

Jiang, B.W., Deguchi, S., Yamamura, I., Nakada, Y., S.H.Cho & Yamagata, T. 1996, ApJS 106, 463

Mathis, J.S. 1990, Ann.Rev.Astr.Astrophy. 28, 37

Nakada, Y., Onaka, T., Yamamura, I., Deguchi, S., Ukita, N., & Izumiura, H. 1993, PASJ 45, 179

Spencer, J.H., Winnberg, A., Olnon, F.M., Schwartz, P.R., Matthews, H.E., & Downes, D. 1981, AJ 86, 392

Chapter IV

Optical identification

This chapter has been published in
The Astronomical Journal, 111:231-259, 1996 October
as
Optical identification of IRAS sources in the outer disk
co-authored by
S. Deguchi and Y. Nakada

ABSTRACT

The optical identifications at both V and I bands are given of 102 color-selected IRAS PSC sources in the outer disk of our Galaxy. The positions were obtained from CCD images by using stars in the same frame and listed in the GSC catalogue (Guide Star Catalogue for Hubble Space Telescope) as references. The identification was judged from the consistency with IRAS parameters in three aspects: the position, color and light variation. About 50% of these sources are found to have optical counterpart. We identified 47 sources as variable stars, 2 as non-variable stars. There are 1 star that has not been checked light variation and 9 sources associated with nebulosity in the sample. We did not find optical counterparts for 43 sources until as faint as 20mag at V band and 19mag at I band. The data suggest that whether or not an IRAS PSC source can be optically identified results from not only the IRAS colors but also the C/O abundance in such a way that an oxygen-rich source may be more likely to be identified than a carbon-rich source.

IV.1. Introduction

The InfraRed Astronomical Satellite (IRAS) surveyed about 96 percent of the sky in bands centered at 12, 25, 60 and 100μm. More than 250,000 point sources were detected and their flux densities and positions are listed in IRAS Point Source Catalogue (IRAS PSC). But because only about 70,000 of these sources are associated with objects in astronomical catalogues, a major identification is required in order to realize and develop the IRAS potential. A lot of work has been devoted to the identification of IRAS point sources such as the identifications of galaxies by Wolstencroft et al.(1986), Wang et al.(1991) and Klass & Elsässer (1993), of pre-main sequence stars by Prusti et al.(1992), of carbon stars by Groenewegen & de Jong(1993), of the IRAS LRS sources by Jiang & Hu(1992), and of the sources in the Ophiuchus molecular cloud by Ichikawa & Nishida(1989).

Usually the identification has two criteria. First is the coincidence with the IRAS PSC position. However the IRAS PSC position is usually as uncertain as about $10'' \times 20''$ so that there may be more than one object locating inside the IRAS position uncertainty area especially in crowded field. Therefore the second criterion is necessary and usually goes to the judgment on physical features of objects. The identification of galaxies can be confirmed by their extended morphologies while stellar objects have to be confirmed in other ways. So far stellar color index has been popularly used because stars in different stages of evolution have different colors in both optical and IRAS color-color diagrams. Besides the color, stellar spectral type was also used for identification (Ichikawa & Nishida 1989). We will use a new parameter, stellar light variation, to identify the IRAS PSC sources in the outer disk of the Galaxy as well as the color index and position coincidence with IRAS sources.

IRAS sources are a good probe for Galactic structure (Weinberg 1992a, 1992b). For such study it is essential to obtain the distances to IRAS sources from, for example, the period-luminosity relation(e.g. Whitelock et al. 1994). We have started a project to identify distant IRAS sources in the outer Galaxy at optical wavelengths, and to measure periods of variable stars. In this paper, we report the first part of this project, optical identification of the IRAS sources.

IV.2. Selection of objects

The sources in the IRAS PSC catalogue (version 2.0) were chosen according to the following criteria:

1) The location is in the northern outer Galaxy with Galactic longitude between 90° and 230°, Galactic latitude between -10° and 10°.

2) The IRAS flux qualities are 333 at 12, 25 and 60μm, i.e. the IRAS photometric results have high-qualitis at relevant wavelengths(Beichman et al. 1985).

3) The IRAS flux density at 12μm is brighter than 3 Jy.

4) The IRAS color $C_{12} \equiv \log_{10}(F_{25}/F_{12})$, in which F_{12} and F_{25} are the IRAS flux densities at 12μm and 25μm, is between -0.3 and 0.3. We will use F_{60} as the IRAS flux density at 60μm.

5) The IRAS variability index is bigger than 50(Beichman et al. 1985).

For the purpose of studying the Galactic kinematics, we try to pick up the candidates for

Mira variables and SiO maser emitters. Optical Miras have some evident features such as red color and light variation with large amplitude. Their IRAS associations locate in some region in the IRAS color-color diagram, i.e. C_{12} in [-0.45, 0.2] and C_{23} ($\equiv \log_{10}(F_{60}/F_{25})$) in [-1.0, -0.6](van der Veen & Habing 1988). As well as the IRAS colors are used to choose Miras, the IRAS variability index is also used corresponding to their light variation. Weinberg(1992a, 1992b) and Allen et al.(1993) chose the IRAS sources with IRAS variability index equal to or bigger than 98 as Miras to study Galactic structure. Whitelock et al.(1994) detected only one non-Mira source of 33 IRAS PSC sources with IRAS variability index bigger than 90. We select the sources with IRAS variability index bigger than 50 because they were surely IRAS-variable when their F_{12} is brighter than 3Jy. Regarding the SiO maser emitters, the sources with IRAS color C_{12} in [-0.3,0.3] and F_{12} brighter than 3Jy were detected SiO masers in high percentage towards the Galactic bulge(Izumiura et al. 1994, 1995a, 1995b, Jiang et al., 1995). That's why we use the above selection criteria. There are 121 sources falling into the selection, 19 of which have been identified as variable stars in light of SIMBAD database. Our observation and identification are then towards the other 102 objects of which nature have not been clarified.

Of course the selection criteria can not pick up all the IRAS sources that are potential Miras. As some Miras are bluer than -0.3 in color C_{12}(van der Veen & Habing 1988), we may miss some Miras which have not so thick circumstellar envelopes (CSE) as to show large infrared excess. We may also miss the Miras which have IRAS variability index less than 50 (Whitelock et al. 1994). The selection may contain some other types of objects besides Miras. There could be semi-regular and irregular variables. In color region where C_{12} is redder than 0.0, there may be some OH/IR stars (van der Veen & Habing 1988) and young stellar objects in star forming regions (Harris et al., 1988) that show excess at 60μm since no constraint is placed on C_{23}.

IV.3. Observation and data reduction

The photometric observations were performed using a 105/150cm Schmidt telescope attached with a CCD camera at Kiso Observatory, University of Tokyo. The CCD camera contains a TI Japan TC215 chip with an array size of 1024 × 1024 pixels. The field of view is about 12.5′× 12.5′ and one pixel is 0.75″ in the sky. The CCD images were taken at both V and I filters for every source. The V filter is the same as that in the Johnson system but the I filter is centered at 8200Å, bluer than 9000Å in the Johnson system. The limiting magnitudes we reached are about 20 mag at V band and 19 mag at I band. All non-nebular sources were observed at least twice with interval mostly longer than 60 days except, IRAS 06181+0406, 22045+6306 and 22103+5120 that we missed. The observations were done from July 1994 to March 1995 about once a month and the observational log is shown in table 1 where the IRAS name and Julian dates of observations for all the sources are listed. The seeing was typically 3″. The raw data were processed using image data reduction software IRAF by subtracting bias and dividing by dome flat field.

IV.4. Method of Identification

IV.4.1. Coincidence with IRAS position

The uncertainties of IRAS PSC positions are approximately elliptical in shape, as a result of the rectangular shape of the individual detectors used in the survey and their distribution in the focal plane (Beichman et al. 1985). In searching for associations of the IRAS PSC sources with objects in catalogues having small position errors, the IRAS team selected an elliptical search area with semi-major and semi-minor axes of 45″ and 8″ (Beichman et al. 1985) which can be regarded as typical values of the uncertainties. In our case the mechanical pointing error of the Kiso Schmidt telescope is bigger than the uncertainties of the IRAS PSC positions. So our approach is divided into two steps: to correct the telescope's pointing error and to take the uncertainties of the IRAS PSC position into account.

About 7 to 10 stars, which are listed in the Guide Star Catalogue (GSC) for Hubble Space Telescope and close to the center of the CCD frame, were taken as position reference stars inside one CCD frame. Their equatorial coordinates (Epoch 2000.0) listed in the GSC catalogue are accurate to 0.2″ - 0.8″ (Russel et al, 1990). Their coordinates in the CCD frame in unit of pixel are measured using IRAF package that calculates the object position from Gaussian fitting to its intensity distribution. This position brings about little error in succeeding calculation as its accuracy, better than 0.1 pixel, is less than 0.075″ in the sky. Because the field of view is only 12.5′ × 12.5′ and the smaller central region is actually used, the transformations between equatorial coordinates and CCD coordinates are calculated by least square linear fitting for every CCD frame. The following are the equations we used to transform the CCD coordinates X and Y to the equatorial coordinates α(right ascension) and δ(declination), vice versa.

$\alpha = a_0 + a_1 \times X + a_2 \times Y$

$\delta = b_0 + b_1 \times X + b_2 \times Y$

The a_0, a_1, a_2, b_0, b_1 and b_2 are the coefficients to be fitted by the least square method. The rms is always less than 1″ and mostly less than 0.5″ for the reference stars. Traditionally the second-order correction of coordinate transformations should be added to the linear terms. It was also tested by us and little was improved. One reason is that the first-order approximation has reached the accuracy limit of the positions of reference stars as that of the GSC catalogue. The other reason is that the reference stars which were added for second-order correction had to be further from the center of the CCD frame than those used for only first-order fitting and thus the second-order correction was compensated for the bigger deviation from the center.

In this way we first find the corresponding position in the CCD frame of given IRAS PSC position (Epoch 2000.0). Searching for optical counterpart will then be constrained to the elliptical area centered at the IRAS position with major and minor axes a little bigger than that of the IRAS position uncertainty ellipse. After the optical counterpart is fixed by examining the color and light variation which will be described in detail in next sections, the equatorial coordinates(Epoch 2000.0) of the counterpart are transformed from its CCD coordinates. The difference of equatorial coordinates (Epoch 2000.0) between the IRAS and optical counterpart is calculated and is very small, normally less than 10″. This value is little different in epoch 2000.0 and 1950.0 so it is offset to the IRAS position (Epoch 1950.0) to calculate the optical-counterpart position(Epoch 1950.0). The position determined in this

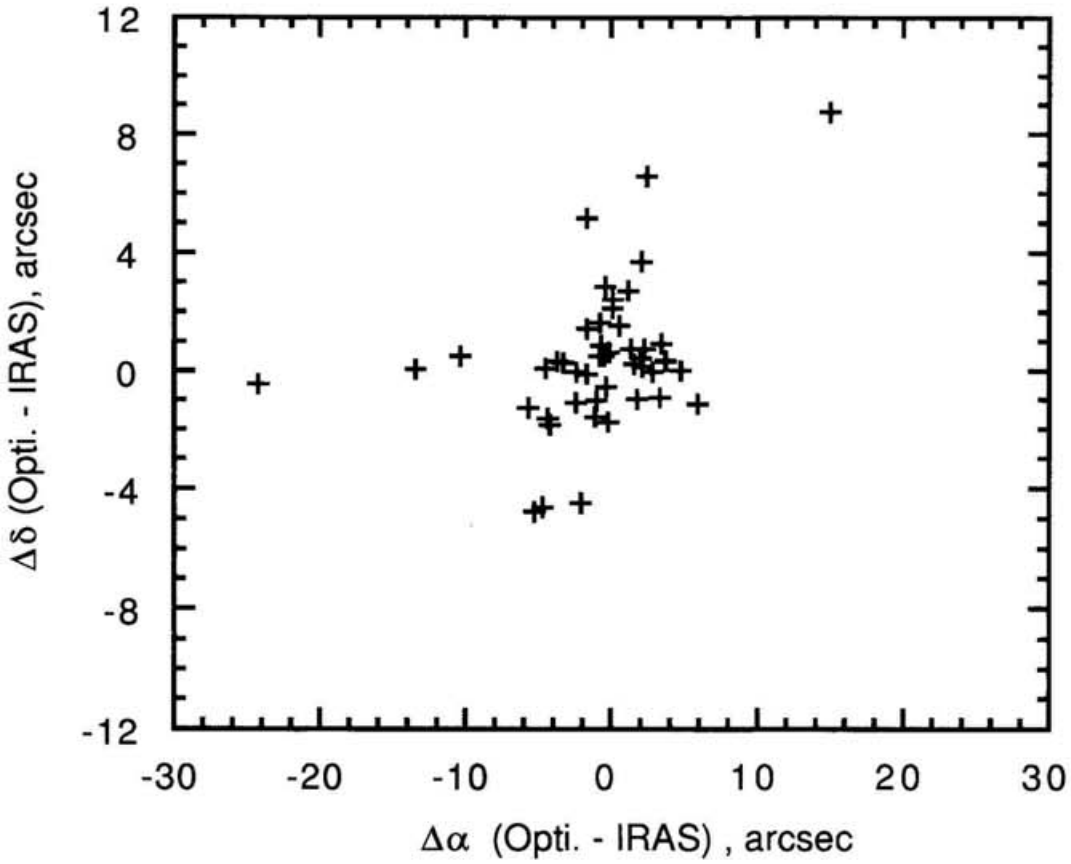

Fig. IV.1.— Position differences between optical counterpart and IRAS PSC coordinates for the 47 identified variable stars. Both $\Delta\alpha$ and $\Delta\delta$ are in unit of aresec.

way is much more accurate than the IRAS PSC position and can be used for further study instead of the IRAS PSC position.

IV.4.2. Red color

The IRAS objects we chose are mainly variable objects with cold circumstellar envelope (CSE) (Van der Veen and Habing 1988). The strong absorption of stellar radiation by the dust in CSE makes the object a) invisible in optical wavelengths when the CSE is optically thick or b) visible and red in the optical wavelengths when the CSE is optically thin. In case a), we can not identify the source in optical image while we can possibly identify it in longer wavelength. In case b), we can identify the object optically as the task of the present work and the source should be brighter at I band than at V band. So an object inside the uncertainty ellipse of IRAS PSC position can be regarded as a candidate for the optical counterpart only if it is brighter at I band than at V band.

IV.4.3. Light variation

The sources in our sample have the IRAS variability indexes bigger than 50, i.e. the IRAS satellite detected more than 10% change in fluxes at both 12 and 25μm consistently. Since the IRAS flux densities of the selected sources are brighter than 3 Jy at 12μm in high quality, the mean IRAS photometric uncertainty for such sources is 7% (Beichman et al. 1985), smaller than the percentage of variation. So these sources were surely detected variable at 12 and 25μm. They are expected to be optically variable too unless the object stopped variation after the IRAS mission.

The weather at Kiso during our observations was not always good enough to calibrate the instrumental magnitude into standard system magnitude by correcting atmospheric extinction as standard reduction, so we measured the light variation by comparing with neighbouring stars. It is assumed that most of the stars are not variable in measurable amplitude as is usually believed. First in a $5' \times 5'$ square area which is centered at the object closest to the IRAS PSC position, we choose all the stars that are detected above 4σ level and in the CCD linear response range. These stars are used as photometric references. The number of the reference stars is usually more than 50 and varies with integration time and field. Their instrumental magnitudes were calculated in a batch mode by the IRAF DAOPHOT (Stetson, 1987) package using the point spread function. Because the sky condition is quite uniform in this small area, the atmospheric extinction can be regarded the same for all these reference stars in a frame when their colors are not very different. Then the IRAF instrumental magnitudes of the reference stars in observations at two separate nights are compared to calculate the shifts with magnitude for non-variable stars by least square linear fitting. The light variation of the source is expressed as the deviation from the fitting line. The rms of fitting is mostly less than 0.05mag. But taking into account the photometric error and the error from stellar color, we assign the source as variable only when the amplitude of light variation is bigger than 0.2mag.

IV.5. Result

IV.5.1. Variable stars

There are 47 IRAS PSC sources identified as variable stars. These stars have been observed to become either brighter or fainter at both V and I band if they are visible at both V and I band. If the source is only visible at I band, more than once the light variations have been observed at I band. In any case, the amplitude of variation is bigger than 0.2 mag, more than the photometric accuracy. The variables with small amplitude and short period (since our observations were performed about once a month), for example the semi-regular and irregular variables of small amplitude, might be missed and our identifications correlate mainly with the characteristics of long-period variables with large amplitude, i.e. Miras.

Table 2 lists their IRAS PSC positions and optical positions with epoch of 1950. Column 1 gives the IRAS PSC name. Columns 2, 3 and 4 are right ascension α in unit of hour, minute and second of IRAS position. Column 5 is α of optical counterpart in unit of second only in which the difference happens between IRAS and optical positions. Column 6 is the uncertainty of optical position, defined as the rms (the method of fitting was described in

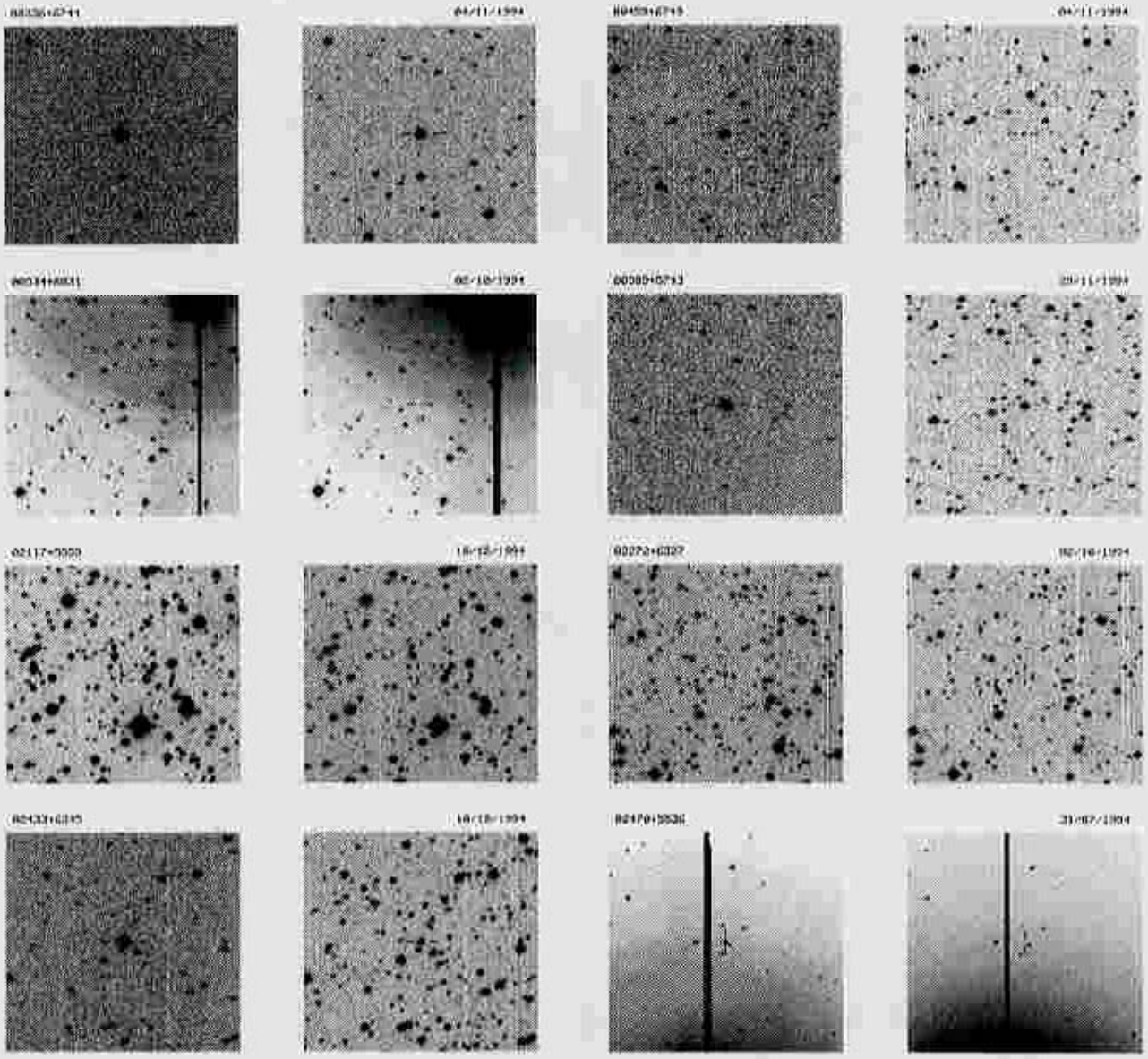

Fig. IV.2.(a)

Fig. IV.2.— Finding charts for the 47 identified variable stars. The size of one frame is $5' \times 5'$ with south up and west left. For every star, both images taken at V(right) and I(left) bands are shown and the date when the images were taken is written at the upright corner in the format date/month/year. The name of the IRAS source locates in the upleft corner. The bars label the identification.

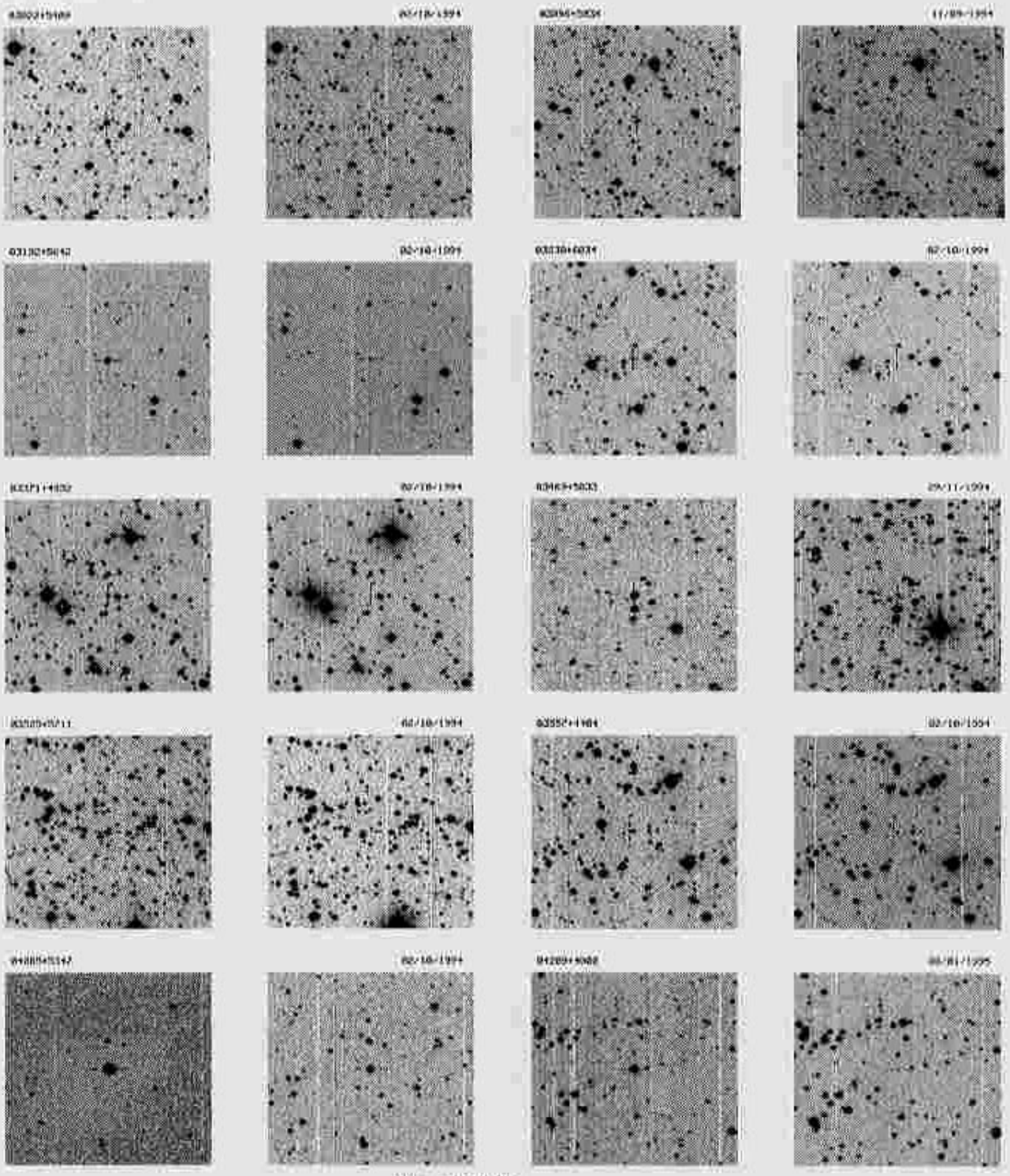

Fig. IV.2.(b)

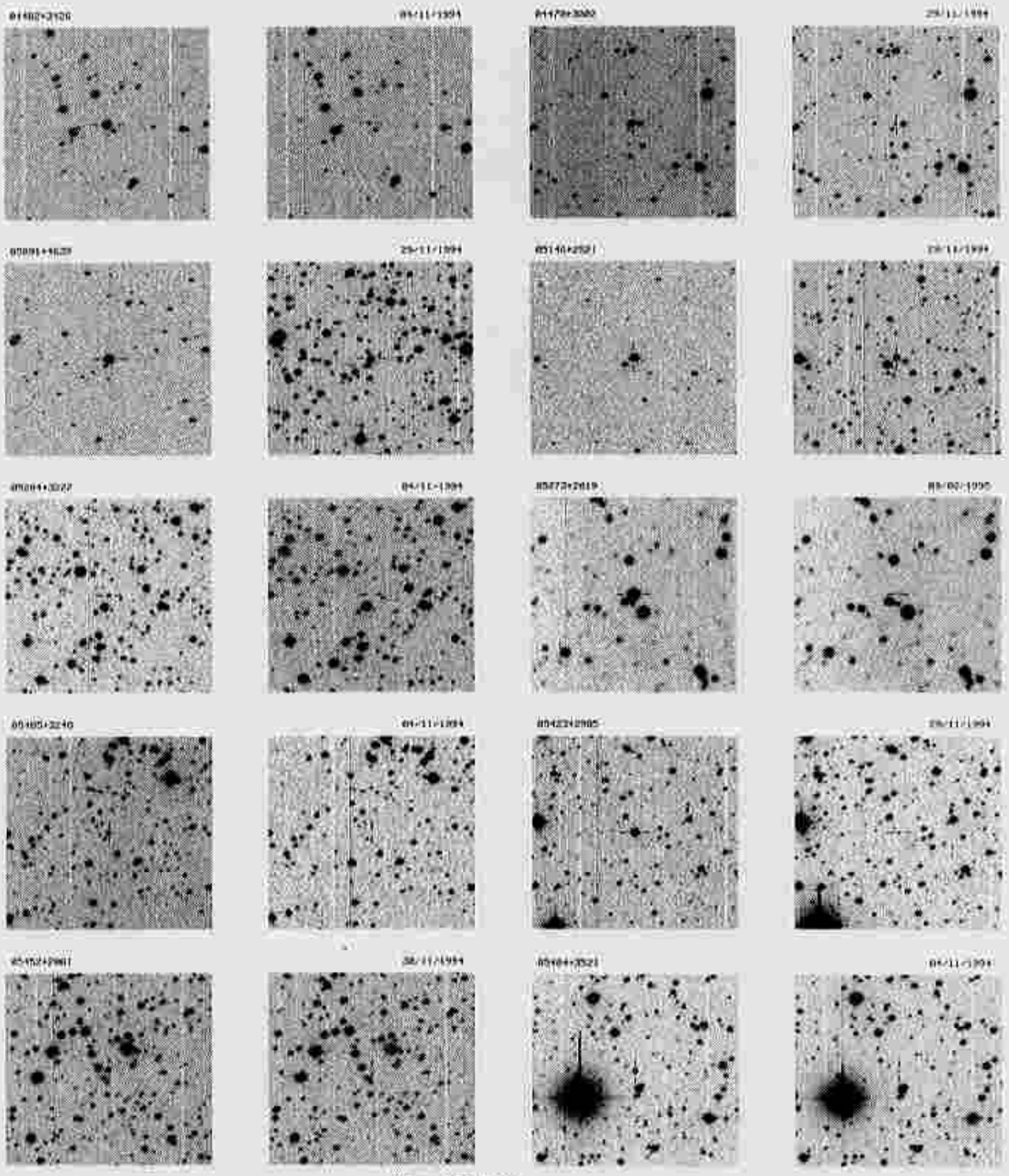

Fig. IV.2.(c)

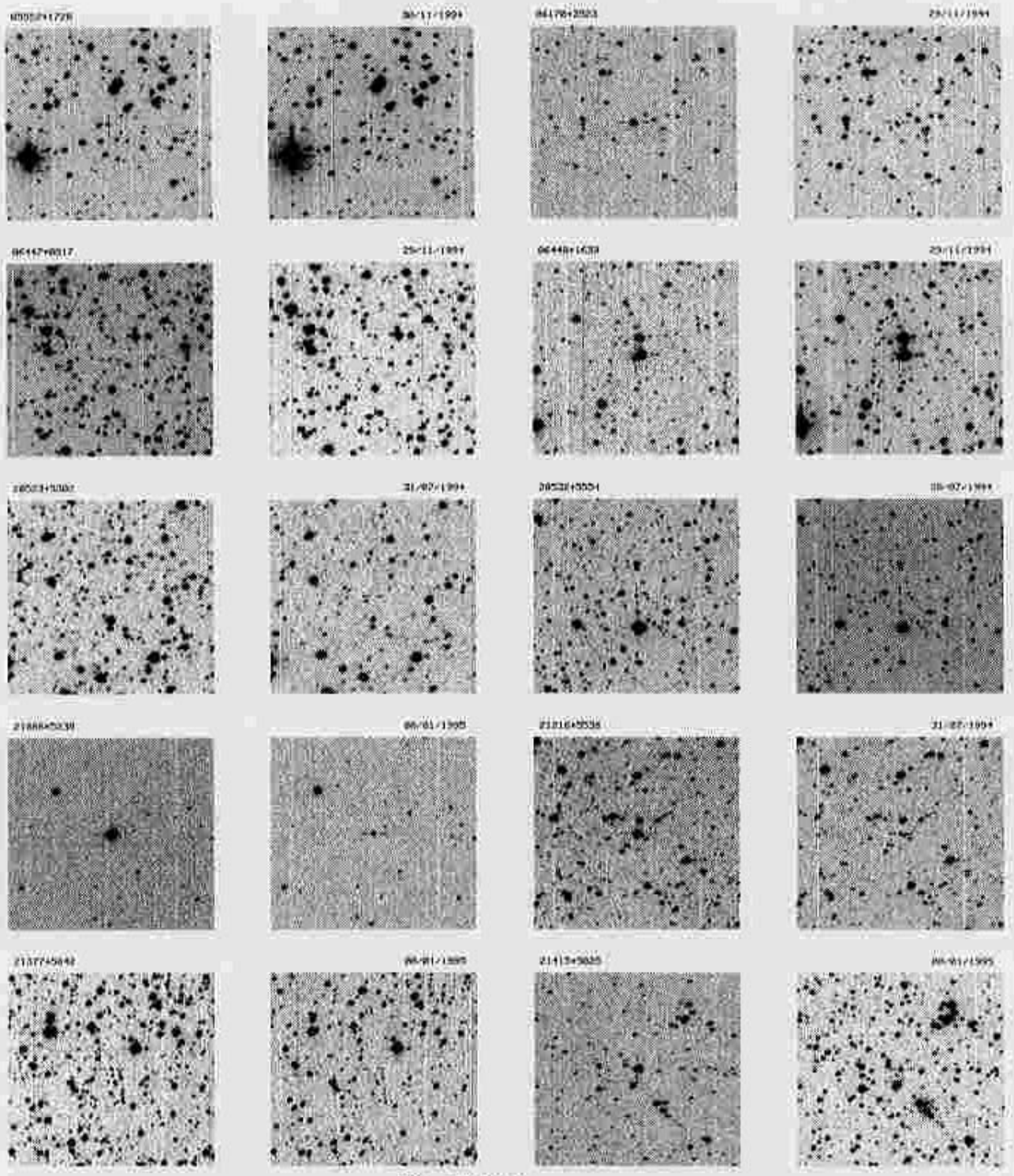

Fig. IV.2.(d)

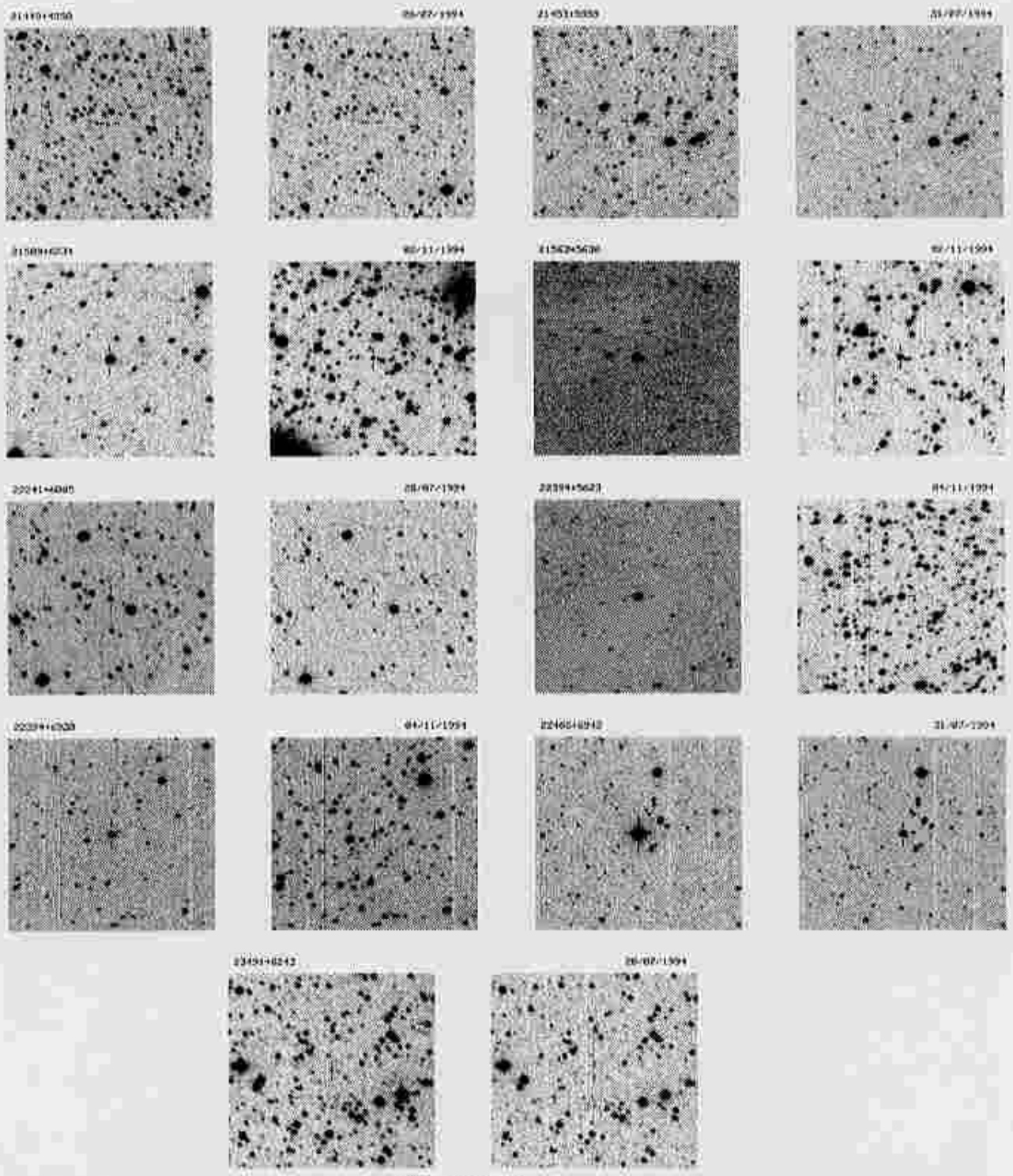

Fig. IV.2.(e)

above section) of position reference stars. Column 7 gives the offset of optical α to IRAS α as α(optical) - α(IRAS). Columns 8 to 13 are the same as columns 2 to 7 but for declination δ and in angular units.

Some IRAS parameters of these sources are shown in table 3 in the order of IRAS PSC name IRASNAME, Galactic longitude GLO, Galactic latitude GLA, flux at 12μm F_{12}, colors C_{12} and C_{23}, IRAS variability index VAR and IRAS LRS type LRS if available.

Fig.IV.1 shows the position difference between the optical star position and the IRAS PSC position of these sources. All the sources are located inside the area, $45'' \times 9''$, which was used by the IRAS team to search for associations of the IRAS PSC sources with stars in catalogue. Most of the sources have not been offset from IRAS position by more than $10''$ in right ascension or $5''$ in declination. The object at the top is IRAS 02433+6345 and the object at the most left is IRAS 04085+5347, they are at the outside edges of the IRAS PSC position uncertainty ellipses. The averages of offsets from the IRAS positions are $-0.39'' \pm 4.3$ and $0.49'' \pm 2.3$ respectively for α and δ. The averages of position uncertainty, which is calculated by the fitting residuals of position reference stars, are $0.24''$ and $0.23''$ for α and δ. Although these sources are located at various parts in the sky, the distribution is still similar to the uncertainty ellipse of the IRAS PSC position, i.e. longer at α direction and shorter at δ direction.

The finding chart, with size as $5' \times 5'$ centering at each optical counterpart, is shown in Fig.IV.2 with south at the top and west to the left. In order to show the color clearly, the CCD images at both V and I bands taken in the same night are shown as the I image on the left and V image on the right. The optical counterpart, or the position where the optical counterpart should be in the case of invisible counterpart in V frame, is labeled by two bars. At the upper-left of the chart is the IRAS PSC name and at the upper-right is the date in the format date/month/year when the images were taken. In order to avoid CCD pixel saturation and to get high signal to noise ratio, the exposure time varies with stellar brightness so that the I image sometimes does not show faint objects which are shown in V image.

As an example, Fig.IV.3 exhibits the light variation of IRAS 02117+5559. The CCD images were taken both at I band on December 10, 1994 and March 21, 1995. This star was 3.57^{m} brightened in 101 days.

IRAS 02433+6345, 05091+4639 and 06170+3523 had ever been identified by Jiang & Hu (1993) in which their positions at K band were different from that of present optical counterparts. Since the present optical counterparts were checked light variation that was not done before, we think they are more potential to be IRAS objects. Further near infrared CCD imaging will be helpful to solve the discrepancy.

Although we have not yet converted the instrumental magnitudes accurately into standard magnitudes, a rough estimation from casually taken standard star fields showed that most of these variable stars have color V-I > 3 indicating that they are late-type such as M, S, C-type stars. Information on light curve and amplitude is necessary in order to distinguish Mira, semi-regular and irregular variables.

The first three volumes of fourth edition General Catalogue of Variable Stars (GCVS) collects about 28435 variables (Samus 1992) of all kinds in all the sky so that the average density of variables with amplitude bigger than 0.2 mag is less than 1 per square degree. The density of variables with amplitude bigger than 0.2mag in the outer disk where the stars are

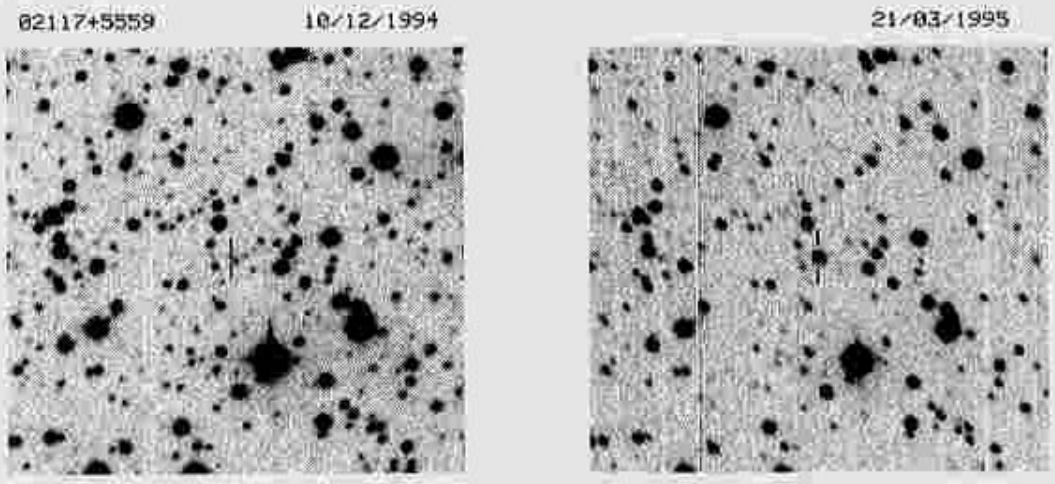

Fig. IV.3.— An example, IRAS 02117+5559, shows the light variation. The two images were taken both at I band but in two dates shown above the image. It is 3.57^m brightened in 101 days.

not as dense as in the inner disk on average is much lower than 1 per square degree according to the GCVS. Even we assume the density as 1 per square degree down to 19 magnitude at I band, the possibilty that an unrelated variable to be found in the searching area (about $10'' \times 30''$) is $(10'' \times 30'')$ / $(3600'' \times 3600'')$, i.e. 2.3×10^{-5}. So the possibility of background detection of a variable star is extremely small in the 47 cases identified here.

IV.5.2. Non-variable stars

There are 3 sources for which light variation have not been detected. They are IRAS 06241+1025, 06364+0450 and 22103+5120. But out of them, IRAS 22103+5120 was observed only once so that no information on light variation is available. IRAS 06241+1025 and 06364+0450 both have an optical counterpart near the IRAS position and no light variation bigger than 0.2mag was detected. Their positions, infrared properties and finding charts are shown in table 4, table 5 and Fig.IV.4.

IV.5.3. Sources associated with nebulosity

Besides stellar objects, there are 9 objects which are associated with optical nebulosities. Table 6 lists their infrared properties in the same format as table 3 for variable stars. Their finding charts are shown in Fig.IV.5. The arrangement of the images is the same as that of Fig.IV.2 except that the IRAS position is labeled by a '+' when there is no associated stellar object. Some of them have ever been identified such as IRAS 02570+6028 as a candidate for star formation region (Sugitani et al. 1991), IRAS 06283+1028 as a Be star associated with reflection nebula (Thé et al. 1994 and references therein), IRAS 21381+5000 as a Herbig-Haro

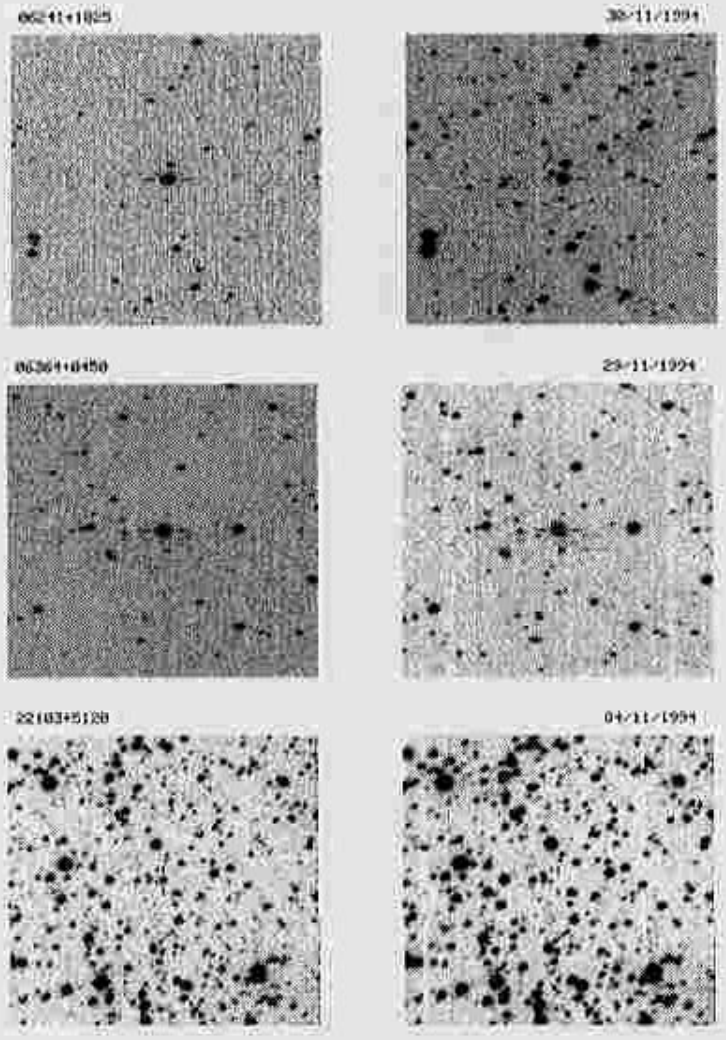

Fig. IV.4.— The finding charts for non-variable stars. Among them, IRAS 22103+5120 has not yet been checked light variation.

object (Molinari et al. 1993 and references therein). In the CCD images, IRAS 02570+6028 is crab like and IRAS 21381+5000 is butterfly like. Among the other sources, only IRAS 01036+5924 has an optical counterpart. But they were all detected in CO (Wouterloot & Brand 1989) and undetected in H_2O (Palla et al. 1991, 1993) except IRAS 01036+5924 which has not been searched for H_2O emission. These sources are possibly associated with young stars in molecular clouds.

IV.5.4. Unidentified objects

In addition to 47 variable stars, 3 non-variable stars and 9 sources associated with nebulosity, there are 43 IRAS PSC sources for which we could not find any optical counterparts. For some of these sources, there are stars inside the IRAS position uncertainty ellipses, but they are usually not red or they are very faint that the photometric results were unreliable. At present we think they have not yet been identified. Table 7 lists the infrared properties of these sources in the same form as table 3. These sources have optically thick CSE and are possibly bright in near-infrared. The study at near-infrared will probably disclose their identifications.

IV.6. Discussion

IV.6.1. IRAS color

The distribution of all these sources in the IRAS color-color diagram is shown in Fig.IV.6 in which $*$ stands for variable star, $\odot$ for non-variable star, $\bullet$ for unidentified source and $\star$ for association with nebulosity. The dash-dot line shows the colors of a blackbody with temperatures between 220K and 550K(cf. van der Veen & Breukers 1989). They are divided into three regions I, II and III separated by solid lines. All the 47 identified variable stars are located in region I, i.e. C_{12} is bluer than -0.03 and C_{23} is bluer than -0.3. There are 27 unidentified sources in this region. All the 9 associations with nebulosity are located in region III, i.e. C_{23} redder than -0.3, where 4 other sources are unidentified. In region II no one of the 12 sources are optically identified.

In the divisions of IRAS color-color diagram by van der Veen & Habing(1988), these objects mainly locate in IIIa, IIIb or IV and they are late-type stars with CSE. As model calculations of continuous mass loss showed that the optical depth is an increasing function of the ratio F_{25}/F_{12} for oxygen-rich late type stars(Bedijn 1987), the unidentification of sources in region II can be explained as that these sources are optically thick due to denser CSE in relatively later stage of stellar evolution than the stars in region I. A rough estimation from the models given by Hashimoto(1995) shows that the late-type stars with $C_{12} > -0.2$ may be fainter than 19 mag at I band at a distance of a few kpc. But starlate-type with $C_{12} < -0.2$ in should be brighter than 19 mag at I band as far as interstellar extinction is not so serious in the direction of the objects.

The mixture of identified and unidentified sources in region I means that the optical depth is not only the function of C_{12}. Because late type stars are divided into oxygen-rich and carbon-rich groups, the abundance is the first parameter to be investigated. The IRAS Low

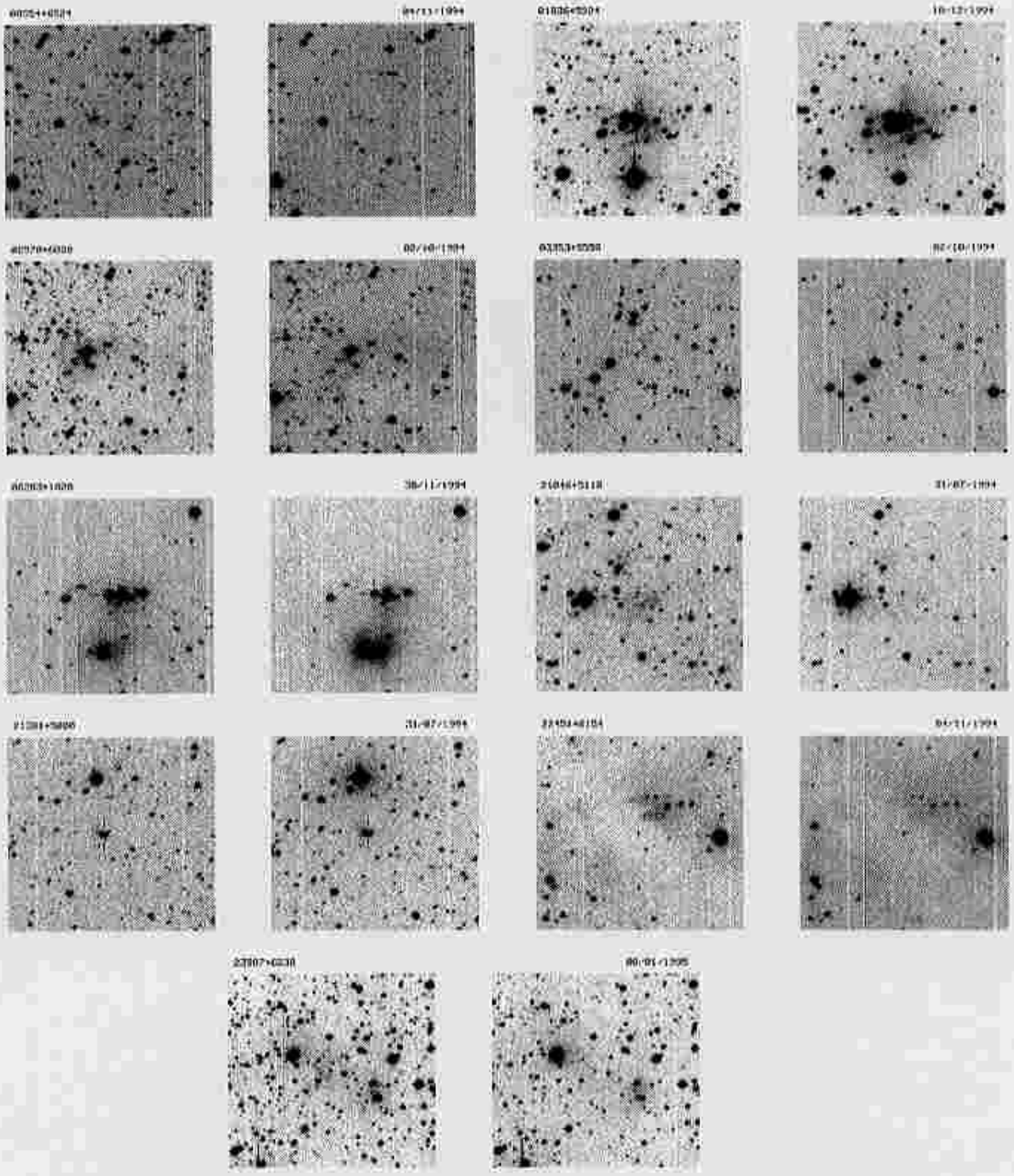

Fig. IV.5.— Finding charts of objects associated with nebulosity

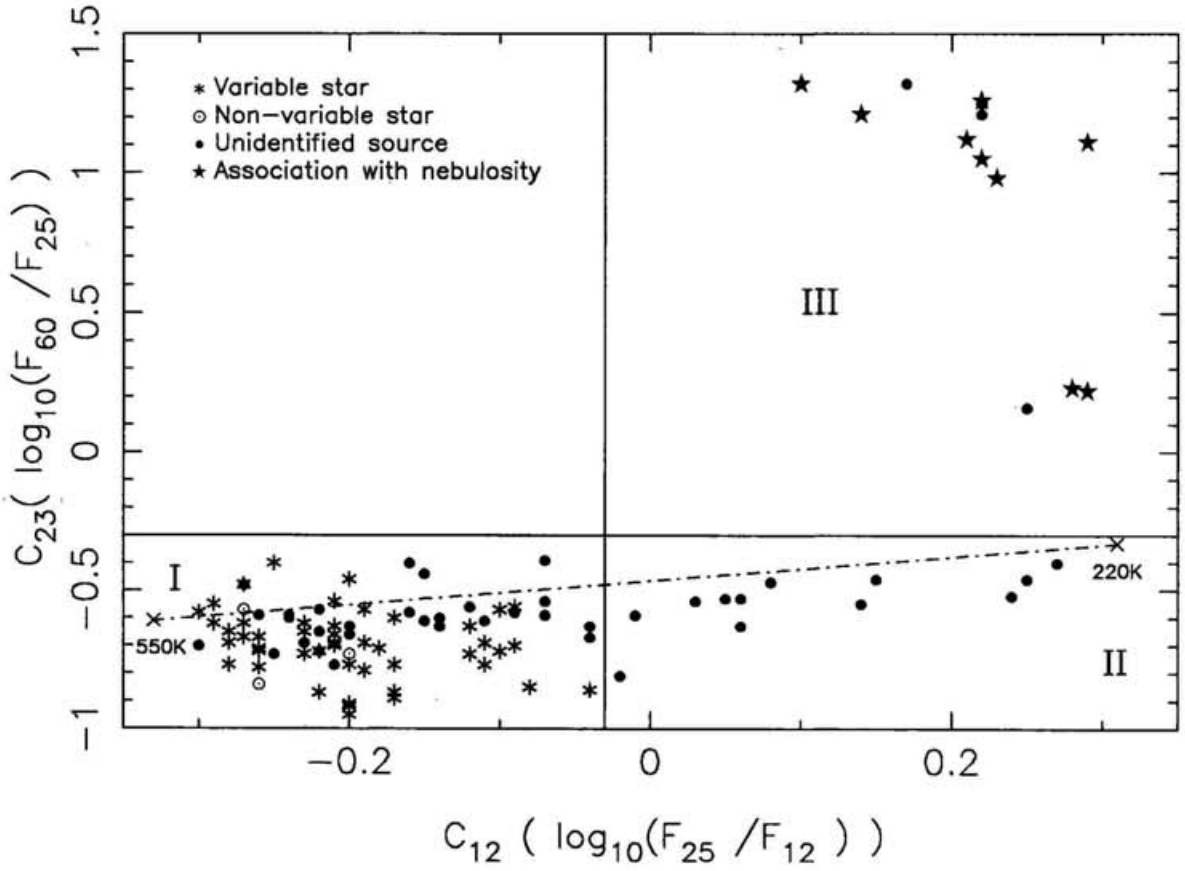

Fig. IV.6.— IRAS color-color diagram for all the 102 sources. The mark $*$ stands for the variable star, the $\odot$ for the non-variable star, the $\bullet$ for the unindentified object and the $\star$ for the source associated with nebulosity. Three regions, I, II and III, are divided by the borderlines. The dot-dash line is for the blackbody of temperatures between 550K and 220K.

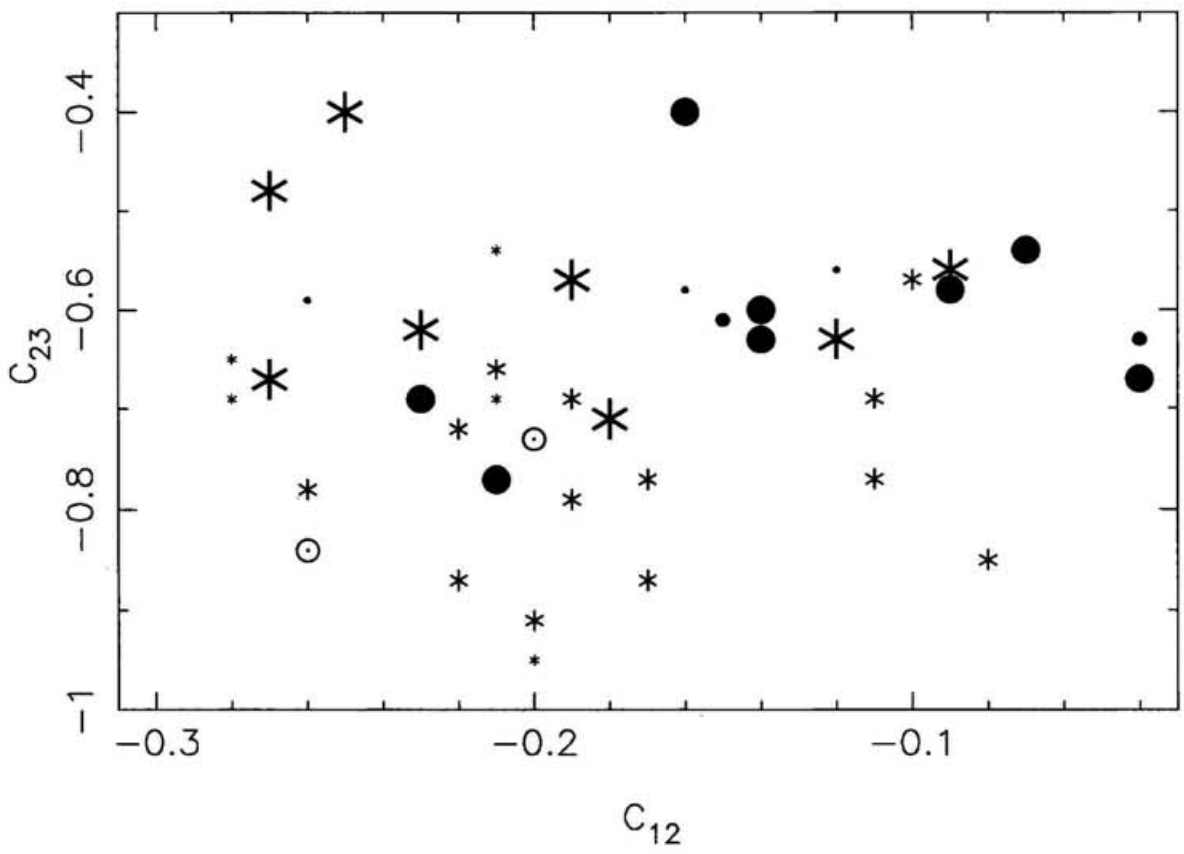

Fig. IV.7.— IRAS color-color diagram for the sources with known IRAS LRS class in region I of Fig.IV.6. The symbols are the same as in Fig.IV.6 while the size of the symbol stands for the IRAS LRS class of the source. The biggest is for the LRS 4n source, the moderate for the LRS 2n source and the smallest for the LRS 1n source.

Resolution Spectra (LRS) are classified based on the slope of the spectrum and the presence of band features between 8 and 23μm(Olnon & Raimond 1986). They are tools to distinguish oxygen-rich and carbon-rich sources by the silicate or SiC features. The sources in region I with known LRS class are plotted in the color-color diagram again (Fig.IV.7). In Fig.IV.7, the symbols have the same meaning as that in Fig.IV.6, furthermore the sizes of the symbol stand for the LRS class of the objects, i.e. the biggest is for LRS 4n source, the moderate for LRS 2n source and the smallest for LRS 1n source. The numbers of LRS class 1n (featureless spectra), 2n (silicate emission) and 4n (SiC feature) sources are shown in table 8 for both variable stars and unidentified sources. The three 2n sources among the unidentification group are IRAS 03313+6058(LRS 22), 06012+0726 (LRS 22), 06181+0406(LRS 23). Their LRS spectra did not show clear silicate feature(Olnon & Raimond 1986). So in region I there is no unidentified oxygen-rich star among the sources with known IRAS LRS class while there are eight 4n sources, possibly C-rich objects.

For the sources having the same C_{12} color, the C-rich sources may have bigger optical depth than O-rich sources. However it is not always the case by noting that there are eight IRAS

LRS 4n sources identified as variable stars. Willems & de Jong(1988) suggested there are two groups of carbon stars and Chan & Kwok(1988) furthermore divided them into optical and radio carbon stars. If the identified and unidentified sources are optical and radio carbon stars respectively, CO emission from identification group should be rare. But among the optically identified 4n sources, three out of five, which were searched for CO emission, IRAS 03192+5642, 20532+5554 and 21449+4950, were detected in CO and two, IRAS 03557+4404 and 05405+3250 were not(Loup et al. 1993 and references therein), i.e. 60 percent. In the unidentification group, four sources were successfully searched for CO emission and there was no negative result. The small number of sources make the statitics not so significant. Nevertheless as well as the CO detection percentage is not as expected, the random location in the color-color diagram of these two groups also suggests that they can not simply be interpreted as optical and radio carbon stars. Maybe to identify optically whether they are really C-rich stars or not will make the situation clear.

IV.6.2. IRAS variability and flux at 12μm

The averages of the IRAS variability index are 90.1, 90.2 and 86.8 and the averages of F_{12} are 29.9, 33.4 and 20.9Jy for variable stars, unidentified objects and sources associated with nebulosity respectively. Because these values do not differ much for identification and unidentification groups, these parameters are irresponsible for the unidentification under our selections. About 96% (47/49) of the identified stars are variables. The selection of the IRAS variability index bigger than 50 works efficiently to find an optical variable star once there is an optical counterpart.

IV.7. Summary

The optical CCD imaging observation at both V and I bands were used to identify objects whose IRAS colors indicate the existence of CSE. There are three criteria, coincidences of optical position with IRAS position, red color and light variation, to judge if an optical object is the IRAS counterpart. The optical position is derived from several position reference stars in GSC catalogue and the light variation between two observations is calculated by comparing the shift of instrumental magnitudes of the stars in the same CCD frame as the object. Out of the 102 observed sources 47 are identified to be variable stars with variation amplitude bigger than 0.2 mag. They are probably Mira type variables. Light variation have not been detected in 2 stars and 1 identified star has not been checked light variation. There are 9 IRAS sources associated with optical nebulosities, some of which are young stellar objects in star formation regions. The 43 unidentified sources are optically thick resulting from dense CSE and maybe the C-rich dust in the CSE.

In order to clarify the classes of variables, we will continue the CCD photometry at V and I bands to plot light curve which can tell us their natures. Furthermore, searching for SiO maser emission and optical spectroscopy will be performed to distinguish O-rich and C-rich stars. Near-infrared imaging will be devoted to the controversial identifications and optically unidentified sources.

One of the authors (B.W.J.) thanks the staff of Kiso Observatory, University of Tokyo for their assistance at the observations and their helpful discussions. They also thank Dr. O. Hashimoto for his valuable comments. This research made use of the SIMBAD database, operated at CDS, Strasbourg, France. B.W.J. is supported by Japanese Government Scholarship.

REFERENCES

Allen, L.E., Kleinmann, S.G, & Weinberg, M.D. 1993, ApJ 411, 188

Bedijn, P.J. 1987, A&A 186, 136

Beichman, C.A., Neugebauer, G., Habing, H.J., Clegg, P.E., & Chester, T.J. 1985, IRAS Catalogues, & Atlases Explanatory Supplement, US Government Printing Office, Washingon DC

Chan, S.J., & Kwok, S. 1988, ApJ 334, 362

Groenewegen, M.A.T., & de Jong, T. 1993, A&AS 101, 267

Hashimoto, O. 1995, ApJ 442, 286

Ichikawa, T., & Nishida, M. 1989, AJ 97, 1074

Izumiura, H., Deguchi, S., Hashimoto, O., Nakada, Y., Onaka, T., Ono, T., Ukita, N., & Yamamura, I. 1994, ApJ 437, 419

Izumiura, H., Catchpole, R., Deguchi, S., Hashimoto, O., Nakada, Y., Onaka, T., Ono, T., Sekiguchi, K., Ukita, N., & Yamamura, I. 1995a, ApJS 98, 271

Izumiura, H., Deguchi, S., Hashimoto, O., Nakada, Y., Onaka, T., Ono, T., Ukita, N., & Yamamura, I. 1995b, ApJ (Nov.10 1995), in press

Jiang, B.W., & Hu, J.Y. 1992, Chin. Astron. Astrophys. 16, 416

Jiang, B.W., Deguchi, S., Izumiura, H., Nakada, Y., & Yamamura, I., PASJ (Dec. 1995), in press

Klass, U., & Elsässer H. 1993, A&AS 99, 71

Loup, C., Forveille, T., Omont, A., & Paul, J.F. 1993, A&AS 99, 291

Molinari, S., Liseau, R., & Lorenzetti, D. 1993, A&AS 101, 59

Olnon, F.M., & Raimond, E. 1986, A&AS 65,607

Palla, F., Brand, J., Cesaroni, R., Comoretto, G., & Felli, M. 1991, A&A 246, 249

Palla, F., Cesaroni, R., Brand, J., Caselli, P., Comoretto, G., & Felli, M. 1993, A&A 280, 599

Persi, P., Ferrari-Toniolo, M., Busso, M., Origlia, L., Robberto, M., Scaltriti, F., & Silvestro, G. 1990, AJ 99, 303

Prusti, T., Whittet, D.C.B., Assendorp, R., & Wesselius, P.R. 1992, A&A 260, 151

Russel, J., Lasker, B., McLean, B., Sturch, C., & Jenkner, H. 1990, AJ 99, 2059

Samus, N. 1992, in 'Variable star research: an international perspective', p.52 Percy J., Mattei, J., & Sterken C.(eds.), Cambridge Univ. Press

Stetson, P.B. 1987, PASP 99, 191

Sugitani, K., Fukui, Y., & Ogura, K. 1991, ApJS 77, 59

Thé, P.S., de Winter, D., & Perez, M.R. 1994, A&AS 104, 315

Wang, G., Clowes, R.G., Leggett, S.K., MacGillivray, H.T., & Savage, A. 1991, MNRAS 248, 112

Weinberg, M.D. 1992a, ApJ 384, 81

Weinberg, M.D. 1992b, ApJ 392, L67

Whitelock, P., Feast, M., & Catchpole, R. 1991, MNRAS 248, 276

Whitelock, P., Menzies, J., Feast, M., Marang, F., Carter, B., Roberts, G., Catchpole, R., & Chapman, J. 1994, MNRAS 267, 711

Willems, F.J., & de Jong, T. 1988, A&A 196, 173

Wolstencroft, R.D., Savage, A., Clowes, R.G., MacGillivray, Leggett, S.K., & Kalafi, M. 1986, MNRAS 223, 279

Wouterloot, J.G.A., & Brand, J. 1989, A&AS 80, 149

van der Veen, W.E.C.J., & Breukers, R.J.L.M. 1989, A&A 213, 138

van der Veen, W.E.C.J., & Habing, H.J. 1988, A&A 194, 125

TABLE 1. Observational log of the sources. The IRAS name and Julian Dates are listed

IRASNAME	Observation Date (Julian Date - 2400000.0)
00070+6503	49606 49697 49726 49741
00336+6744	49661 49687 49700 49726 49741 49759
00459+6749	49661 49687 49726 49741 49759
00534+6031	49610 49628
00554+6524	49661 49687 49726
00589+5743	49607 49628 49659 49686 49700 49726 49741 49759
01036+5924	49565 49697
01557+5759	49565 49687
02117+5559	49607 49697 49725 49726 49742 49759 49798
02173+6322	49565 49660
02272+6327	49607 49628 49660 49686 49700 49726 49742 49759 49798
02408+5458	49628 49697 49759
02433+6345	49565 49606 49697 49725 49742 49759 49798
02470+5536	49565 49606 49627
02535+5555	49565 49606 49658 49686 49700
02570+6028	49606 49628 49658 49760
03022+5409	49610 49628 49697 49725 49742 49759 49798
03078+6046	49610 49628 49697 49726
03096+5936	49607 49628 49658 49686 49725 49743 49759 49798
03192+5642	49607 49628 49658 49686 49700 49725 49742 49759 49798
03206+6521	49607 49697 49726 49760
03238+6034	49628 49658 49686 49700 49726 49742 49759 49798
03293+6038	49628 49697 49726 49760
03301+5658	49607 49690 49700 49726 49760
03313+6058	49610 49628 49658 49726 49760 49799
03353+5550	49628 49726
03371+4932	49628 49658 49726 49742 49759 49799
03385+5927	49660 49686 49700 49726 49742 49759 49760 49799
03434+5818	49660 49686 49726 49760
03448+4432	49607 49690 49760
03469+5833	49660 49686 49700 49725 49742 49759 49799
03525+5711	49628 49658 49686 49700 49725 49726 49742 49759 49799
03557+4404	49628 49697 49726 49743 49760 49799
04085+5347	49628 49658 49686 49705 49726 49741 49757 49797
04209+4800	49660 49687 49697 49726 49741 49757 49797
04254+5255	49628 49658 49686 49726
04256+4435	49660 49661 49687 49726
04340+4623	49628 49658 49742 49757 49760
04402+3426	49661 49686 49700 49726 49741 49757 49798
04470+3002	49660 49686 49705 49726 49741 49757 49799
05091+4639	49660 49686 49700 49741 49757 49797
05131+4530	49660 49686
05146+2521	49660 49686 49705 49743 49758 49797
05204+3227	49661 49686 49743 49758 49797
05273+2019	49687 49706 49725 49743 49758 49797
05405+3240	49661 49686 49743 49758 49797
05423+2905	49660 49686 49706 49725 49741 49757 49799
05452+2001	49687 49706 49726 49743 49758 49799

TABLE 1. (continued)

IRASNAME	Observation Date (Julian Date - 2400000.0)
05484+3521	49661 49686 49725 49743 49758 49797
05552+1720	49687 49706 49726 49743 49759 49760 49799
06012+0726	49687 49706 49743 49799
06069+2142	49687 49743 49800
06170+3523	49660 49686 49705 49725 49741 49757 49797
06181+0406	49687
06241+1025	49687 49706 49725 49743 49799
06242+2830	49687 49725 49726 49743 49800
06283+1028	49687 49743
06364+0450	49686 49705 49726 49743 49800
06447+0817	49686 49743 49758 49798
06448+1639	49686 49705 49743 49798
20479+5336	49565 49606 49697
20523+5302	49565 49606 49697 49726 49741
20532+5554	49562 49607 49658 49687 49697 49726 49742
21046+5110	49565 49606 49707
21086+5238	49562 49606 49627 49658 49690 49701 49726 49742
21122+4900	49565 49628 49707
21147+5110	49562 49606 49707
21216+5536	49565 49606 49628 49658 49690 49701 49726 49742
21223+5114	49565 49606
21269+5030	49610 49707 49726
21290+4919	49565 49606 49707
21297+5251	49562 49610 49707
21377+5042	49562 49707 49726 49743
21381+5000	49565
21415+5025	49562 49607 49628 49658 49690 49706 49726 49743
21444+5053	49562 49628 49690 49708
21449+4950	49562 49708
21453+5959	49565 49607 49659 49726
21489+5301	49562 49628 49708 49726
21509+6234	49565 49628 49659 49690 49706 49708 49726 49741 49760
21533+5844	49565 49708
21563+5630	49565 49606 49628 49659 49690 49706 49708 49726 49741 49760
22045+6306	49661
22103+5120	49661
22130+5634	49565 49607 49659 49690 49706
22147+5948	49659
22177+5936	49565 49628 49659
22224+5736	49562 49607 49708
22241+6005	49562 49628 49659 49690 49706 49726 49741 49760
22367+5537	49562 49628 49708
22394+5623	49661 49726 49741 49760
22394+6930	49661 49726 49741 49760
22451+6154	49661
22466+6942	49565 49610 49628 49659 49686 49706 49726 49741 49760
23030+5719	49661
23183+6151	49661 49726

TABLE 1. (continued)

IRASNAME	Observation Date (Julian Date - 2400000.0)
23361+6437	49562 49606 49658
23389+6529	49562 49690
23491+6243	49562 49690
23507+6230	49565 49606 49690 49726
23516+6430	49565 49690
23592+6228	49565 49690

TABLE 2. Positions of the IRAS PSC source and its optical counterpart for the 47 identified variable stars. The meaning of each column is explained in text.

IRASNAME	α (h)	α (m)	α(s) (IR)	α(s) (Op)	$\sigma(\alpha)$ (s)	$\Delta\alpha$ (s)	δ (°)	δ (′)	δ(″) (IR)	δ(″) (Op)	$\sigma(\delta)$ (″)	$\Delta\delta$ (″)
00336+6744	0	33	37.5	37.92	0.02	0.42	+67	44	43.0	49.59	0.40	6.59
00459+6749	0	45	59.4	59.26	0.07	-0.14	+67	49	25.0	26.64	0.19	1.64
00534+6031	0	53	27.1	26.46	0.01	-0.64	+60	31	1.0	-3.60	0.16	-4.60
00589+5743	0	58	57.5	56.97	0.02	-0.53	+57	43	43.0	41.17	0.30	-1.84
02117+5559	2	11	45.8	45.60	0.01	-0.20	+55	59	5.0	6.43	0.03	1.43
02272+6327	2	27	17.5	17.81	0.02	0.31	+63	27	0.0	3.70	0.58	3.70
02433+6345	2	43	21.0	23.26	0.06	2.26	+63	45	42.0	50.76	0.28	8.76
02470+5536	2	47	5.7	5.65	0.02	-0.05	+55	36	36.0	38.87	0.22	2.87
03022+5409	3	2	13.0	12.50	0.02	-0.50	+54	9	20.0	18.36	0.15	-1.63
03096+5936	3	9	37.2	36.71	0.03	-0.49	+59	36	52.0	52.33	0.33	0.33
03192+5642	3	19	13.8	13.71	0.04	-0.09	+56	42	3.0	3.88	0.24	0.88
03238+6034	3	23	52.3	52.37	0.06	0.07	+60	34	30.0	31.53	0.26	1.53
03371+4932	3	37	11.9	12.08	0.05	0.18	+49	32	16.0	15.04	0.20	-0.96
03469+5833	3	46	59.0	58.42	0.02	-0.58	+58	33	23.0	23.08	0.23	0.08
03525+5711	3	52	33.4	33.41	0.01	0.01	+57	11	45.0	47.12	0.62	2.12
03557+4404	3	55	42.1	42.31	0.01	0.21	+44	4	39.0	39.75	0.07	0.75
04085+5347	4	8	30.5	27.76	0.02	-2.74	+53	47	25.0	24.56	0.19	-0.44
04209+4800	4	20	58.7	58.91	0.02	0.21	+48	0	32.0	32.15	0.16	0.15
04402+3426	4	40	12.1	12.40	0.01	0.30	+34	26	43.0	43.33	0.10	0.33
04470+3002	4	47	3.1	2.91	0.01	-0.19	+30	2	39.0	37.91	0.09	-1.09
05091+4639	5	9	9.0	9.46	0.01	0.46	+46	39	30.0	30.01	0.17	0.01
05146+2521	5	14	38.5	38.77	0.01	0.27	+25	21	49.0	49.35	0.21	0.35
05204+3227	5	20	24.7	24.25	0.01	-0.45	+32	27	32.0	30.74	0.12	-1.26
05273+2019	5	27	19.5	19.92	0.01	0.42	+20	19	47.0	45.86	0.19	-1.14
05405+3240	5	40	33.1	33.26	0.02	0.16	+32	40	48.0	48.44	0.07	0.44
05423+2905	5	42	18.9	19.16	0.01	0.26	+29	5	54.0	54.93	0.09	0.93
05452+2001	5	45	17.6	17.71	0.01	0.11	+20	1	1.0	1.23	0.08	0.23
05484+3521	5	48	25.5	25.36	0.02	-0.14	+35	21	36.0	35.89	0.06	-0.11
05552+1720	5	55	13.9	12.96	0.03	-0.94	+17	20	44.0	44.06	0.32	0.06
06170+3523	6	17	0.2	0.43	0.01	0.23	+35	23	42.0	41.97	0.27	-0.03
06447+0817	6	44	42.5	41.80	0.01	-0.70	+8	17	18.0	18.50	0.12	0.50
06448+1639	6	44	53.7	53.93	0.02	0.23	+16	39	55.0	54.08	0.35	-0.92
20523+5302	20	52	19.6	19.23	0.02	-0.37	+53	2	32.0	32.28	0.08	0.28
20532+5554	20	53	15.8	15.77	0.03	-0.03	+55	54	6.0	4.24	0.08	-1.76
21086+5238	21	8	39.2	39.21	0.05	0.01	+52	38	44.0	46.41	0.26	2.41
21216+5536	21	21	37.8	37.70	0.01	-0.10	+55	36	20.0	20.51	0.12	0.51
21377+5042	21	37	46.9	47.02	0.02	0.12	+50	42	49.0	51.72	0.36	2.72
21415+5025	21	41	31.8	31.62	0.05	-0.18	+50	25	22.0	27.17	0.61	5.17
21449+4950	21	44	56.2	55.66	0.01	-0.55	+49	50	8.0	3.23	0.32	-4.77
21453+5959	21	45	23.1	23.05	0.04	-0.05	+59	59	53.0	52.44	0.12	-0.56
21509+6234	21	50	54.5	54.47	0.01	-0.03	+62	34	30.0	30.62	0.08	0.62
21563+5630	21	56	19.6	19.31	0.08	-0.29	+56	30	28.0	27.98	0.23	-0.02
22241+6005	22	24	7.1	6.82	0.06	-0.28	+60	5	31.0	26.54	0.22	-4.46
22394+6930	22	39	27.6	27.50	0.10	-0.10	+69	30	32.0	32.52	0.65	0.52
22394+5623	22	39	27.7	27.86	0.07	0.16	+56	23	26.0	26.76	0.33	0.76
22466+6942	22	46	37.1	36.90	0.07	-0.20	+69	42	37.0	35.99	0.40	-1.01
23491+6243	23	49	9.1	8.93	0.05	-0.17	+62	43	57.0	55.43	0.22	-1.57

TABLE 3. IRAS parameters for the 47 variable stars. From left to right are IRAS name, Galactic longitude, Galactic latitude, flux density at 12μm, IRAS colours $C_{12}(\log(F_{25}/F_{12}))$, $C_{23}(\log(F_{60}/F_{25}))$, IRAS variability index and IRAS LRS class if available.

IRASNAME	GLO (°)	GLA (°)	F_{12} (Jy)	C_{12}	C_{23}	VAR	LRS
00336+6744	121.5	5.2	6.373	-0.20	-0.77	65	
00459+6749	122.7	5.2	8.069	-0.28	-0.77	80	
00534+6031	123.5	-2.1	4.691	-0.20	-0.46	98	
00589+5743	124.3	-4.8	4.284	-0.23	-0.73	59	
02117+5559	134.4	-4.8	7.399	-0.04	-0.86	78	
02272+6327	133.7	2.9	8.261	-0.29	-0.62	95	
02433+6345	135.2	3.9	20.080	-0.08	-0.85	99	29
02470+5536	139.2	-3.2	29.280	-0.20	-0.92	76	
03022+5409	141.8	-3.5	11.160	-0.17	-0.87	72	29
03096+5936	139.9	1.7	16.330	-0.21	-0.54	99	14
03192+5642	142.6	-0.1	16.880	-0.25	-0.40	99	44
03238+6034	140.9	3.5	70.430	-0.27	-0.67	97	43
03371+4932	148.8	-4.5	5.420	-0.27	-0.62	92	
03469+5833	144.5	3.6	7.343	-0.26	-0.72	99	
03525+5711	145.9	3.0	7.132	-0.21	-0.70	99	
03557+4404	154.8	-6.7	36.300	-0.09	-0.56	99	43
04085+5347	149.9	1.9	29.530	-0.26	-0.78	99	27
04209+4800	155.3	-0.9	24.870	-0.11	-0.77	99	27
04402+3426	167.7	-7.5	3.394	-0.23	-0.65	75	
04470+3002	172.1	-9.2	5.950	-0.12	-0.73	99	
05091+4639	161.6	4.4	17.210	-0.17	-0.77	99	27
05146+2521	179.6	-7.1	19.960	-0.22	-0.87	99	29
05204+3227	174.4	-2.0	23.010	-0.17	-0.89	99	
05273+2019	185.4	-7.5	5.242	-0.17	-0.60	99	
05405+3240	176.6	1.6	196.000	-0.19	-0.57	99	42
05423+2905	179.8	0.1	49.810	-0.10	-0.57	99	29
05452+2001	187.9	-4.1	15.740	-0.21	-0.69	99	15
05484+3521	175.1	4.4	8.001	-0.29	-0.55	99	
05552+1720	191.4	-3.4	8.673	-0.10	-0.72	99	
06170+3523	177.9	9.5	22.840	-0.20	-0.91	99	28
06447+0817	205.1	2.9	21.250	-0.28	-0.65	88	
06448+1639	197.7	6.7	5.756	-0.30	-0.58	97	
20523+5302	91.8	5.4	11.070	-0.09	-0.70	97	
20532+5554	94.1	7.1	58.530	-0.12	-0.63	99	42
21086+5238	93.1	3.3	54.320	-0.28	-0.69	94	14
21216+5536	96.6	4.0	11.410	-0.19	-0.69	51	29
21377+5042	95.0	-1.2	94.490	-0.20	-0.95	99	15
21415+5025	95.3	-1.8	8.293	-0.21	-0.63	93	
21449+4950	95.3	-2.6	67.070	-0.18	-0.71	68	42
21453+5959	101.9	5.1	24.380	-0.11	-0.69	98	23
21509+6234	104.0	6.7	23.990	-0.22	-0.72	96	27
21563+5630	100.8	1.5	84.300	-0.21	-0.66	99	26
22241+6005	105.8	2.4	181.500	-0.23	-0.62	52	41
22394+6930	112.0	9.7	5.606	-0.26	-0.71	90	
22394+5623	105.7	-1.8	6.833	-0.26	-0.67	63	
22466+6942	112.7	9.6	16.180	-0.19	-0.79	91	29
23491+6243	116.2	0.9	40.610	-0.27	-0.48	94	43

TABLE 4. Positions for three non-variable stars. The columns are the same as Table 2.

IRASNAME	α (h)	α (m)	α(s) (IR)	α(s) (Op)	$\sigma(\alpha)$ (s)	$\Delta\alpha$ (s)	δ (°)	δ (′)	δ(″) (IR)	δ(″) (Op)	$\sigma(\delta)$ (″)	$\Delta\delta$ (″)
06241+1025	6	24	6.7	6.92	0.01	0.22	+10	25	41.0	40.44	0.26	-0.56
06364+0450	6	36	27.2	27.46	0.01	0.26	+ 4	50	27.0	29.72	0.45	2.72
22103+5120	22	10	20.0	20.22	0.05	0.22	+51	20	12.0	11.99	0.43	-0.01

TABLE 5. IRAS parameters for the 3 non-variable stars. The columns are the same as Table 3.

IRASNAME	GLO (°)	GLA (°)	F_{12} (Jy)	C_{12}	C_{23}	VAR	LRS
06241+1025	200.9	-0.6	37.120	-0.26	-0.84	99	29
06364+0450	207.3	-0.5	6.633	-0.27	-0.57	95	
22103+5120	99.4	-3.9	15.780	-0.20	-0.73	92	29

TABLE 6. IRAS parameters for the 9 associations with nebulosity. The columns are the same as Table 3.

IRASNAME	GLO (°)	GLA (°)	F_{12} (Jy)	C_{12}	C_{23}	VAR	LRS
00554+6524	123.7	2.8	4.574	0.29	1.11	95	
01036+5924	124.9	-3.1	3.693	0.10	1.32	77	
02570+6028	138.2	1.7	4.823	0.23	0.98	99	
03353+5550	144.9	0.5	3.721	0.22	1.26	53	
06283+1028	201.3	0.3	35.000	0.29	0.22	85	50
21046+5110	91.6	2.7	7.183	0.21	1.12	99	
21381+5000	94.6	-1.8	114.200	0.28	0.23	78	32
22451+6154	109.0	2.7	5.910	0.14	1.21	99	
23507+6230	116.3	0.7	9.288	0.22	1.05	96	14

TABLE 7. IRAS parameters for the 46 unidentified sources. The columns are the same as Table 3.

IRASNAME	GLO (°)	GLA (°)	F_{12} (Jy)	C_{12}	C_{23}	VAR	LRS
00070+6503	118.6	2.8	4.203	0.22	1.21	97	
01557+5759	131.8	-3.5	5.236	-0.24	-0.60	71	
02173+6322	132.7	2.5	9.849	-0.07	-0.59	99	
02408+5458	138.6	-4.2	11.700	0.25	-0.46	83	
02535+5555	139.9	-2.6	11.850	-0.26	-0.59	93	15
03078+6046	139.2	2.6	13.640	0.05	-0.53	69	13
03206+6521	138.0	7.3	95.760	0.14	-0.55	98	34
03293+6038	141.5	3.9	46.200	-0.23	-0.69	99	43
03301+5658	143.6	1.0	15.120	-0.01	-0.59	99	43
03313+6058	141.5	4.3	30.870	0.15	-0.46	50	22
03385+5927	143.1	3.6	59.410	-0.21	-0.77	99	42
03434+5818	144.3	3.1	4.199	-0.11	-0.61	82	
03448+4432	152.9	-7.6	130.300	-0.14	-0.63	99	42
04254+5255	152.3	3.1	3.124	-0.15	-0.44	97	
04256+4435	158.3	-2.7	14.260	-0.24	-0.59	99	
04340+4623	158.0	-0.4	38.600	-0.09	-0.58	95	42
05131+4530	163.0	4.3	27.800	0.24	-0.52	99	42
06012+0726	200.8	-7.0	319.600	-0.15	-0.61	81	22
06069+2142	189.0	1.1	7.740	0.25	0.16	79	
06181+0406	205.8	-4.9	35.280	-0.04	-0.63	99	23
06242+2830	184.9	7.8	17.770	-0.20	-0.66	99	14
20479+5336	91.8	6.3	5.085	-0.02	-0.81	99	
21122+4900	90.9	0.4	14.430	0.06	-0.53	93	13
21147+5110	92.7	1.6	65.610	-0.14	-0.60	87	42
21223+5114	93.6	0.8	69.980	-0.16	-0.40	81	42
21269+5030	93.6	-0.2	4.459	-0.07	-0.39	96	
21290+4919	93.0	-1.3	5.375	-0.20	-0.63	93	
21297+5251	95.5	1.2	7.985	-0.30	-0.70	91	
21444+5053	95.9	-1.8	17.160	-0.04	-0.67	98	43
21489+5301	97.8	-0.6	110.900	-0.07	-0.54	99	42
21533+5844	101.9	3.5	7.298	-0.22	-0.65	93	
22045+6306	105.6	6.2	11.690	0.06	-0.63	97	
22130+5634	102.7	0.2	10.960	0.08	-0.47	99	
22147+5948	104.7	2.8	3.418	0.22	1.25	99	
22177+5936	104.9	2.4	123.200	0.27	-0.40	82	38
22224+5736	104.4	0.4	3.215	0.17	1.32	92	
22367+5537	105.1	-2.3	10.170	-0.22	-0.72	81	
23030+5719	109.1	-2.4	14.430	-0.25	-0.73	93	
23183+6151	112.5	1.1	8.106	-0.27	-0.48	97	
23361+6437	115.3	3.1	4.075	0.03	-0.54	74	
23389+6529	115.8	3.9	10.180	-0.22	-0.57	79	
23516+6430	116.9	2.6	41.600	-0.12	-0.56	75	14
23592+6228	117.3	0.4	23.180	-0.16	-0.58	79	14

TABLE 8. Statistics on the number of different LRS classes of the sources in Fig.IV.7.

LRS classes	2n	1n	4n
variable and non-variable stars	15	5	8
unidentification	3	3	8

Chapter V

Near-IR observation and optical spectroscopy

This chapter is submitted to
The Astronomical Journal, 1996
as
Identification of IRAS sources in the outer disk of the Galaxy
co-authored by
S. Deguchi, J.Y. Hu, T.Yamashita, E.Nishihara, S.Matsumoto and Y. Nakada

ABSTRACT

Near infrared imaging and photometric observations at J, H and K (or K′) bands were performed toward 95 IRAS sources in the outer disk of the Galaxy, most of which had been searched for SiO maser emission and are candidates for variable late-type stars with cold circumstellar envelopes. Low resolution optical spectroscopic observations were made to 19 stars of them for classifying the spectral types. Thirty-eight of them, for which there are no counterparts found at I band brighter than 19mag, were taken near infrared images for identification. All are identified in the near-infrared brighter than 16 mag at K′ band except two that could be in the faint phase of variation when observed. So most of the IRAS late-type stars perhaps have a near-infrared counterpart although many have no optical counterpart. In the near-infrared color-color diagram, the stars with O-rich and C-rich circumstellar envelopes(CSEs) are separated from each other. The stars with C-rich CSE are redder than those with O-rich CSE in general but there are three very red stars in this sample being SiO maser sources, i.e. with O-rich CSE. By combining the near-infrared colors and infrared spectral energy distribution shapes, the two types of circumstellar envelopes are discriminated. 48 percent are stars with C-rich CSE in the entire sample and the number ratios of C-rich to O-rich stars are 14:43 and 32:6 for the optically identified and unidentified groups respectively. This indicates an increasing proportion of C-rich stars with galacto-centric distance and stellar evolutionary stage. The result is applied to explain the low detection rate of SiO maser emission in a physically similar and bigger-scale sample in the outer disk of the Galaxy.

V.1. Introduction

The InfraRed Astronomical Satellite (IRAS) surveyed about 96 percent of the sky in bands centered at 12, 25, 60 and 100μm. More than 250,000 point sources were detected and their flux densities and positions are listed in IRAS Point Source Catalogue (IRAS PSC) (Beichman et al. 1988). About 70,000 of the IRAS PSC sources are associated with objects in astronomical catalogues. In the IRAS PSC sources, a large population are Asymptotic Giant Branch(AGB) stars that are low- and intermediate-mass stars losing mass in the late stage of evolution. The AGB star is embedded in the cold gas/dust circumstellar envelope which absorbs the light from stellar photosphere and re-emit in infrared. IRAS measured their flux densities at four bands and took Low Resolution Spectrum (LRS) ranging from 7 to 23 μm for some sources bright at 12μm. However, the sources of different types can have the same IRAS colors and even show very similar profiles in LRS (see e.g. Noguchi et al. 1993). More observations are necessary to clarify their nature.

We observed 95 IRAS PSC sources whose IRAS colors are of late-type stars. The sources are picked up according to the following criteria. First, they are confined to be in the second quadrant of the Galactic plane, i.e. $90° < l < 180°$ and $|b| < 10°$. Second, the IRAS colors are as $-0.3 < C_{12} < 0.3$ and $C_{23} < -0.4$ (where $C_{12} \equiv \log_{10}(F_{25}/F_{12})$, $C_{23} \equiv \log_{10}(F_{60}/F_{25})$ and F_λ is the flux density at λ). These sources are mostly in the IIIa and IIIb regions of the IRAS color-color diagram divided by van der Veen & Habing(1988) (hereafter VH). The study of IRAS PSC sources by VH concluded that these are variable stars with evolved and/or thick O-rich circumstellar shells. But some IRAS LRS 4n sources that exhibit SiC features have similar colors, the stars with thick C-rich circumstellar shells may be included in the sample besides the stars with O-rich CSEs. Third, the IRAS variability index (cf. Beichman et al. 1988) is > 50. Fourth, $F_{12} > 3$Jy. The sources satisfying the third and fourth criterion are variable within the accuracy of IRAS photometry. There are 92 sources complying with the above criteria. Seventy-eight of them are included in the present observations and 14 (6 M-type, 3 C-type and 5 unknown) are not due to observational restrictions. Instead additional 17 sources (9 M-type, 4 C-type and 4 unknown), which slightly deviate from the above criteria such as in the third quadrant of the Galaxy other than in the second, are complemented. The sources consist an almost unbiased subsample of IRAS PSC sources in selected IRAS color ranges in the Galactic outer disk. They are very possibly variable stars in the AGB evolutionary stage.

Optical identification of these sources was already made by using the 105cm Schmidt telescope with a CCD detector at Kiso Observatory, The University of Tokyo (Chapter IV). The optical counterparts were looked out based on the coincidences with IRAS observations in three aspects, i.e. position, color and light variation. 48 sources were identified as optically variable stars and 40 sources were un-identified. According to the optical identifications, a star with C-rich CSE tends to be more optically thick than a star with O-rich CSE of the same IRAS colors and thus is less likely to have an optical counterpart. So more C-rich stars are suspected to be included in the optically unidentified group than in the optically identified. But it is difficult to tell whether a CSE is C-rich or O-rich from available optical and IRAS data. Near-infrared observations would be helpful to investigate their specific nature. Here we report the results of observations mainly in near-infrared.

V.2. Observations

V.2.1. Near-infrared imaging observation and data reduction

The Near-InfraRed (NIR) imaging observations were carried out on November 08-12, 1995. The NIR detector OASIS with a 256×256 NICMOS3 array(Yamashita et al. 1994) was attached at the Cassegrain focus of the 188cm telescope at Okayama Astrophysical Observatory(OAO). The field of view was about $4.2' \times 4.2'$. Because of strong background radiation in NIR, every imaging frame was exposed for no longer than 60s, 15s and 10s at J, H and K′(cutoff at 2.2μm) bands respectively. In order to improve the detection limit and to avoid the effect of bad pixels, 9 frames were taken for every source at each band by shifting the center position of image little by little. The observations were as deep as 18mag, 17mag and 16mag at J, H and K′ bands respectively at 5σ level. The atmospheric seeing varied from $1''$ through $2.5''$.

The NIR images were at first corrected for dark current. Since the NIR sky background is bright and varies in sites and with time of observation, the flat field correction was performed individually for each object at each band by combining the 9 frames. But when the object (e.g. the standard star) was so bright to cause saturation in array pixels, the observation had to be done by defocusing so that caused unflatness by the artificially extended morphology. In such case, the flat field extracted from the context sources was adopted.

Plate scale and rotation angle

Because the field of view of OASIS is about 4.2 arcmin square and there are usually less than 4 stars listed in HST-GSC catalogue(Russel et al. 1990) in a so small area, the method used for the optical identification(Paper 1), i.e. to take stars in the same frame listed in HST-GSC catalogue as position references, can not be fulfilled of conditions. So the plate scale and rotation angle of OASIS are first determined in order to calculate the equatorial positions of the NIR counterparts from their array coordinates.

Five fields inside which there are more than 5 reference stars in the HST GSC catalogue taken in different nights are selected for calculating the plate scale and rotation angle. The equatorial coordinates (α, δ) of the reference stars are extracted from the HST-GSC catalogue. The positions at OASIS imaging frames (x,y) are measured by the IRAF package. From such measurements it is possible to fit the transformations between pixel and equatorial coordinates (Hunt et al. 1996). The results of the linear fit give the plate scales in the array $x-$ and $y-$axis, as well as the coupling between the two directions. If $(\Delta\alpha, \Delta\delta)$ are the offsets in equatorial coordinates with respect to some reference point, then the coefficients $C_{11}, C_{12}, C_{21}, C_{22}$ in following equations are obtained:

$\Delta\alpha = C_{11}x + C_{12}y + O_\alpha(2)$

$\Delta\delta = C_{21}x + C_{22}y + O_\delta(2)$

With neglecting the second order terms, the coefficients are derived for each of the five fields and the results follow as:

$C_{11} = -0.969(\pm 0.004)$; $C_{12} = 0.006(\pm 0.008)$

$C_{21} = 0.007(\pm 0.004)$; $C_{22} = 0.957(\pm 0.001)$

So the plate scales along the α- and δ- axis. the angle between the x-axis and the negative-

RA axis are then drawn from the relations between the coefficients:

$s_\alpha = (C_{11}^2 + C_{12}^2)^{1/2}$

$s_\delta = (C_{21}^2 + C_{22}^2)^{1/2}$

$tan(\omega_r) = (C_{12}/C_{11} - C_{21}/C_{22})/2$

The results are $s_\alpha = 0.969'' \pm 0.004$/pixel, $s_\delta = 0.957'' \pm 0.001$/pixel and $\omega_r = -0.325° \pm 0.307$. The quite small standard deviations from the five fields indicate the stability of the telescope system.

Calculation of the positions of NIR counterparts

These results are applied to derive the equatorial coordinates of the other objects for which there are not enough position-reference stars. One reference star, whose equatorial coordinates can be extracted from HST-GSC, is measured the coordinates in an OASIS frame. Then according to above formula, the corresponding position in the same frame of the IRAS PSC object is calculated by the known offsets of the object from the reference star in equatorial coordinates. Hereafter the NIR identification is made easily because these objects are so red that they are much brighter at K′ band than at J band. After its IRAS PSC position in the imaging frame is determined, the object can be recognized by eyes. Once the NIR counterpart is fixed, the offsets in equatorial coordinates from the reference star are transformed from its offsets in the imaging frame coordinates. The uncertainty of this method mainly originates from the measurement of coordinates of stars in the imaging frame, which is about 0.5 pixel or 0.5″.

Results

Thirty-eight stars are found to have NIR counterparts at K′ band and their equatorial coordinates are derived in the way discussed in previous section. The average offsets from IRAS PSC positions are 0.52″(±5.08″) in Right Ascension and 1.73″(±3.30″) in Declination which are on the similar magnitude of optical identifications (Chapter IV). There are still 2 sources for which identifications could not be figured out: IRAS 02408+5458 and IRAS 22045+6306. However, they are not peculiar in that they are brighter than 10Jy at 12μm with IRAS colors of late-type stars. Since the stars were chosen to be variables by IRAS variability index and some of then were confirmed variable by the optically identified stars(Chapter IV), these two sources were probably at a so faint phase of light variation when observed that they could not been detected at the observational sensitivity. They may be identified in brighter phase. On basis of this NIR identification, IRAS late-type stars with $F_{12} > 3$ Jy are mostly (98% in this sample) brighter than 16mag at K′ band.

In Table 1 we list the positions of NIR identified counterparts and the offsets from IRAS PSC positions in epoch of 1950.0. Column 1 gives the IRAS PSC name. Columns 2, 3 and 4 are right ascension α in sequence of hour, minute and second of IRAS PSC position. Column 5 is the second part of α of NIR counterpart. Column 6 gives the offset of NIR α to IRAS α as α(NIR) - α(IRAS) in unit of second. Columns 7 to 11 are the same as columns 2 to 6 but for declination δ and in angular units. Each identification chart, centering on the NIR counterpart with size of 2′× 2′, is shown in Fig.V.1 with north up and east to the left. In

TABLE 1. Positions of NIR identified counterparts.

IRASNAME	α (h)	α (m)	α(s) (IRAS)	α(s) (NIR)	$\Delta\alpha$ (s)	δ (o)	δ (′)	δ(″) (IRAS)	δ(″) (NIR)	$\Delta\delta$ (″)
00127+5437	0	12	44.6	45.3	0.7	54	37	35.0	42.5	7.5
01557+5759	1	55	43.7	43.4	-0.3	57	59	42.0	42.8	0.8
02173+6322	2	17	22.1	21.7	-0.4	63	22	35.0	36.2	1.2
02535+5555	2	53	32.7	32.5	-0.2	55	55	14.0	14.1	0.1
03078+6046	3	7	52.1	52.3	0.2	60	46	4.0	4.7	0.7
03206+6521	3	20	41.6	41.8	0.2	65	21	31.0	32.4	1.4
03293+6038	3	29	21.6	21.7	0.1	60	38	20.0	21.4	1.4
03301+5658	3	30	11.4	11.4	0.0	56	58	42.0	43.0	1.0
03313+6058	3	31	20.0	20.8	0.8	60	58	49.0	52.8	3.8
03385+5927	3	38	34.1	33.1	-1.0	59	27	30.0	27.9	-2.1
03434+5818	3	43	26.5	27.2	0.5	58	18	52.0	56.4	4.4
03448+4432	3	44	49.2	47.5	-1.7	44	32	51.0	4.6	13.6
04254+5255	4	25	24.9	25.3	0.4	52	55	45.0	46.0	1.0
04256+4435	4	25	38.1	38.0	-0.1	44	35	33.0	33.3	0.3
04340+4623	4	34	1.2	2.8	1.6	46	23	27.0	32.4	5.4
05131+4530	5	13	6.6	7.0	0.4	45	30	48.0	49.6	1.6
05284+1945	5	28	27.2	27.5	0.3	19	45	8.0	8.0	0.0
06012+0726	6	1	17.1	17.8	0.7	7	26	3.0	2.4	-0.6
06181+0406	6	18	7.3	7.1	-0.2	4	6	36.0	33.7	-2.3
06242+2830	6	24	15.2	15.3	0.1	28	30	20.0	19.0	-1.0
20479+5336	20	47	54.4	54.4	0.0	53	36	49.0	52.6	3.6
21122+4900	21	12	16.3	16.5	0.2	49	0	17.0	20.5	3.5
21147+5110	21	14	45.8	46.0	0.2	51	10	5.0	12.5	7.5
21223+5114	21	22	21.7	21.5	-0.2	51	14	5.0	4.3	-0.7
21269+5030	21	26	59.8	0.1	0.3	50	30	23.0	24.8	1.8
21290+4919	21	29	3.0	2.6	-0.4	49	19	57.0	54.7	-2.3
21297+5251	21	29	42.8	42.7	-0.1	52	51	35.0	35.5	0.5
21444+5053	21	44	26.8	26.9	0.1	50	53	33.0	34.8	1.8
21489+5301	21	48	59.2	59.2	0.0	53	1	23.0	23.4	0.4
21533+5844	21	53	20.2	20.0	-0.2	58	44	52.0	51.8	-0.2
22130+5634	22	13	0.4	0.4	0.0	56	34	20.0	21.4	1.4
22177+5936	22	17	43.1	43.0	-0.1	59	36	16.0	16.4	0.4
22367+5537	22	36	46.9	47.1	0.2	55	37	58.0	2.5	4.5
23030+5719	23	3	4.3	4.1	-0.1	57	19	17.0	17.7	0.7
23183+6151	23	18	23.4	23.3	-0.1	61	51	45.0	45.0	0.0
23389+6529	23	38	59.6	0.2	0.6	65	29	55.0	3.2	8.2
23516+6430	23	51	41.8	41.4	-0.4	64	30	48.0	46.9	-1.1
23592+6228	23	59	12.2	12.0	-0.2	62	28	16.0	13.6	-2.4

order to show the color of the identified counterpart directly, the OASIS images at both J and K′ bands (in case that K′ band image is defocused, H band image replaces) are presented with the filter type labelled in the up-right corner. The NIR counterpart, or the position where the NIR counterpart should be is labelled by two bars. At the upper-left of the chart is the IRAS PSC name.

V.2.2. Near infrared photometry

Observation and data reduction

While the OASIS array imagings were aiming at the identification as described above, they were also used to measure the brightness of objects at JHK′ bands. Besides the imaging observation at OAO, some more photoelectric observation at JHK bands was done at XingLong observational station, Beijing Astronomical Observatory(BAO). By using the InSb detector attached to the 1.26m infrared telescope, 37 sources brighter than 8 mag at K band were detected on October 26 and 29, 1995.

For the BAO data, correction for the atmospheric absorption was made by comparing the object with a standard star which was located at close position. The accuracy is about 0.1mag. While during the OAO observations, several standard stars in the Elias list (Elias et al. 1982), ranging the zenith of program stars, were used to correct for atmospheric absorption. The following equation of instrumental magnitude $m_{I\lambda}$ and standard magnitude m_λ is solved for the observational data of standard stars:

$m_\lambda = m_{I\lambda} - k_\lambda * X_\lambda + Z_\lambda$

where k_λ, X_λ and Z_λ are the atmospheric absorption coefficient, airmass and instrumental zero point at λ.

The parameters were calculated by interactive fitting to k_λ and Z_λ simultaneously night by night except that of Nov. 10. Because only the late half night of Nov. 10 was fine for observations and only three calibration observations were made in that run. So the instrumental zero point was fixed based on its stability of about 0.05mag during the other 4 nights, then only the atmospheric absorption coefficient was independently calculated. The results with standard deviations are shown in table 2. The atmospheric absorption coefficients changed from night to night and the instrumental zero point was stable at the

TABLE 2. Atmospheric absorption coefficients and instrumental zero points for OAO OASIS observations.

	Nov08	Nov09	Nov10	Nov11	Nov12
k_J	0.086±0.069	0.158±0.094	0.315±0.043	0.243±0.065	0.164±0.047
Z_J	5.959±0.088	5.896±0.117	5.950	5.912±0.077	6.015±0.060
k_H	0.142±0.082	0.057±0.090	0.260±0.027	0.114±0.049	0.109±0.042
Z_H	5.913±0.109	6.017±0.113	5.950	6.029±0.058	6.043±0.054
$k_{K'}$	0.140±0.117	0.151±0.086	0.231±0.010	0.191±0.077	0.184±0.043
$Z_{K'}$	6.541±0.153	6.505±0.108	6.540	6.542±0.093	6.541±0.054

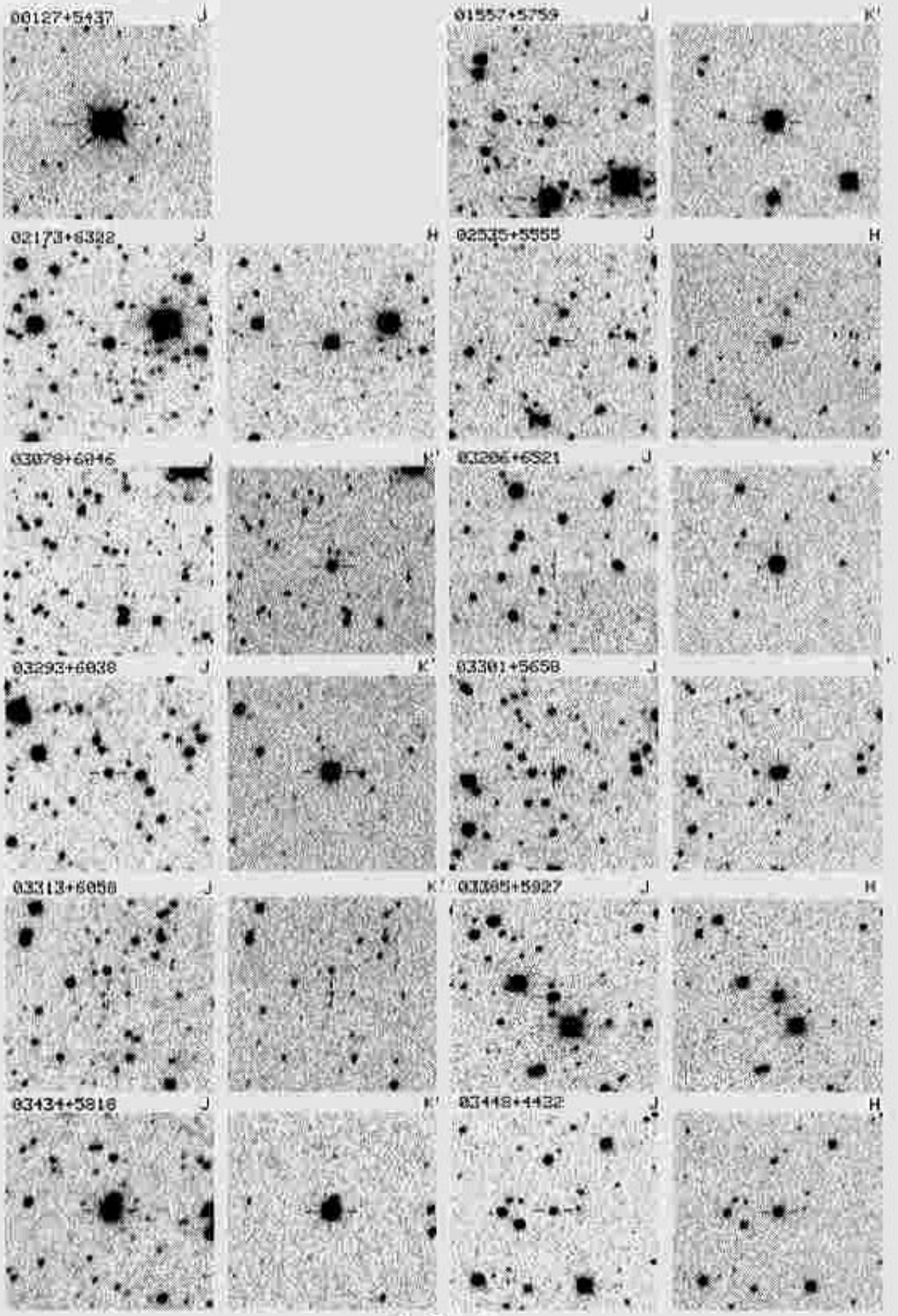

Fig.V.1 (a)

Fig. V.1.— Identification charts of 38 stars at two near-infrared bands.

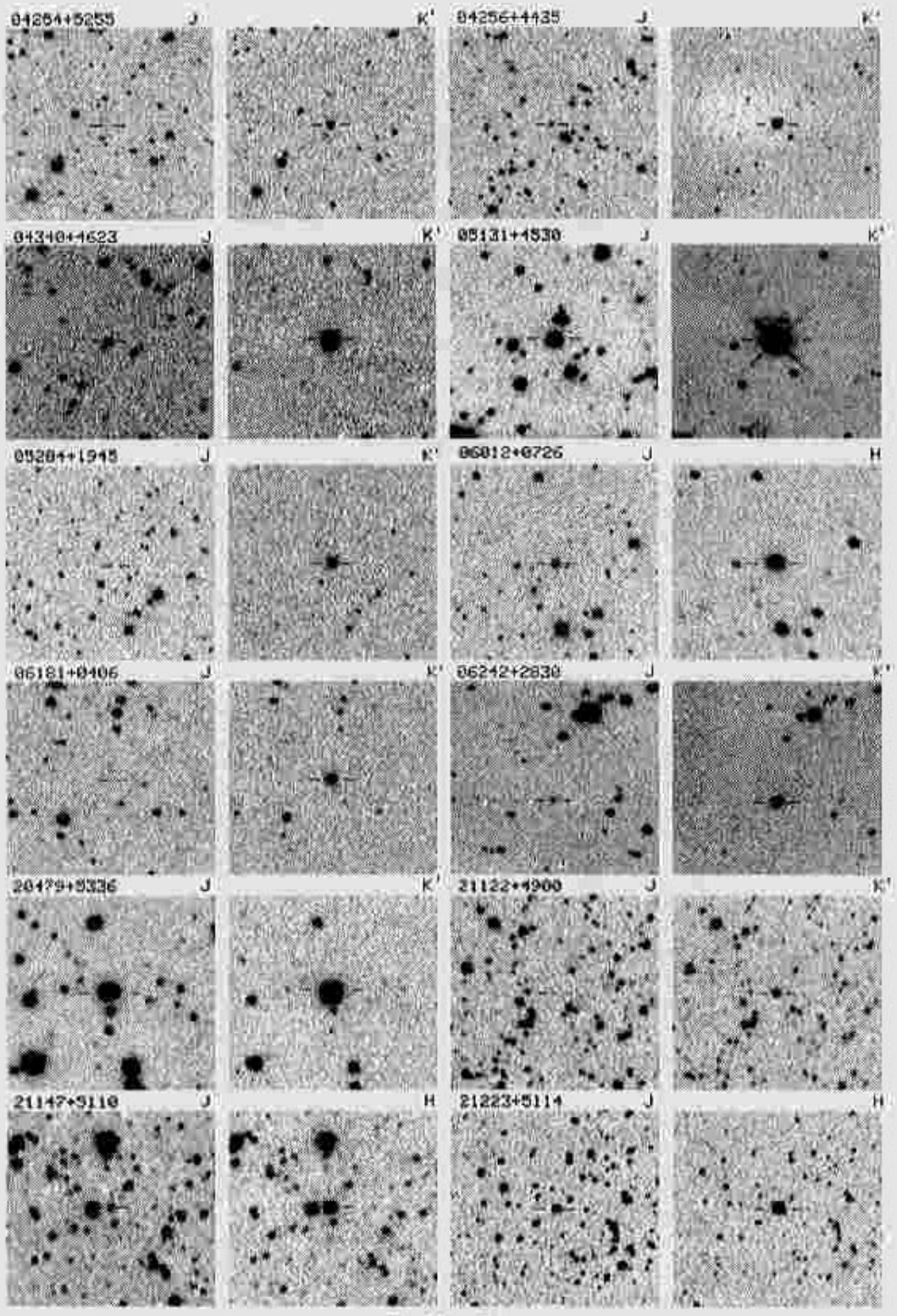
04284+5255 J K'
04256+4435 J K'
04340+4623 J K'
05131+4530 J K'
05284+1945 J K'
06012+0726 J H
06181+0406 J K'
06242+2830 J K'
20479+5336 J K'
21122+4900 J K'
21147+5110 J H
21223+5114 J H

Fig.V.1 (b)

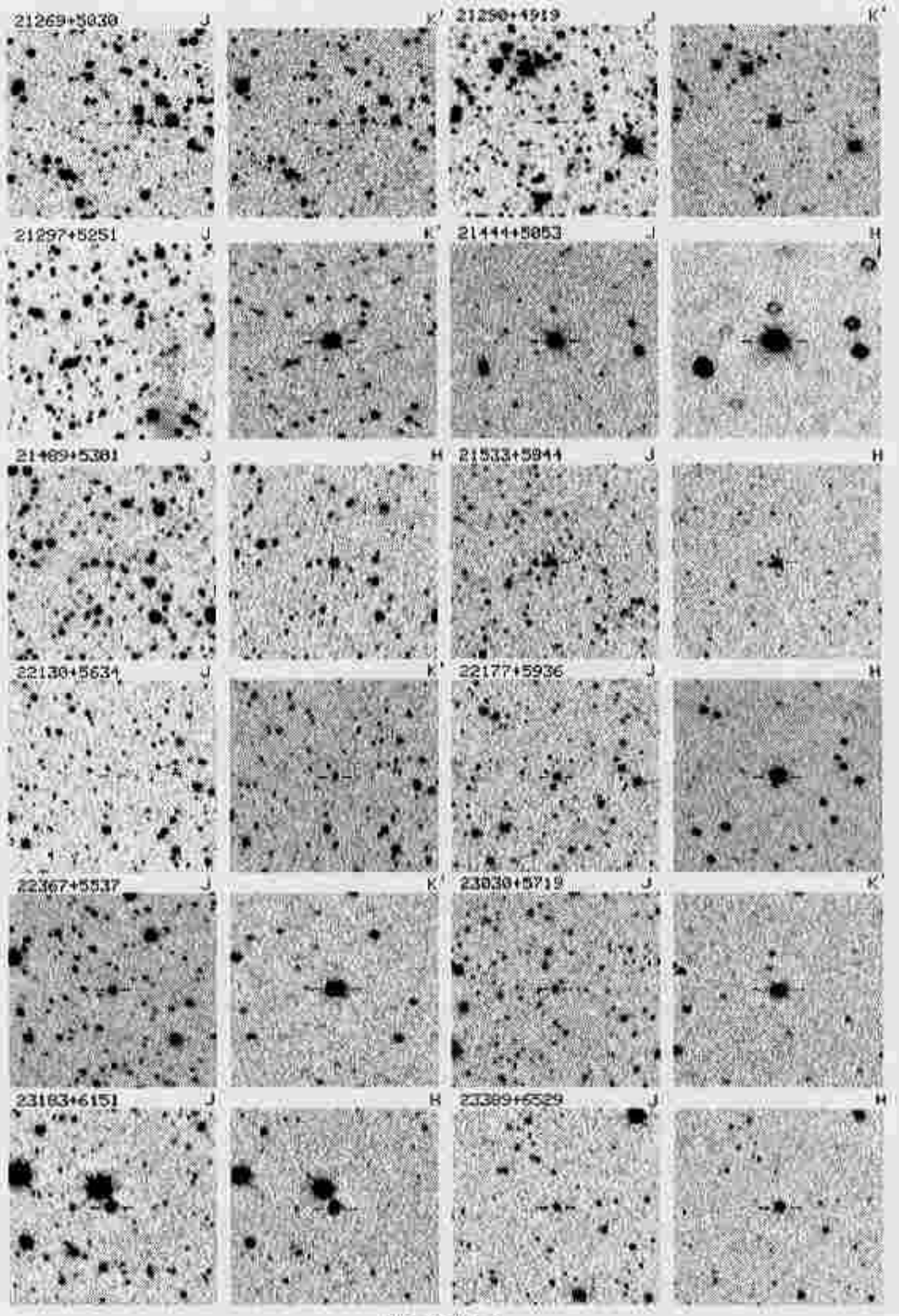
21269+5030
21250+4919
21297+5251
21444+5853
21469+5381
21533+5944
22130+5634
22177+5936
22367+5537
23030+5712
23163+6151
23389+6529

Fig.V.1 (c)

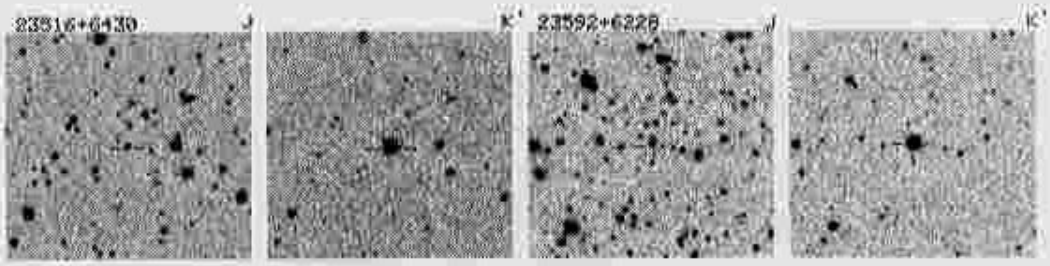

Fig.V.1 (d)

order of 0.05mag. The data analysis on photometry was proceeded by IRAF DAOPHOT package(Stetson, 1987) using Point Spread Function and the errors are usually less than 0.1mag.

Correction for interstellar extinction

The objects in our sample are located at low Galactic latitude ($|b| < 10°$) and most of them are expected to be located at further than 1kpc, thus interstellar reddening correction has been applied to the NIR fluxes. For purposes of computing distances to individual stars, a uniform absolute luminosity is assumed to be $8000L_{\odot}$(cf. Jiang et al. 1993) and the bolometric correction formulae(van der Veen & Breukers 1989) of calculating the apparent flux based on IRAS flux and colors are used. The bolometric corrections are applied to C-rich and O-rich stars respectively while the separation of C-rich and O-rich stars is discussed in upcoming sections. (The method of distance determination has been described in details in Chapter II). The reddening law by Cardelli et al. (1989) is adopted. The interstellar gradient at K band is poorly known. Schechter et al.(1991) reported a value corresponding to 0.03 mag kpc^{-1} based on HI column densities, while Jura et al. (1989) used a much higher value of 0.15 mag kpc^{-1} in the outer Galactic plane. We adopted the value of 0.03 mag kpc^{-1}. As the method of distance determination and assuming a universal value of interstellar extinction result in some uncertainties, the corrections are not very precise. However, most of these sources are intrinsically very red which can be seen from their IRAS color C_{12}, the results are essentially insensitive to interstellar reddening. Therefore, the uncertainty in corrections for interstellar reddening is of little effect on the calculations of intrinsic colors.

In table 3, we listed the photometric results without correction for interstellar extinction (but in the discussion section, the data after correction for interstellar extinction are used), together with IRAS flux at 12μm, IRAS colors C_{12} and C_{23}, type of CSE as C-rich or O-rich, estimated distance. Some sources are only detected at K′ or K′ and H bands, then the lower limit color is calculated assuming the limiting magnitudes are 18 mag at J and 17 mag at H and 'L' is appended to the reduced magnitude. The photometric errors of BAO observations are all taken as 0.1mag and the errors of OAO observations are only that of the IRAF DAOPHOT. The accuracy of correction for atmospheric correction can be seen in Table 2.

Based on the model for spatial distribution of AGB stars by Habing(1988), there is an

outer cutoff (only 1kpc beyond the solar circle) of the disk AGB stars. Later Jura et al.(1989) found there are C-rich AGB stars in further area and concluded that the cutoff may be only applicable to O-rich AGBs. However, one very red SiO maser source, IRAS05284+1945 is located at further than 9kpc (cf. Table 3) away from the sun according to the distance estimation from IRAS colors and flux. So it is doubtful if such cutoff exists and where is the spatial boundary of AGB stars if it exists.

TABLE 3. Photometric results in NIR and by IRAS

IRASNAME	K	errK	J-K	err(J-K)	H-K	err(H-K)	F_{12}	C_{12}	C_{23}	CSE	D(kpc)
00127+5437	4.747	0.013	2.921	0.016	1.202	0.015	55.970	-0.15	-0.86	O	1.332
00336+6744	4.821	0.009	1.605	0.012	0.699	0.011	6.373	-0.20	-0.77	O	3.350
00459+6749	4.554	0.012	2.000	0.020	0.872	0.015	8.069	-0.28	-0.77	O	2.257
00534+6031	5.230	0.100	1.580	0.150	0.520	0.150	4.691	-0.20	-0.46	O	3.904
00589+5743	4.560	0.100	2.230	0.150	0.550	0.150	4.284	-0.23	-0.73	O	3.689
01557+5759	8.459	0.016	5.165	0.024	2.430	0.027	5.236	-0.24	-0.60	C:	7.398
02173+6322	8.069	0.004	5.160	0.020	2.368	0.040	9.849	-0.07	-0.59	C:	5.450
02272+6327	6.740	0.100	1.500	0.150	1.560	0.150	8.261	-0.29	-0.62	O:	5.792
02433+6345	4.329	0.004	2.313	0.014	0.986	0.014	20.080	-0.08	-0.85	O	2.746
02469+5646	2.410	0.100	1.800	0.150	0.510	0.150	90.580	-0.06	-0.72	O	1.367
02470+5536	4.313	0.006	2.312	0.026	1.015	0.011	29.280	-0.20	-0.92	O	1.563
02535+5555	8.628	0.008	5.368	0.053	2.412	0.044	11.850	-0.26	-0.59	C:	4.893
03022+5409	5.172	0.009	2.140	0.028	0.867	0.011	11.160	-0.17	-0.87	O	2.796
03078+6046	11.670	0.037	6.33L	...	4.04	0.105	13.640	0.05	-0.53	C:	4.633
03096+5936	6.077	0.012	4.720	0.076	2.096	0.013	16.330	-0.21	-0.54	C	4.209
03192+5642	4.804	0.018	4.097	0.027	1.712	0.019	16.880	-0.25	-0.40	C	4.111
03206+6521	9.396	0.017	8.291	0.136	3.670	0.030	95.760	0.14	-0.55	O	1.933
03238+6034	5.277	0.011	4.753	0.019	2.096	0.016	70.430	-0.27	-0.67	C	2.001
03293+6038	9.013	0.010	6.212	0.031	2.857	0.021	46.200	-0.23	-0.69	C	2.495
03301+5658	10.386	0.023	6.915	0.081	3.360	0.051	15.120	-0.01	-0.59	C	4.400
03313+6058	15.640	0.140	2.36L	...	1.36L	...	30.870	0.15	-0.46	C	3.080
03371+4932	9.488	0.049	4.718	0.062	2.251	0.069	5.420	-0.27	-0.62	C:	7.212
03385+5927	7.689	0.004	5.600	0.023	2.768	0.040	59.410	-0.21	-0.77	C	2.206
03434+5818	8.688	0.012	2.610	0.028	1.441	0.027	4.199	-0.11	-0.61	O:	5.503
03448+4432	8.459	0.002	5.998	0.050	3.054	0.068	130.300	-0.14	-0.63	C	1.497
03469+5833	5.410	0.100	1.410	0.150	0.540	0.150	7.343	-0.26	-0.72	O	2.539
03513+4827	3.480	0.100	2.520	0.150	0.940	0.150	18.650	-0.26	-0.74	O	1.593
03525+5711	4.620	0.100	1.700	0.150	0.460	0.150	7.132	-0.21	-0.70	O:	3.061
03557+4404	7.804	0.000	5.700	0.049	2.648	0.059	36.300	-0.09	-0.56	C	2.838
03572+5509	2.740	0.100	2.340	0.150	0.530	0.150	45.330	-0.12	-0.81	O	1.625
04085+5347	3.474	0.015	1.712	0.017	0.704	0.016	29.530	-0.26	-0.78	O	1.266
04209+4800	4.304	0.007	2.771	0.017	1.140	0.011	24.870	-0.11	-0.77	O	2.261
04254+5255	12.980	0.047	6.02L	...	3.58	0.200	3.124	-0.15	-0.44	C:	9.662
04256+4435	10.209	0.046	6.672	0.098	3.451	0.093	14.260	-0.24	-0.59	C:	4.483
04340+4623	8.735	0.012	6.921	0.036	3.173	0.022	38.600	-0.09	-0.58	C	2.753
04402+3426	4.902	0.013	1.914	0.019	0.733	0.013	3.394	-0.23	-0.65	O	4.145
04470+3002	5.352	0.005	1.710	0.011	0.699	0.008	5.950	-0.12	-0.73	O	4.485
05091+4639	3.629	0.016	1.578	0.024	0.698	0.016	17.210	-0.17	-0.77	O	2.252
05131+4530	5.602	0.007	5.575	0.025	2.376	0.007	27.800	0.24	-0.52	C*	3.245
05146+2521	4.790	0.100	2.100	0.150	0.920	0.150	19.960	-0.22	-0.87	O	1.769
05204+3227	5.204	0.009	2.531	0.017	0.967	0.012	23.010	-0.17	-0.89	O:	1.947
05284+1945	10.500	0.073	7.50L	...	4.01	0.080	4.174	0.33	-0.43	O	9.817
05325+2351	3.100	0.100	2.810	0.150	0.640	0.150	25.510	-0.34	-0.72	O	1.024
05354+2458	0.340	0.100	2.180	0.150	0.580	0.150	104.200	-0.25	-0.70	O	0.698
05367+3736	1.450	0.100	1.580	0.150	0.560	0.150	154.000	-0.28	-0.84	O	0.517
05368+2841	2.310	0.100	1.050	0.150	0.630	0.150	31.350	-0.32	-0.65	O	0.993
05384+3854	0.570	0.100	0.730	0.150	0.260	0.150	61.430	-0.40	-0.69	O	0.530
05405+3240	6.322	0.010	6.017	0.020	2.758	0.015	196.000	-0.19	-0.57	C	1.217

V.2.3. Optical spectroscopy

All the sources were searched for SiO maser emission except the IRAS LRS 4n sources which are possibly with C-rich circumstellar shells. The observational results are reported in a separate paper(Chapter II). Since the SiO masers are from O-rich CSEs, they have O-rich CSE in spite that there are a small number of S stars with SiO maser emission. In order to unveil the SiO non-detections, spectra were taken of 19 sources brighter than 15 mag at I band at XingLong observational station, Beijing Astronomical Observatory by using the UNIVERSAL spectrograph at the Cassegrain focus of the 2.16m telescope on October 24, 25 and 26, 1995. The 1024×1024 CCD detector was used with a grating resulting in a dispersion of 193Å/mm and a wavelength coverage from about 4900Å to 9200Å. The weather was fine and atmospheric seeing was about 2-2.5″. The width of slit was chosen as 3″ to match the seeing. All the spectra were corrected for bias and flat-field, transformed to linear wavelength and, with the help of observed flux standard star, calibrated to absolute flux. Based on the presence of CN bands at 7945, 8125 and 8320Å or TiO band at 7667Å, the objects are classified into C-type or M-type stars. The M-type stars are further sub-classified according to the absorption depth of VO group around 7900Å and with reference to the standard stars for MS classification in the same wavelength range by Lundgren(1989). The sub-classification is about 1 sub-type uncertain. The C-type stars are not further divided into sub-classes. No attempt is made to clarify their luminosity classes because spectral resolution is low and all the atomic lines are blended with ubiquitous molecular bands. As can be seen from table 4, all the 8 SiO maser sources are late M-type stars. In the SiO non-detection sources, 4 are C-type stars and 7 are late M-type stars. The spectra of 4 C-type stars and, as an example, of 1 M-type star are shown in Fig.V.2 with their IRAS PSC names and prominent molecular bands. Only the part of spectra from 6000Å to 9000Å is presented because the stars are very faint at the shortward of 6000Å.

V.3. Discussion

V.3.1. Discriminations of stars with C-rich and O-rich CSEs

It has been known that there are two groups of red giants, M-type and C-type, both characterised by strong molecular absorption bands in red spectral region. A similar dichotomy also exists in stellar CSE with silicate or carbonaceous dust. We divided the CSE of some stars in our sample into C-rich and O-rich groups based on three kinds of observations. First is the observations in molecular lines. Molecular maser or thermal emissions are found abundant in late-type stars. OH, SiO, H_2O maser lines are detected in O-rich CSEs and HCN line in C-rich CSEs(cf. Bujarrabal 1994). The sources detected in SiO maser lines (Chapter II) are classified as O-rich and sources detected in HCN lines(Loup et al. 1993) are classified as C-rich. Second is the mid-infrared IRAS LRS spectra(Olnon et al. 1986). The LRS 2n and 3n sources exhibiting silicate feature at 9.7μm are classified as O-rich and LRS 4n sources with SiC feature at 11.3μm as C-rich. In our sample, an LRS 2n source is classified as O-rich only when its LRS class is >25 if no SiO maser emission was detected. Third is the optical

TABLE 3. (continued)

IRASNAME	K	errK	J-K	err(J-K)	H-K	err(H-K)	F_{12}	C_{12}	C_{23}	CSE	D(kpc)
05423+2905	2.898	0.010	2.320	0.015	1.015	0.011	49.810	-0.10	-0.57	O	1.646
05443+2707	2.840	0.100	1.060	0.150	0.820	0.150	19.680	-0.33	-0.83	O	1.208
05452+2001	6.194	0.000	4.565	0.044	1.981	0.001	15.740	-0.21	-0.69	C	4.287
05484+3521	7.218	0.003	4.278	0.021	1.934	0.015	8.001	-0.29	-0.55	C:	5.886
05552+1720	5.402	0.006	2.651	0.017	1.116	0.012	8.673	-0.10	-0.72	O	3.944
05559+3825	3.420	0.100	2.130	0.150	0.970	0.150	117.800	-0.23	-0.87	O	0.704
06012+0726	6.207	0.010	7.194	0.055	3.180	0.011	319.600	-0.15	-0.61	C	0.955
06170+3523	5.586	0.004	2.883	0.011	1.183	0.008	22.840	-0.20	-0.91	O	1.769
06181+0406	11.390	0.020	6.61L	...	3.760	0.030	35.280	-0.04	-0.63	C:	2.880
06242+2830	11.422	0.008	5.001	0.053	2.303	0.033	17.770	-0.20	-0.66	C:	4.039
06346+1444	3.600	0.100	1.250	0.150	0.450	0.150	16.100	-0.19	-0.68	O	2.179
06447+0817	7.050	0.010	5.161	0.050	2.346	0.011	21.250	-0.28	-0.65	C:	3.628
06448+1639	6.741	0.024	3.657	0.034	1.647	0.025	5.756	-0.30	-0.58	C	6.901
20479+5336	7.481	0.020	3.633	0.022	1.446	0.021	5.085	-0.02	-0.81	O	6.388
21086+5238	1.980	0.100	2.850	0.150	0.890	0.150	54.320	-0.28	-0.69	O	0.870
21122+4900	12.770	0.027	6.23L	...	3.22	0.150	14.430	0.06	-0.53	C:	4.505
21147+5110	7.882	0.012	7.054	0.027	3.217	0.021	65.610	-0.14	-0.60	C	2.109
21216+5536	4.500	0.100	1.730	0.150	0.760	0.150	11.410	-0.19	-0.69	O	2.589
21223+5114	7.423	0.001	6.012	0.046	2.785	0.052	69.980	-0.16	-0.40	C	2.041
21269+5030	12.267	0.027	5.202	0.192	2.469	0.056	4.459	-0.07	-0.39	C:	8.100
21290+4919	9.586	0.040	5.965	0.087	2.486	0.079	5.375	-0.20	-0.63	C:	7.343
21297+5251	8.763	0.025	5.915	0.041	2.727	0.041	7.985	-0.30	-0.70	C:	5.859
21341+5101	2.740	0.100	1.870	0.150	0.490	0.150	24.830	-0.27	-0.77	O	1.333
21377+5042	4.407	0.012	4.596	0.021	1.981	0.015	94.490	-0.20	-0.95	C	1.751
21415+5025	3.936	0.008	1.475	0.013	0.541	0.011	8.293	-0.21	-0.63	O	2.839
21444+5053	6.115	0.006	3.796	0.038	1.790	0.006	17.160	-0.04	-0.67	C	4.130
21449+4950	6.168	0.011	5.348	0.028	2.475	0.013	67.070	-0.18	-0.71	C	2.082
21453+5959	5.880	0.100	1.560	0.150	1.320	0.150	24.380	-0.11	-0.69	O	2.284
21489+5301	8.506	0.006	6.698	0.037	3.138	0.030	110.900	-0.07	-0.54	C	1.624
21509+6234	3.470	0.100	1.900	0.150	0.360	0.150	23.990	-0.22	-0.72	O	1.613
21522+6018	3.150	0.100	1.830	0.150	0.760	0.150	13.290	-0.28	-0.78	O	1.759
21533+5844	8.526	0.005	5.307	0.047	2.571	0.074	7.298	-0.22	-0.65	C:	6.287
21563+5630	1.655	0.019	1.899	0.019	0.755	0.022	84.300	-0.21	-0.66	O	0.890
22103+5120	5.390	0.100	1.870	0.150	1.230	0.150	15.780	-0.20	-0.73	O	2.129
22130+5634	13.180	0.073	4.82L	...	3.82L	...	10.960	0.08	-0.47	C	5.169
22177+5936	5.920	0.007	8.450	0.077	3.618	0.014	123.200	0.27	-0.40	O	1.815
22241+6005	4.114	0.006	5.366	0.036	2.396	0.012	181.500	-0.23	-0.62	C	1.259
22367+5537	8.426	0.006	5.438	0.067	2.386	0.062	10.170	-0.22	-0.72	C:	5.326
22394+5623	3.730	0.100	0.930	0.150	0.550	0.150	6.833	-0.26	-0.67	O	2.632
22394+6930	4.894	0.000	2.211	0.018	0.887	0.007	5.606	-0.26	-0.71	O	2.906
22466+6942	3.769	0.007	1.649	0.009	0.671	0.011	16.180	-0.19	-0.79	O	2.174
23030+5719	8.539	0.012	6.106	0.054	2.847	0.064	14.430	-0.25	-0.73	C:	4.446
23183+6151	7.629	0.020	4.887	0.052	2.543	0.105	8.106	-0.27	-0.48	C:	5.897
23389+6529	8.238	0.005	5.936	0.121	2.508	0.047	10.180	-0.22	-0.57	C:	5.324
23491+6243	5.856	0.019	5.361	0.025	2.424	0.025	40.610	-0.27	-0.48	C	2.635
23516+6430	9.477	0.035	6.358	0.071	3.033	0.068	41.600	-0.12	-0.56	C:	2.650
23592+6228	9.830	0.054	6.249	0.150	3.030	0.085	23.180	-0.16	-0.58	C:	3.546

*c.f. Section 3.3 for discussion on the C-rich or O-rich nature of this object.

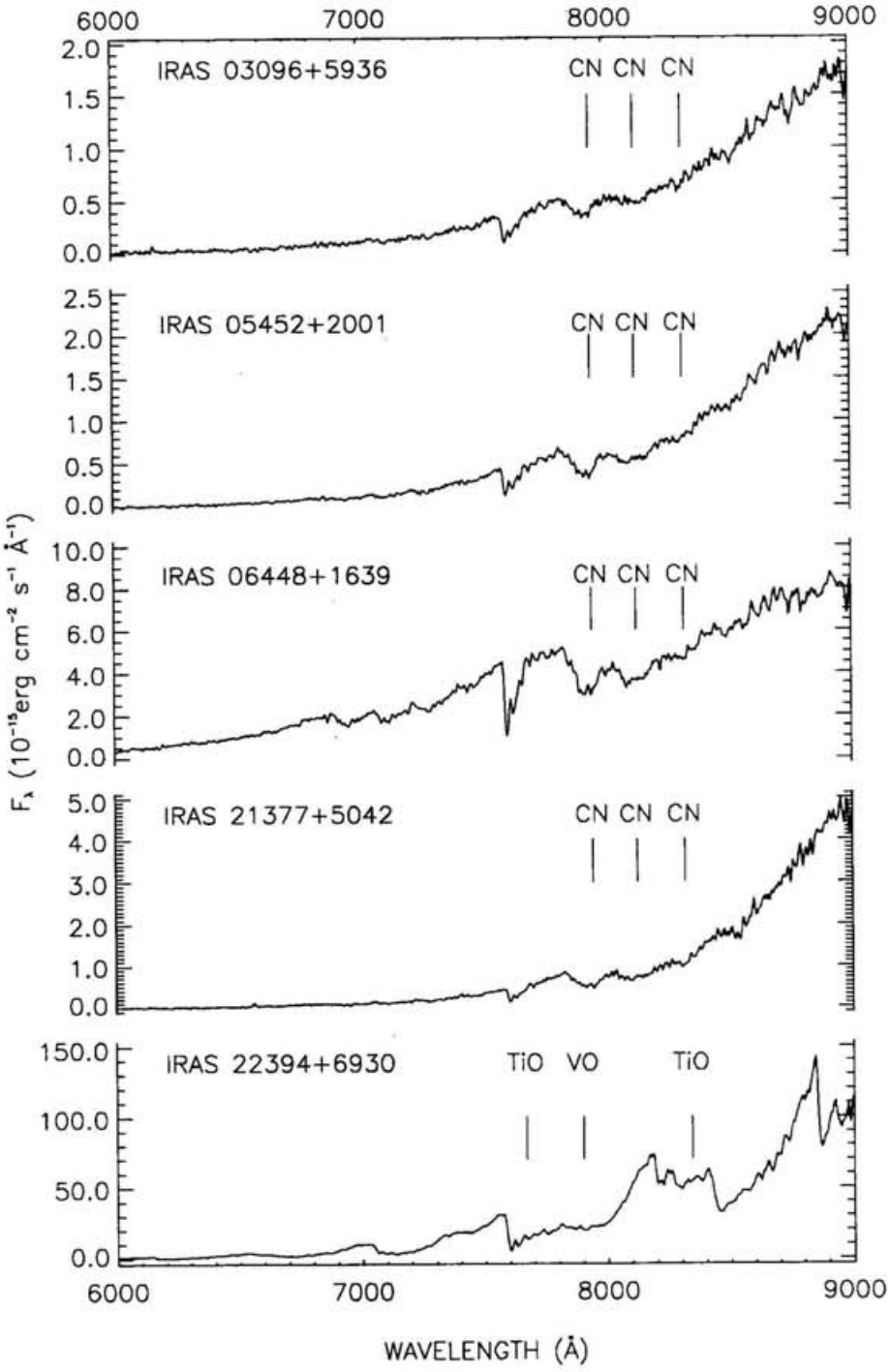

Fig. V.2.— Spectra of 4 C-type stars and 1 M-type star.

TABLE 4. Spectral classes of 19 stars

IRASNAME	SiO*	Spectral Type
00336+6744	Y	M8
00459+6749	Y	M8
00589+5743	N	M6
02117+5559	N	M8
02433+6345	Y	M9
03022+5409	N	M6
03096+5936	N	C
04402+3426	N	M8
04470+3002	N	M8
05452+2001	N	C
06448+1639	N	C
21377+5042	N	C
21415+5025	N	M5
21509+6234	Y	M8
21563+5630	Y	M8
22103+5120	Y	M8
22394+5623	Y	M6
22394+6930	N	M8
22466+6942	Y	M6

*cf Chapter II, Y is for detection and N for non-detection

spectra. Stars with TiO bands are classified as O-rich and stars with CN bands as C-rich (cf. Section 2.3). If one of the above three features has been found for a star, its CSE is clear of C-rich or O-rich. If more than one kind of observations was performed, the priority first goes to optical spectrum, then SiO/HCN line and finally IRAS LRS class. As a result, 45 stars have O-rich CSEs and 24 have C-rich CSEs. In the column 'CSE' of Table 3, they are represented by O and C respectively. The stars with unknown chemical type of CSE are then 26 SiO maser non-detections for which no observational data like these three types are available to classify their CSEs.

V.3.2. Near Infrared color-color diagram

This sample

Because stars with C-rich and O-rich CSEs are entangled together in IRAS Color-Color (CC) diagram, hard effort is devoted to distinguish them by ground-based NIR observations. By a great deal of observations, Epchtein et al.(1990) found the solution to this problem by using the NIR colors relating to L band. Noguchi et al.(1991) drew the same conclusion from observations towards a number of M-type and C-type stars. But the photometry at L band is usually difficult and inaccurate due to strong background radiation, only the photometries at JHK bands were made during our observations and hereafter the NIR color-color diagram refers to the J-K vs. H-K plot.

The NIR colors of all the observed sources are shown in Fig.V.3 where a cross denotes an O-rich star, a lozenge denotes a C-rich star and a circle denotes an SiO non-detection with unknown CSEs (the symbol convention is kept in Fig.V.4.1 and Fig.V.4.2). The blackbody line as a reference is also plotted indicating the color temperatures ranging from 4000K to 500K. The arrows mark the lower limits of colors in the case of stars that can be detected at only K′ or K′ and H bands. The two color indices, J-K and H-K, correlate linearly well.

The CC diagram is divided into three regions bordered by the dot-dash lines in Fig.V.3. It can be seen that (1) in region I most stars are with O-rich CSEs though there are 4 SiO non-detections and 1 star with C-rich CSE that could be in region II since its colors are given in lower limits; (2) in region II are all except one C-rich stars and most of SiO non-detections; (3) in region III there are 2 O-rich stars (which are SiO maser sources IRAS 03206+6521 and 22177+5936). Outside the three regions, there are stars potentially in region III after taking the lower limits of colors into account: 1 SiO maser source IRAS 05284+1945, 1 C-rich star and 2 SiO non-detections. The C-rich and O-rich stars mostly have different NIR colors, i.e. in general the O-rich stars have relatively bluer NIR colors than the C-rich stars. But the presence of three very red O-rich stars in region III can not be accidental and it seems irreasonable that the NIR colors of O-rich stars have some gap between region I and region III shown in this figure. There should be some O-rich stars in region II if the color sequence of O-rich stars is continuous. The lack of O-rich stars in region II of this figure can be caused by the few proportion of O-rich stars having such colors and the small number of objects in the sample. Anyway the O-rich and C-rich stars are clearly separated as O-rich stars in region I, C-rich stars in region II and few of both in region III.

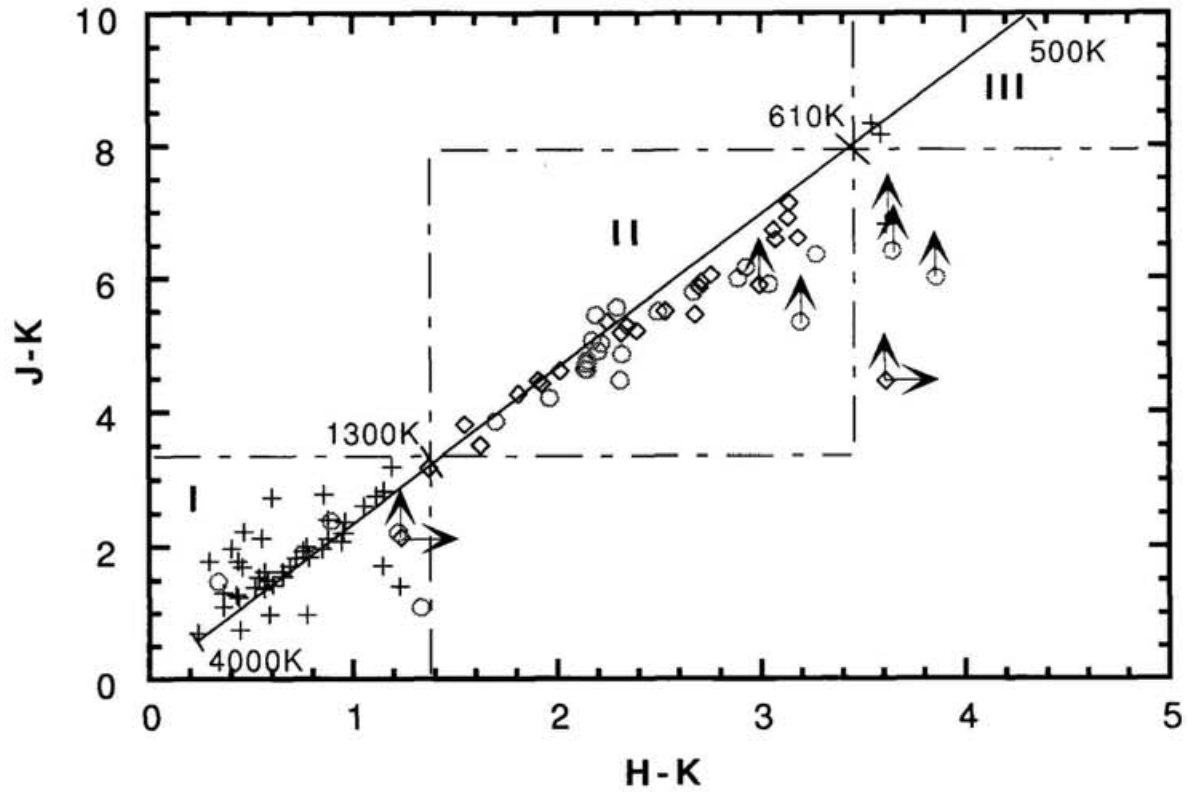

Fig. V.3.— Near infrared color-color diagram of the stars in our sample, a cross denotes an O-rich star, a lozenge denotes a C-rich star and a circle denotes an SiO non-detection.

The other samples

Because the present sample is not big, statistical fluctuation may be able to affect the results. Whether the discrimination between O-rich and C-rich stars in NIR CC diagram is true or not should be attested by larger sample. Though there are a lot of NIR photometric observations of late-type stars in references, many are not clear if the object is C-rich or O-rich. Here we give two systematic and representative samples as examples.

Since IRAS LRS sources are bright and readily classified into O-rich or C-rich stars, many of them have been observed in NIR before. For example, the IRAS LRS 2n and 3n sources, whose LRS spectra exhibit silicate features, in the northern sky were observed by Jiang et al.(1992) and Wang et al.(1994). The IRAS LRS 4n sources, whose LRS spectra exhibit SiC feature, in the southern sky were observed by Epchtein et al.(1990). The locations of these sources are plotted in the NIR color-color diagram Fig.V.4.1 where there are 82 O-rich and 207 C-rich stars. The divisions of three regions in Fig.V.4.1 are quite similar to that in Fig.V.3. Only because interstellar reddening is not corrected for the IRAS LRS 2n and 3n sources, the boundary between region I and region II is slightly shifted to red side. Different from Fig.V.3, in region I there are C-rich stars besides O-rich stars. But it is the same as Fig.V.3 that in region II, there is no O-rich source intruding into this territory of C-rich stars, $1.5 < H - K < 3.5$ and $4.0 < J - K < 8.0$. In region III no source is present, which can be attributed to the sensitivity limit of BAO NIR telescope(cf. Jiang et al. 1992).

Blanco et al. (1980) made the grating-prism survey of selected fields in the Magellanic Clouds(MCs) and bifurcated the C-type and later-than-M5-type stars. The succeeding broad-band NIR photometry towards some of those red stars was done by Cohen et al.(1981). From that observational data (Cohen et al. 1981), the NIR CC diagram of 74 late-type stars in the MCs is shown in Fig.V.4.2. Here the diagram is divided into two regions. As in Fig.V.4.1, in region I there are also C-type stars though M-type stars are dominants. But there is no difference from Fig.V.3 and Fig.V.4.1 that region II is occupied completely by carbon stars. Comparing Fig.V.4.2 with Fig.V.3 and Fig.V.4.1, one can easily find that the MCs C-type stars are not so red in NIR colors as the Galactic C-type stars. The reason could be difference in metallicity or that they are in different stages of stellar evolution. This question will not be discussed further in this paper because more scrutiny has to be made. Though we do not show result here, the sample of OH/IR stars in the southern hemisphere (Lepine et al. 1995) exhibits the same tendency that the stars with O-rich CSEs are conserved in region I.

Both the two samples indicate that in region I of NIR color-color diagram not only O-rich stars are seen but also C-rich stars. It has been known that the NIR colors of optically visible C-type stars are not quite different from that of M-type stars. For example, the observations by Noguchi et al.(1991) towards the optically visible C stars in solar neighbourhood show that their H-K colors are < 2.0. However, the mixture of C-rich stars with O-rich stars in region I is not seen in the sample we observed. Our sample is composed of stars with few catalogue associations and mostly optically faint (Chapter IV). Therefore the stars with C-rich CSE could be more evolved or at further distance than the optical C stars listed in catalogues. On the other hand, region II only sees the C-rich stars in all the three samples even its boundary is different for C-type stars in the MCs. The stars with C-rich CSEs that have the similar IRAS colors as O-rich CSE yet have redder NIR colors so that they can be

separated out based on NIR colors. In light of this criterion, 22 of the 26 SiO non-detections are with C-rich CSE. By far region III has objects only in our sample. This could be caused by the detection limit of previous observations. A system can detect a source in region III

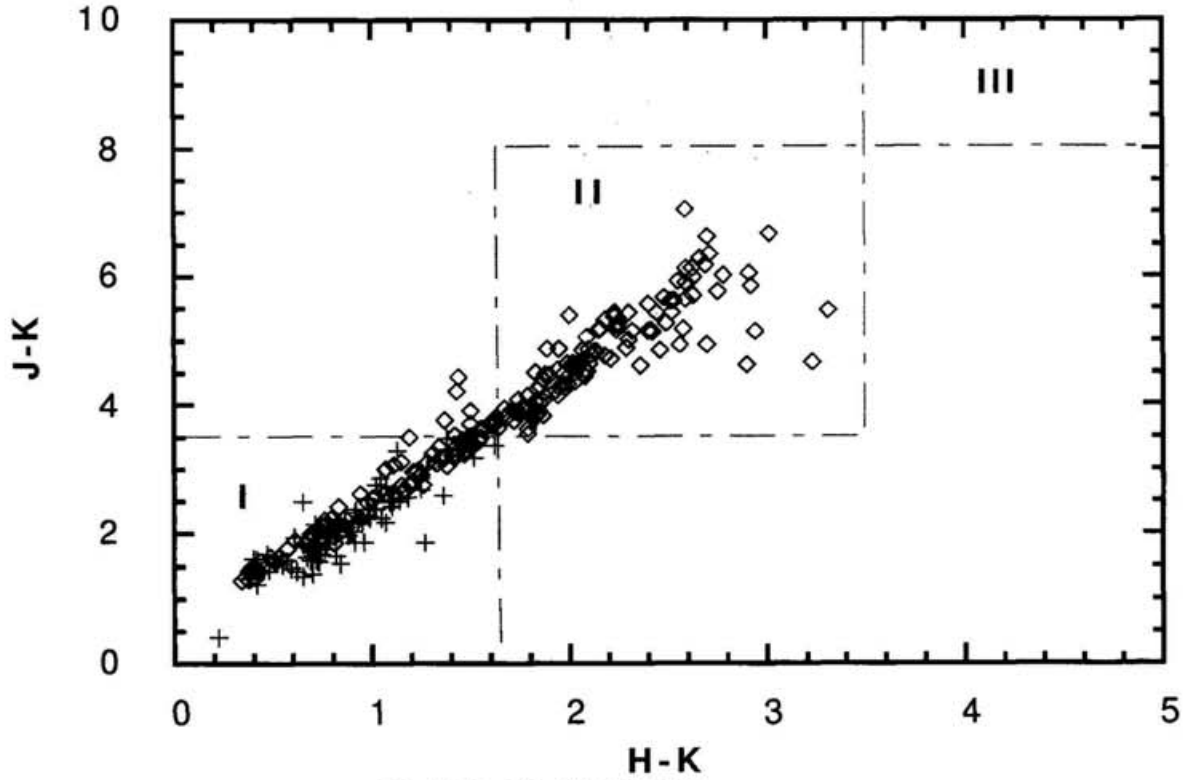

Fig.V.4.1 The IRAS LRS sources.

Fig. V.4.— Near infrared color-color diagram

V.3.3. Near-mid-IR color-color diagram

As is seen in Fig. V.3 that the near-IR colors J-K and H-K correlate linearly, either can represent the near-IR color of the objects. It will be more informative to combine the near-IR color with IRAS color. So Fig. V.5 is a plot of all the stars with their colors H-K and C_{12}, where the symbols obey the same conventions used in Fig. V.3. The separation of C-rich stars from O-rich stars by color H-K is repeated here for stars in region I and region II even they have quite similar IRAS color C_{12}. The new result from this figure is that the O-rich stars in region III of Fig. V.3 stand out from the C-rich stars by their redder IRAS color C_{12}. A further investigation of the spectral energy distribution between 1.2μm and 60μm revealed that the O-rich stars in region III actually show the radiation excess at 25μm while

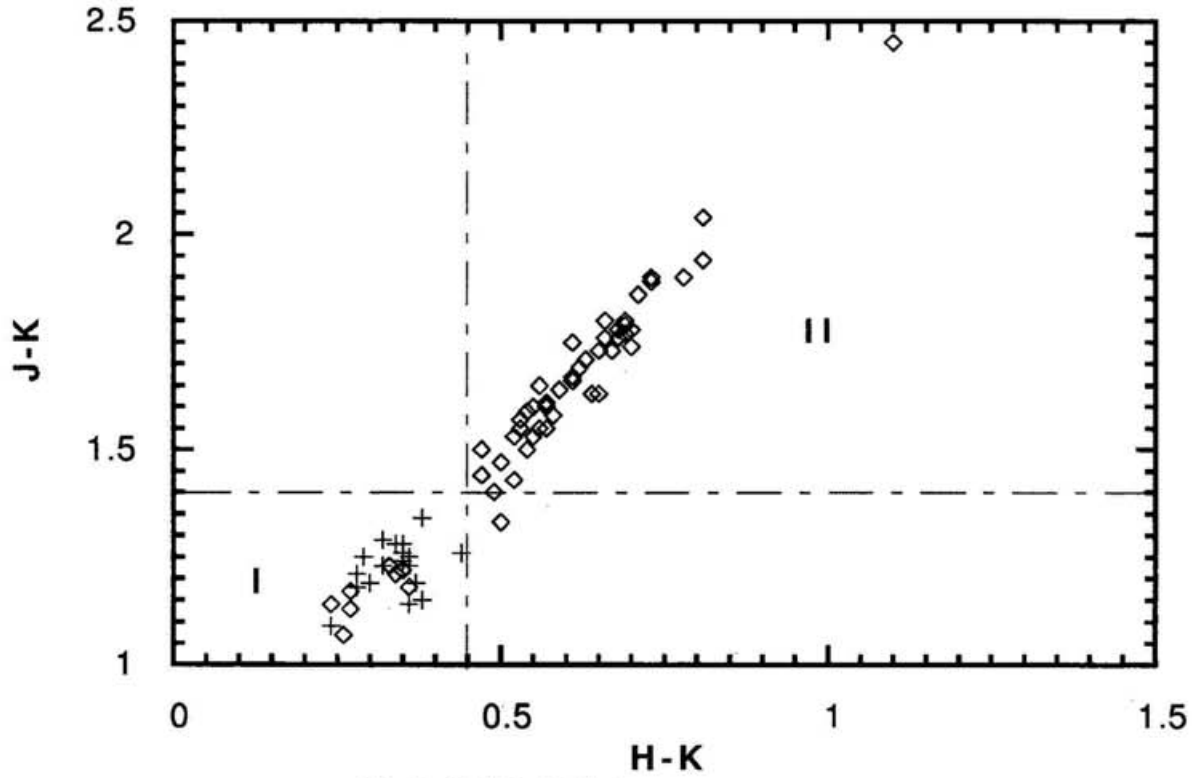

Fig.V.4.2 The MCs late-type sources.

the C-rich stars with similar near-IR colors do not show such excess. There is one exception, IRAS 05131+4530 that was classified as C-rich according to the IRAS LRS class, having emission excess at 25μm. This object is also an OH maser source(te Lintel Hekkert et al. 1991) so that it may be an O-rich star and a misclassified IRAS LRS 4n source. Meanwhile, IRAS 05131+4530 locates in region II of Fig. V.3. So if it is an O-rich star, there is one object between bluer (region I) and redder (region III) groups of O-rich stars in Fig. V.3. But the conclusion drawn from previous section holds on, that is, the possibility to find an O-rich star in region II is very low. Again the SiO non-detections assemble in region II where the C-stars reside and only 4 of them are in region I as O-rich candidates. This population of the 26 SiO non-detections is the same as drawn from Fig. V.3.

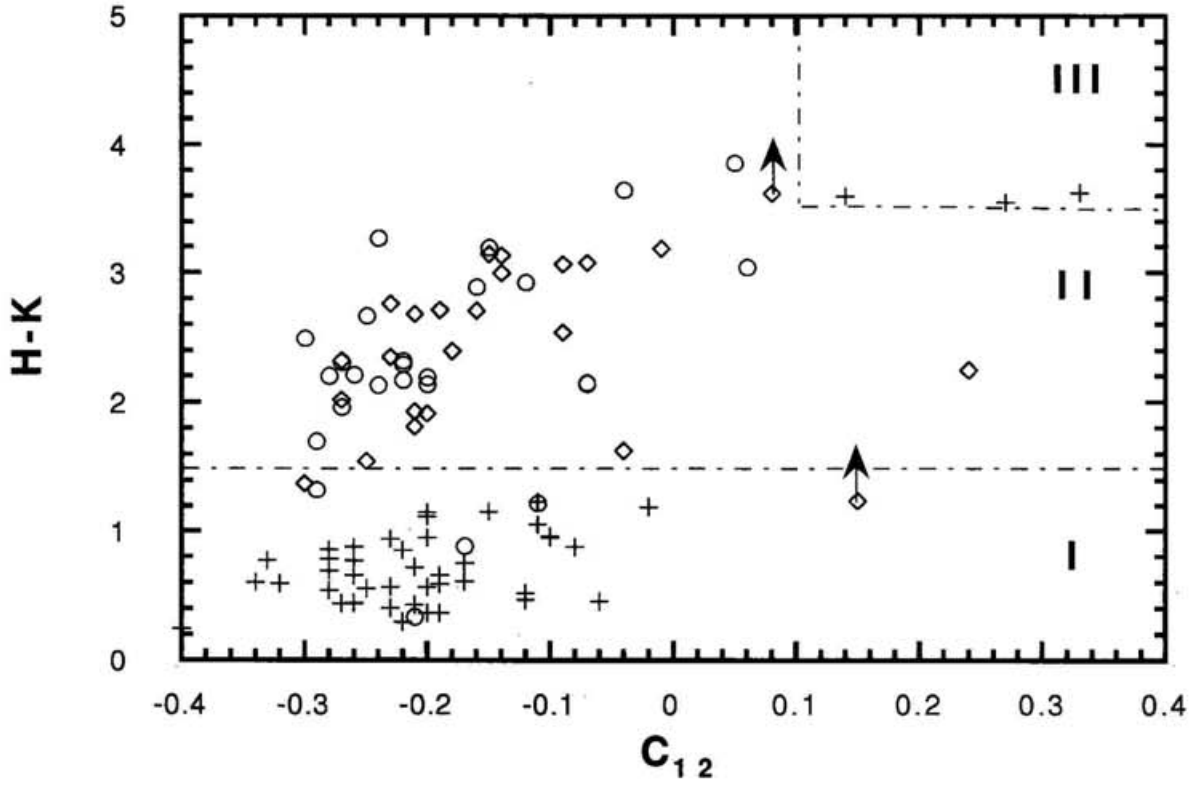

Fig. V.5.— Near-mid-IR color-color diagram. The convention of sysmbols is the same as in Fig. V.3.

V.3.4. Implication on stellar population

According to the above discrimination between O-rich and C-rich CSEs of SiO non-detections on the basis of IR colors as well as molecular lines and optical spectroscopic observational data, the sample is composed of 49 stars with O-rich CSEs and 46 stars with C-rich CSEs. Forty-eight percent of them are C-rich stars. In this sample for NIR observation, the number ratio of stars with C-rich to O-rich CSE is almost unity. Here we would like

to emphasize the features of this sample: (1) in the second quadrant of the Galactic plane and (2) late-type stars with cold (about 660K to 200K) circumstellar envelopes. The half proportion of C-rich stars is 10 times that of C-type stars in the solar neighbourhood which is only 10 percent of M-type stars(Westerlund 1965).

To know why the high proportion of C-rich stars occurs in this sample of late-type stars, it is further divided into optically identified and optically unidentified groups(Paper I). The number ratios of stars with C-rich to O-rich CSEs (hereafter C:O ratio) are found to be 14:43 and 32:6 respectively. This result is consistent with the implication from optical identification (Paper I) as mentioned in Introduction that an optically unidentified object is more likely to be C-rich than O-rich. Though there are more O-rich stars in optically identified group among which C:O is 0.35, the number of stars with C-rich CSEs is 5 times that with O-rich CSEs in the optically unidentified group. The optical unidentification of the object can be caused by two reasons. One is that the source is too far to be detected. Then the increase of C:O ratio in the optical unidentification group means the increasing proportion of C stars with distance from the sun as well as from the Galactic center. The study of late-type stellar content of galaxies shows that the C- to M-type star number ratio anti-correlates with metallicity, i.e. the ratio is high in low metallicity environment(Pritchet et al. 1987). In our Galaxy, the observations of globular clusters found the decreasing gradient of metallicity in the disk with increasing Galactocentric distance (Friel 1995). So the higher proportion of C stars in the optically unidentified group could be caused by the lower metallicity at further distances. The other reason for optical unidentification is that the source has so thick CSEs not to be seen optically. In this case, the change of C:O ratio with optical identification status means there are more C-rich stars in the later stage of stellar evolution if CSE becomes thick with evolution. This conclusion is supported by the theory that some of the O-rich stars evolve to C-rich stars due to dredge-up of stellar core materials to the surface(Iben & Renzini 1983). In the IRAS LRS sample (Omont et al. 1993) that are generally bright at 12μm and thus close to the sun, the ratio of C-rich to O-rich CSEs is 0.29 for the stars with similar IRAS color C_{12} as those in our sample. In one hand, 0.29 is slightly lower than the value (0.33) for optically identified group in our sample, which could be attributed to the inclusion of inner disk sources in the IRAS LRS sample. On the other hand, 0.29 is much bigger than the value (0.1) for the optical C- to M-type stars in the solar neighbourhood too. It means there are more C stars in the IRAS LRS sample than in the optical visible late-type stars even both are in the solar neighbourhood. The main difference between these two samples is that the IRAS LRS sources are in later stage of evolution with cold CSEs. So the difference might be explained by that some of the IRAS LRS sources may have experienced the third dredge-up phase to become C-rich in their photospheres or CSEs, which could also be the case of many optically unidentified stars in our sample. The two reasons for optical unidentification both exist and the high proportion of stars with C-rich CSEs can be due to both the low metallicity in the outer disk and objects having experienced the third dredge-up in late stage of evolution.

This high value of proportion of C-rich stars can explain the low detection rate of SiO maser surveys in a similar color-selected IRAS PSC sample. A survey in SiO maser lines to a sample of late-type stars in the outer disk resulted in a much lower detection rate than the survey to a bulge sample(Jiang et al. 1996b), even though the SiO-surveyed samples in

the outer disk and bulge were picked up under quite similar criteria and both observed by the 45m telescope at Nobeyama Radio Observatory. So more inclusion of C-rich stars in the outer disk was suspected to be the reason for lower detection rate. Because SiO maser survey towards the bulge (Izumiura et al. 1994, 1995a and 1995b) (1) looked almost only O-rich stars in that less than 0.3% C-type stars are found by optical grating-prism survey of the bulge (Blanco & Terndrup 1989), and (2) resulted in 66% detections, the detection rate of SiO maser in the bulge is then the possibility to detect the SiO maser emission in a group of stars with O-rich CSE, i.e. $\sim$ 66%. The non-detection of SiO maser in an O-rich star may be caused by: (a) that the SiO maser intensity of the star is lower than the sensitivity limit of the telescope or (b) that the star has no SiO maser emission intrinsically. But in the outer disk sample, there are 48% stars with C-rich CSEs, much higher than the bulge sample. Therefore, the detection rate of SiO maser emission in the outer disk IRAS sample should be $\sim 66\% \times 52\% = 34\%$ where 52% is the percentage of stars with O-rich CSE. In fact, the detection rate is 39%(63/161) (Jiang et al. 1996b). If we consider the fact that the outer disk SiO maser survey was biased to bright O-rich stars (Jiang et al. 1996b), the two values (34% and 39%) are quite close. The differences in SiO maser detection rates can then be explained by the differences in C stars proportion in the samples for bulge and outer disk surveys.

The half proportion of C-rich stars in the AGB stars in the outer disk is also in agreement with the result of Arecibo OH maser survey. The OH maser survey at Arecibo in IRAS PSC sources with colors of late-type stars showed that the OH detection rate towards the Galactic center is 4 times that towards the anticenter. Lewis(1994) explained most of the difference is attributable to ultra-violet intensity changes. Except some bluer objects, the OH maser survey(Eder et al. 1988; Lewis et al. 1990; Chengalur et al. 1993; Lewis 1994) searched the objects with similar IRAS colors of the stars in present NIR observation sample. According to above analysis on population of O-rich and C-rich CSEs , there must be many stars with C-rich CSE in the Arecibo OH maser survey sample towards the anticenter as well. So the much lower OH maser detection rate towards the anticenter should be at least partly attributed to the inclusion of a numerous star with C-rich CSE since OH maser emission is not seen in stars with C-rich CSE.

V.4. Summary

Near-infrared identification and photometry are made to 95 IRAS sources with colors of late-type stars in the outer disk of the Galaxy. These sources had been searched for SiO maser emission. For most of them there is a counterpart of very red color and brighter than 16mag at K′ band in the near-infrared images taken by using a NICMOS3 array detector. Their accurate positions are calculated based on the array scalar factors in reference to a star with known equatorial coordinates. The stars with O-rich and C-rich CSEs show difference in NIR colors. This characteristics is also attested by the IRAS LRS sample in the Galaxy and the late-type stars in the Magellanic Clouds. Besides in the NIR colors, the stars also exhibit some differences in the infrared spectral energy distribution between a C-rich and O-rich CSE. Both the near-infrared colors and spectral energy distribution shape are used to clarify whether the CSEs are C-rich or O-rich for stars without SiO detection. By combining together

with the observational results in optical spectroscopy, molecular lines and IRAS LRS, stars with C-rich CSE compose as high as 48% of the sample. This can explain main difference in SiO maser detection rate between the IRAS color selected samples in the Galactic bulge and outer disk. Meanwhile, the number ratios of C-rich to O-rich stars are very different for optically identified and unidentified groups, which can possibly be caused by more C stars at further outer disk or in later stage of stellar evolution.

The authors are grateful to the Telescope Management Group at XingLong Observatory for their help and kindness through our observation. They also thank Drs. H. Maehara, H. Izumiura, K. Noguchi and K. Utsumi for valuable discussions. B.W.J. is supported by Japanese Government Scholarship and her travel to BAO is sponsored by the Hayakawa Foundation of Japanese Astronomical Society. This research is supported by grant in-aid for Scientific Research(C), No 08640337 of Ministry of Education, Science, Sports and Culture.

REFERENCES

Beichman, C.A., Neugebauer, G., Habing, H.J., Clegg, P.E., & Chester, T.J. 1988, IRAS Catalogues & Atlases Explanatory Supplement, US Government Printing Office, Washingon DC

Blanco, V.M., McCarthy, M.F., & Blanco, B.M. 1980, ApJ 242, 938

Blanco, V.M., & Terndrup, D.M. 1989, AJ 98, 843

Bujarrabal, V. 1994, A&A 285, 953

Cardelli, J.A., Clayton, G.C., & Mathis, J.S. 1989, ApJ 345, 245

Chengalur, J.N., Lewis, B.M., Eder, J., & Terzian, Y., 1993, ApJS 89, 189

Cohen, J.G., Frogel, J.A., Persson, S.E. & Elias, J.H. 1981, ApJ 249, 481

Eder, J., Lewis, B.M., & Terzian, Y. 1988, ApJS 66, 183

Elias, J.H., Frogel, J.A., Matthews, K. & Neugebauer, G. 1982, AJ 87, 1029

Epchtein, N., Le Bertre, T., & Lépine, J.R.D. 1990, A&A 227, 82

Friel, E.D. 1995 Ann. Rev. Astro. Astrophy. 33, 381

Habing, H.J. 1988, A&A 200, 40

Hunt, L.K., Lisi, F., Testi, L., Baffa, C., Borelli, S., Maiolino, R., Moriondo, G. & Stanga, R.M., 1996, A&AS 115, 181

Iben,I.Jr. & Renzini, A. 1983, Ann. Rev. Astro. Astrophy. 21, 271

Izumiura, H., Deguchi, S., Hashimoto, O., Nakada, Y., Onaka, T., Ono, T., Ukita, N., & Yamamura, I. 1994, ApJ 437, 419

Izumiura, H., Catchpole, R., Deguchi, S., Hashimoto, O., Nakada, Y., Onaka, T., Ono, T., Sekiguchi, K., Ukita, N., & Yamamura, I. 1995a, ApJS 98, 271

Izumiura, H., Deguchi, S., Hashimoto, O., Nakada, Y., Onaka, T., Ono, T., Ukita, N., & Yamamura, I. 1995b, ApJ 453, 837

Jiang, B.W., Deguchi, S., Izumiura, H., Nakada, Y., & Yamamura, I. 1995, PASJ 47, 815

Jiang, B.W., Deguchi, S., & Nakada, Y. 1996a, AJ 111, 231(Chapter IV)

Jiang, B.W., Deguchi, S., Yamamura, I., Nakada, Y., S.H. Cho., & Yamagata, Y. 1996b, ApJS in press

Jiang, B.W., & Hu, J.Y. 1993, Chin. Astron. Astrophys.17, 321

Jura, M., Joyce, R.R., & Kleinmann, S.G. 1989, ApJ 336, 924

Lewis, B.M. 1994, ApJS 93, 549

Lewis, B.M., Eder, J., & Terzian, Y. 1990, ApJ 362, 634

Lepine, J.R.D., Ortiz, R., & Epchtein, N. 1995, A&A 299, 453

Loup, C., Forveille, T., Omont, A., & Paul, J.F. 1993, A&AS 99, 291

Lundgren, K. 1989, Upp. Ast. Obs. Rep. 51

Noguchi, K., Sun, J.H., & Wang, G. 1991, PASJ 43, 275

Noguchi, K., Qian, Z., Wang, G. & Wang J. 1993, PASJ 45, 65

Olnon, F.M., & Raimond, E. 1986, A&AS 65, 607

Omont, A., Loup, C., Forveille, T., te Lintel Hekkert, P., Habing, H. & Sivagnanam, P. 1993, A&A 267, 515

Pritchet, C.J., Richer, H.B., Schade, D., Crabtree, D. & Yee, H. 1987, ApJ 323, 79

Russel, J., Lasker, B., McLean, B., Sturch, C., & Jenkner, H. 1990, AJ 99, 2059

Schechter, P.L., Aaronson, M., Blanco, V.M., & Cook, K.H. 1991, AJ 101, 1756

Stetson, P.B. 1987, PASP 99, 191

te Lintel Hekkert, P., Caswell, J.L., Habing, H.J., Haynes, R.F., & Norris, R.P. 1991, A&AS 90, 327

van der Veen, W.E.C.J. & Breukers, R.J.L.H. 1989, AAp 213, 133

van der Veen, W.E.C.J. & Habing, H.J. 1988, A&A 194, 125

Wamsteker, W. 1981, AAp 97, 329

Wang, J.J., Jiang, B.W., & Hu, J.Y. 1994, Acta Astrophysica Sinica 14, 239

Westerlund, B.E. 1965, MNRAS 130, 45

Yamashita, T., Nishihara, E., Okumura, S., Mori, A. & Watanabe, E. 1994, in Scientific and Engineering Frontiers for 8-10m telescopes, edited by Iye, M. & T. Nishimura, p.285

Chapter VI

Summary

Asymptotic Giant Branch(AGB) stars are low- and intermediate-mass stars that have developed an electron-degenerate C-O core after the exhaustion of central helium. They are detected in large amount by IRAS due to the strong middle- and far-infrared radiation from their cold circumstellar envelopes which are resulted from the mass loss at a rate of about 10^{-7} to 10^{-5} $M_{\odot}$ yr^{-1}. The third dredge-up process in AGB phase digs out the newly produced C (and/or N) in the burning shells and transforms some stars into C-rich. Because these stars play an important role to recruit the interstellar medium as well as the evolution to the end of a stellar life, observations in multi-wavelength and by versatile methods have been made. This thesis puts emphasis on these AGB stars in the outer disk of the Galactic plane.

The survey in SiO maser lines was performed to the IRAS PSC sources in the outer disk of the Galaxy, which are candidates for AGB stars according to their IRAS colors. In May of 1994, 1995 and 1996, 244 AGB stars in the second and third quadrants of the Galactic plane were searched for the ^{28}SiO J=1-0, v=1 and v=2 transitions and the isotopic ^{29}SiO J=1-0, v=0 transition simultaneously by taking the wide-band advantage of the 45m telescope system. The SiO maser emission stronger than 1Jy was detectable at 5 sigma level and at a velocity resolution of 0.3 km s^{-1}. 76 stars were detected the ^{28}SiO maser emissions with 64 new detections. It's found that the v=1 and v=2 lines appear simultaneously in most cases as also shown in the bulge SiO maser emitters. The ^{29}SiO maser emission was detected in 12 stars, adding 10 new members to the previously known 20 such rare stars partly due to that the ^{29}SiO is only about 1-20th abundant as ^{28}SiO in the circumstellar envelopes of AGB stars. The isotopic maser lines are found to be detectable only in strong SiO maser sources, located at the same velocity and about 1-10th to 1-100th strong in terms of integrated intensity as the normal SiO maser lines.

The SiO maser sources are mostly associated with long-period large-amplitude variables. Except several of them, the others are all optically identified in the observations made at V and I bands by using the Kiso Schimdt telescope. By taking the CCD images about once a month for more than one year that started from 1994 August, these stars are found to be as red as $V - I > 2mag$ and their amplitudes of variability are $> 2mag$ at I band. The low

resolution spectra taken by using the 216cm telescope in 1995 October at Beijing Astronomical Observatory (BAO) showed that all the 10 observed SiO maser sources are late-M5-type stars. They could be Mira-type or semi-regular variables as the bulge SiO maser stars are. In spite that there is no clear difference in the properties of SiO maser spectra or SiO maser stars when compared with that in the bulge, the survey in the outer disk was out of expected high detection rate. Previously a survey in the SiO maser lines towards the bulge direction yielded the historically highest detection rate (66%) and it's attributed to the good sensitivity of the 45m telescope system at Nobeyama Radio Observatory and appropriate selection of sources in IRAS colors. The sample of the outer disk survey was selected under similar criteria and the same sensitivity was reached as in the bulge survey. However the detection rate, 31%, is less than half that of the bulge survey.

The outer disk sample was suspected to be consisted of more C-rich AGB stars responsible for the much lower detection rate. As is known that the non-detection of SiO maser emission in AGB stars can be caused by the weakness of SiO maser line beyond the detection limit or no emission intrinsically as in case of a C-rich AGB star. While the former reason could not bring about big difference since the same detection limit was achieved in both the bulge and the outer disk surveys and the outer disk sample stars are even averagely closer. In order to investigate how much proportion of C-rich AGB stars is in the AGB stars in the outer disk, optical spectroscopy and near-infrared photometry were carried out to 19 and 95 sources respectively, a subsample of the SiO maser-searched. The optical spectroscopy to 9 SiO non-detections revealed 4 C-rich stars. Because many of the stars are optically invisible, near-infrared identification and photometry were supplemented by using the 126cm infrared telescope at BAO and the 188cm telescope at Okayama Astrophysical Observatory in the fall of 1995. Combining the data of molecular lines, IRAS LRS spectra and optical spectroscopy, we found that the separation of C-rich from O-rich AGBs is feasible based on their near-infrared colors J-K and H-K. About half of the stars are then of typical near-infrared colors of C-rich AGB stars. Though this proportion of C-rich stars is quite high compared with the value of 10% among the neighbourhood late-type stars, it is consistent with the low metallicity in the outer disk since the proportion of C-rich stars is high in metal poor environment as seen in external galaxies. The content of 50% C stars can explain the major difference in SiO maser detection rate between the outer disk sample and the bulge sample. It is also in agreement with the results of Arecibo OH maser survey towards a similar sample of AGB stars in the outer disk.

摘要

渐近巨星支（ＡＧＢ）星是中心Ｈｅ燃烧完、擁有一个簡并Ｃ/Ｏ核的中小質量恒星。他們以 10^{-7}至 $10^{-5}M_{\odot}/yr$ 的速度流失質量, 従而形成一个紅外輻射強列的冷星周包層, 所以工作在中遠紅外的ＩＲＡＳ衛星大量地探測到了這類天体。在ＡＧＢ演化階段, 有的恒星経歴所謂第三次”dredge-up”過程, 把在核反応層中新形成的Ｃ或Ｎ通過激烈的対流伝送到恒星表面, 変成富Ｃ星。由于ＡＧＢ星在星際物質的演化中扮有重要角, 同時又是恒星演化的最後階段, 人們已経做了大量的観測, 本篇論文則通過多波段観測集中研究銀河面内、太陽系外銀盤的ＡＧＢ星。

首先, 我們進行了 SiO 脈澤観測, 観測様本主要是根据ＩＲＡＳ顔色挑選出来的外銀盤ＡＧＢ星候選体。１９９４年、１９９５年、１９９６年的三个５月我們一共観測了銀河面的第二和第三象限的２４４个ＡＧＢ星, 同時搜尋^{28}SiOJ=1-0 v=1 和 v=2, 和同位素^{29}SiOJ=1-0 v=0 発射。使用野辺山射電天文台的４５ｍ望遠鏡系統使我們能観測到強度為１Ｊｙ的源（Ｓ/Ｎ＞５）而同時達到０．３ｋｍ/ｓ的速度分辨率。７６个星被発現有^{28}SiO 脈澤輻射, 其中６４个源是第一次被観測到；１２个源被観測到了同位素^{29}SiO 脈澤輻射, 其中１０个是第一次被観測到。由于在ＡＧＢ星的星周包層中, ^{29}SiO 的豊度只有^{28}SiO 的大約１/２０, 以前只発現了２０个這様的^{29}SiO 脈澤源。一般来講, ^{29}SiO 脈澤線只在強的^{28}SiO 脈澤源中才被探測到, 速度与^{28}SiO 的最強線一致, 積分強度只有^{28}SiO 的１/１０到１/１００。

SiO 脈澤源絶大部分是長周期、大幅度的変星。除了幾个源以外, 別的都有在Ｉ波段亮于１９等的光学対応体。我們使用東京大学木曽観測所的１０５/１５０ｃｍ施米特望遠鏡加一个ＣＣＤ探測器、従１９９４年８月開始進行了将近両年的跟踪観測, 発現這些星一般都很紅Ｖ－Ｉ＞２ｍａｇ、変幅ΔＩ＞２ｍａｇ。而１９９５年１０月使用北京天文台２１６望遠鏡得到的低分辨光譜則表明観測的１０个 SiO 脈澤源全是晚于Ｍ５的Ｍ型星。所以, 他們很可能是Ｍｉｒａ型或半規則変星, 与銀河系核球中的 SiO 脈澤星没有区別。

尽管在 SiO 脈澤星的性質或 SiO 脈澤光譜方面、銀河系核球和外銀盤没有明星的不同, 但外銀盤的巡天却是出乎意外地没有象銀河系核球巡天那様有高的探測率。在外銀盤巡天之前進行的銀河系核球巡天観測的探測率是６６％, 曾被帰功于野辺山天文台４５ｍ望遠鏡系統在這个波段的高霊敏度和正確的ＩＲＡＳ顔色的選択。而外銀盤巡天的様本是

基于極為相似的選択判据並達到了同様的探測霊敏度, 但探測率只有３１％, 不足銀河系核球巡天的一半。

我們推測外銀盤様本可能包含更多的富Ｃ ＡＧＢ星、因而造成低的探測率。没被探測到 SiO 脈澤的天体可以帰于両類：第一類天体有 SiO 脈澤輻射、但視強度弱于観測的霊敏度；還有一類天体則本身就没有 SiO 脈澤輻射, 富Ｃ ＡＧＢ星就属于這一類。第一類的天体応該不会対銀河系核球和外銀盤的観測結果帯来太大的区別, 因為探測極限是一様、而且外銀盤的天体平均来講更近一些。所以第二類天体的差別才会是造成探測率不同的主要因素。為了弄清楚有多少富Ｃ星被包括在外銀盤的観測様本中, 我們選択一个亜様本進行光学光譜和近紅外測光観測, 得到１９个源的光学光譜和９５个源的近紅外測光結果。通過光譜観測我們発現 9 个没有観測到 SiO 脈澤的源中有 4 个是Ｃ型星。但大多数没被探測到 SiO 脈澤的天体是光学不可見的, 我們于１９９５年秋天用北京天文台的１２６ｃｍ紅外望遠鏡和岡山天体物理観測所的１８８ｃｍ的望遠鏡做了近紅外証認和測光観測。結合射電分子線、ＩＲＡＳ的低分辨率光譜和光学光譜数据, 我們発現富Ｃ和富Ｏ ＡＧＢ星可以従他們的近紅外色指数Ｊ－Ｋ和Ｈ－Ｋ区別開来, 而在我們観測的様本中約有５０％的星呈現富Ｃ星的近紅外顔色。在太陽附近的光学晩型星中只有１０％是富Ｃ的, 所以５０％這个比例看起来太高, 但這个結果与外銀盤的低金属豊度是一致的, 因為対銀河系的研究表明：在貧金属環境下、富Ｃ星的比例偏高。而５０％的富Ｃ星可以很好地解釋外銀盤和銀河系核球的 SiO 脈澤探測率的不同, 也与在 Arecibo 進行的ＯＨ脈澤巡天的結果相吻合。